KERNFORSCHUNGSANLAGE JÜLICH GmbH
Institut für Reaktorwerkstoffe

Plasma Induced Material Defects and Threshold Values for Thermal Loads in High Temperature Resistant Alloys and in Refractory Metals for First Wall Application in Fusion Reactors

by

Harald Bolt
Helmut Hoven
Erich Kny
Karl Koizlik
Jochen Linke
Hubertus Nickel
Erich Wallura

Jül-2086
October 1986
ISSN 0366-0885

Metallwerk Plansee GmbH
A-6600 Reutte/Tirol
Austria

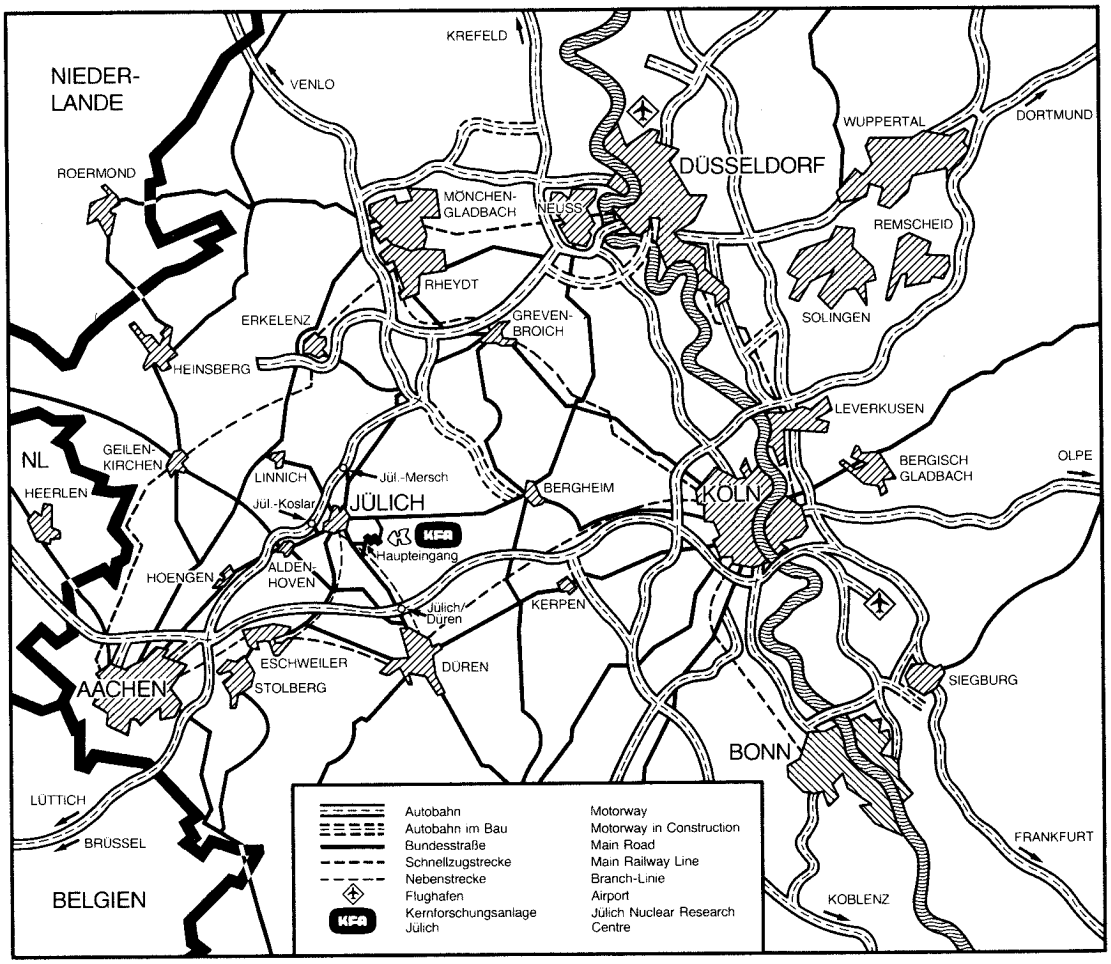

Als Manuskript gedruckt

Berichte der Kernforschungsanlage Jülich - Nr. 2086

Institut für Reaktorwerkstoffe Jül - 2086

Zu beziehen durch: ZENTRALBIBLIOTHEK der Kernforschungsanlage Jülich GmbH
Postfach 1913 · D-5170 Jülich (Bundesrepublik Deutschland)
Telefon: 02461/610 · Telex: 833556-0 kf d

Plasma Induced Material Defects and Threshold Values for Thermal Loads in High Temperature Resistant Alloys and in Refractory Metals for First Wall Application in Fusion Reactors

by

Harald Bolt
*Helmut Hoven
Erich Kny
Karl Koizlik
Jochen Linke
Hubertus Nickel
Erich Wallura

*Metallwerk Plansee GmbH
A-6600 Reutte/Tirol
Austria

Plasma-induzierte Werkstoffschäden und Grenzwerte für thermische Belastungen in hochwarmfesten metallischen Legierungen und in Refraktär-Metallen für den Einsatz im Bereich der ersten Wand von Fusionsreaktoren

von

H. Bolt, H. Hoven, E. Kny, K. Koizlik,
J. Linke, H. Nickel, E. Wallura

Kurzfassung

Werkstoffe der ersten Wand von Fusionsreaktoren vom Tokamak-Typ werden durch gepulste Flüsse thermischer Energie belastet, die von 0,5 MW m^{-2} bis 10 MW m^{-2} während des Normalbetriebs der Anlage reichen und die 1000 MW m^{-2} bei Plasmaabbrüchen überschreiten können. Die dadurch verursachten Werkstoffschäden und Werkstoffermüdung werden untersucht und in Form von Belastungs-Grenzkurven dargestellt. Zusätzlich werden die Ergebnisse, soweit möglich, mit theoretischen, quantitativen Daten verglichen. Diese Art der Auswertung erlaubt eine halb-quantitative Bewertung der Verwendbarkeit der genannten metallischen Werkstoffe für die erste Wand von Fusionsreaktoren.

Kernforschungs-
anlage Jülich
GmbH IRW

Jül-2086

January 1987

Plasma Induced Material Defects and Threshold Values for Thermal Loads in High Temperature Resistant Alloys and in Refractory Metals for First Wall Application in Fusion Reactors

by

H. Bolt, H. Hoven, E. Kny, K. Koizlik,
J. Linke, H. Nickel, E. Wallura

Abstract

Materials for the application in the first wall of fusion reactors of the Tokamak type are subjected to pulsed heat fluxes which range from some 0.5 MW m^{-2} to 10 MW m^{-2} during normal plasma operation, and which can exceed 1000 MW m^{-2} during total plasma disruptions. The structural defects and material fatigue caused by this types of plasma wall interaction are investigated and the results are plotted in threshold loading curves. Additionally, the results are, as far as possible, compared with quantitative, theoretical calculations. These procedures allow a semi-quantitative evaluation of the applicability of the mentioned metals in the first wall of fusion reactors.

Contents

1. Introduction

The technical concept for the construction of a thermo-nuclear fusion reactor which presently is investigated most frequently is the magnetic confinement of the Tokamak type /1,2/. Here, the deuterium-tritium gas mixture is heated by direct current flow, the so called ohmic heating /3/, by ion /4/ or electron cyclotron resonance /5/ heating, and/or by high energy neutral particle injection /6/. The resulting hot plasma is compressed by suitable magnetic fields forming a torus-shaped tube. Thus, on the one hand, the hot plasma is kept away from the material first wall of the plasma chamber. On the other hand, the Tokamak concept as being used at present allows only a pulsed operation of the plasma machine and, in the future, of the fusion reactor, thus giving rise to an intermittent load on the first wall.

The magnetically confined plasma tube is surrounded by a material wall which is in the technical reality a complex system of different assemblies with various service requirements such as limiters and/or divertors, liner (if existing), vacuum vessel, cooling facilities, blanket, etc.. From the point of view of the problem discussed in this presentation the term "first wall" means those parts, components and materials of the whole first wall which are directly facing the plasma. In that sense, first wall means those components and materials of the toroidal plasma chamber that can interact with the plasma, either by direct contact with the hot plasma or parts of it or on a secondary way by temperature radiation (electromagnetic radiation). On the other hand, this definition of the first wall covers just those components and materials which affect the properties of the plasma, primarily its purity. In the course of this presentation the term "first wall" is always used in this described sense.

During operation of a plasma machine of a fusion reactor, the first wall and its materials interact with the hot plasma. This plasma wall interaction causes a pulsed application of load to the first wall which can give rise to material damage, at least to a degradation of the material parameter values. Thus, the plasma wall interaction can have life time limiting consequences for the first wall or some of its components.

This presentation attempts to give a contribution to the quantitative determination of plasma induced effects in the first wall material, primarily under the aspect of highly loaded first wall components.

2. First Wall of Fusion Reactors

The first wall of already operating plasma machines and of future fusion reactors is affected by the hot plasma and, on the other hand, affects the plasma by contaminating it with material atoms and ions. The intensity of the plasma wall interaction and therefore also the induced affections of the wall materials and the arising contaminations of the plasma depend on the respective first wall material, the actual component, the dominating type of interaction process and - this is corresponding at least partially with the just mentioned type of interaction - on the mode of plasma operation. These relationships shall be briefly pointed out.

2.1 First Wall Components

From the aspect of plasma wall interaction, the first wall of fusion reactors of the Tokamak type can be devided into two parts. The larger part of the plasma facing inner wall area remains relatively cold /7/, although being near by the many million K hot plasma - the target temperature is more than 10^8 K corresp. to about 10 keV. Depending on the respective Tokamak machine, this part of the first wall can have an average temperature of few hundred ^oC which is kept constant - except for a small "ripple" of few degrees caused by the pulsed operation of the plasma - by an active cooling of the first wall. Another concept with a radiation cooled "curtain" in front of the plasma facing surface leads to temperatures up to 1800^oC of the "curtain" material. This area should also never come in direct contact with the hot plasma, e.g. during plasma disruptions.

To guarantee this last-mentioned requirement the first wall is partly protected by suitable components: The inboard area of the first wall is covered with high temperature resistent protective tiles /8/ to shield this part of the first wall from disruptions and the so-called shine-through of the neutral beams, when neutral beam injection heating of the plasma is applied.

The outboard area is protected by special first wall components, namely the limiters /9/. An additional limiter can also be used for increasing the protection of the inner first wall. Limiters are also used for the shielding of special facilites of the first wall from possible contacts with the fusion plasma, e.g. the high frequency antennae when electron or ion cyclotron resonance heating (ECRH or ICRH) is used as an additional heating procedure for the plasma.

Limiters can also be used as exhaust for the "ash" of the burning plasma, the He, which results form the D-T-fusion reaction, and other impurities or contaminations of the plasma and for density control, e.g. after neutral beam injection. For that purpose, they are constructed as pumped limiters /10, 11/, the leading edge of which or their pumping duct extends into the boundary layer of the plasma. Another Tokamak concept transfers this task of plasma cleaning to a particular first wall component, the divertor /12/.

Even under normal, regular plasma operation, limiters and divertors reach elevated temperatures already after a sequence of few ten plasma discharges. A standard value of the temperature may be some 10^3 ^oC which is superimposed by a temperature variation of some 100^oC caused by the pulsed plasma /12, 13/.

During unstable plasma states, e.g. by a premature break-down of the plasma current, i.e. a so called plasma disruption, limiters can reach temperatures far above the melting temperature (or sublimation temperature or decomposition temperature, depending on the resp. material) of the limiter material. This is also true for the armor tiles when the shine-through of the neutral beam is very intense e.g. due to a low density plasma state.

2.2 Plasma Wall Interaction

During operation, the fusion plasma of a Tokamak interacts with the first wall of the plasma chamber. This interaction has to be examined depending on the working conditions of the plasma.

Normal plasma operation gives rise to plasma wall interaction /14,15/ which is pulsed due to the non-continuous operation of present type Tokamaks. In this connection, the term plasma wall interaction summarizes a system of individual sub-processes which each by itself affect the first wall material.

Moreover, the sub-processes can mutually influence themselves thus reducing or intensifying the effects of each single, individual process on the material. Such so called synergistic effects /16, 17/ are not subject of this presentation.

Considering this restriction the plasma wall interaction during normal plasma operation consists mainly of
- electron and ion bombardment,
- neutral particle bombardment
- electromagnetic radiation,
- unipolar arcs (arcing).

If realistic fusion conditions are considered another highly important interaction process has to be taken into account, namely the irradiation of the first wall with the fusion neutrons. These neutrons have a very high energy, e.g. for the D-T-fusion process about 14 MeV.

Neutrons of such high energies have long ranges of mean free path, and on their way through the material they generate lattice damage in the crystalline material and transmutation products. Although this plasma wall interaction process is of fundamental importance it remains disregarded in this report.

The arcing /18/, mentioned as one of the plasma wall interaction sub-processes during normal plasma operation seems to be in reality a process in the transition range between normal and instable plasma operation. This latter plasma state can be characterized by low plasma density which can be the reason for the high-energetic run-away electrons /19/. The run-away electrons - which can have a kinetic energy up to some 10 MeV and thus far above that of the "normal" electrons interacting with the first wall - can leave the magnetic confinement and strike the protection components of the first wall.

Another characteristic process during instable plasma states is the plasma disruption /20,21/, a premature, abrupt termination of the discharge. Depending on plasma and process parameters plasma disruptions can deposit huge amounts of the plasma energy during very short periods of time on relatively small areas of the first wall. Thus, from the aspect of first wall materials, plasma disruptions and run-away electron events are the most dangerous processes of plasma wall interaction.

2.3 Loading Parameters

The plasma wall interaction causes energy deposition and direct surface erosion in the first wall and, as a consequence, the material removed from the first wall contaminates /22/ the hot plasma.

This plasma contamination has to be avoided or at least minimised, in particular contamination by medium and high Z material.

The material erosion /23,24/ by physical or chemical processes, or both mechanisms simultaneously, is an interaction mechanism which affects the very surface of the first wall material. From the material side of view, it results in a decrease of wall thickness which can reach values up to few millimeters per year of Tokamak operation.

Electromagnetic radiation from the plasma is another component of plasma wall interaction. It deposites its energy within a depth of less than one wavelength in the case of a metallic first wall or, when the interacting surface is a ceramic material, the energy deposition may occur in considerably greater distance below the surface, depending on the type of ceramic or its transmission coefficient.

The depth of the energy deposition /25, 26/ by bombardment with corpuscular particles - not regarding neutrons - depends, - besides the values of density and atomic number of the material - whether electrons or ions/neutrals are examined: Without regarding diffusions processes, ions and neutrals seem to deposit their energy in a surface - near area of few hundred micrometers at most, independent of the type of material. This may of course be sufficient to distroy a first wall component by thermal shock cracking, fig. 2.1. The deposition depth of energy by electrons on the other hand seems to depend on the electrical conductivity of the first wall material and should be great in the case of insulators, fig. 2.2, and in the same order of magnitude as with ions and neutrals in the case of metals.

These statements are based on experimental results from simulation experiments and are of course related to the energy range of the particles coming from the plasma to the first wall.

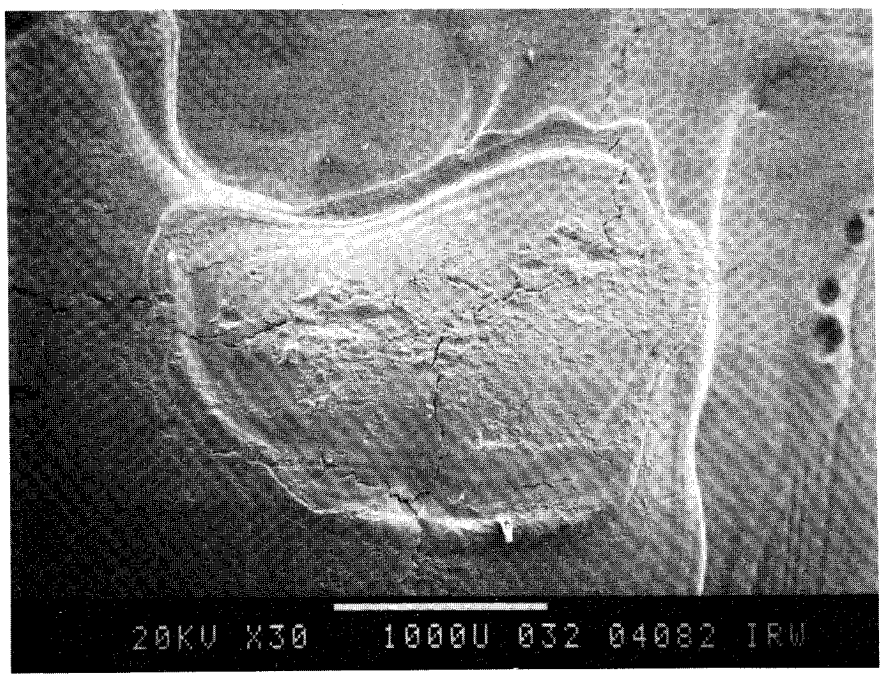

Fig. 2.1: Thermal shock cracking in the surface of an INCONEL 600 limiter of TEXTOR by a touchdown of the plasma

Finally, the neutrons have to be mentioned which are generated by the fusion process and the energy of which depends on the resp. fusion reaction. So, for example, the deuterium-tritium (D-T) fusion reaction generates neutrons with a lower energy threshold of about 14 MeV. In an actual fusion reactor about 80 % of the energy originated from the fusion reaction is carried by the neutrons /27/. They transfer their energy during the moderation process to the surrounding matter mainly behind the first wall in the adjacent blanket. In the plasma machines operating today the neutron generation can be neglected.

Although during plasma wall interaction thus a broad spectrum of different and interfering processes contributes to the wall loading at least for a first approach it seems to be allowed to classify these mechanisms by the following parameters:

Erosion /28,29/ is regarded to be a pure surface-relevant process caused by particle bombardment which leads to a more or less homogeneous excavation of material from the first wall and, on the other hand, to a plasma contamination. At a better approach, also synergistic effects would have to be taken into account. Erosion occurs "continuously" during all states of plasma operation.

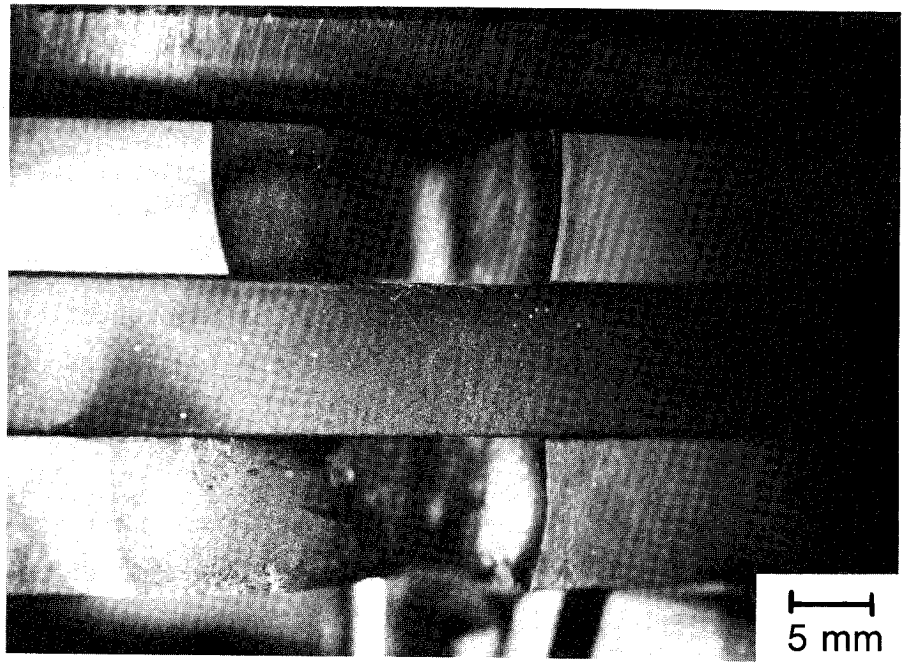

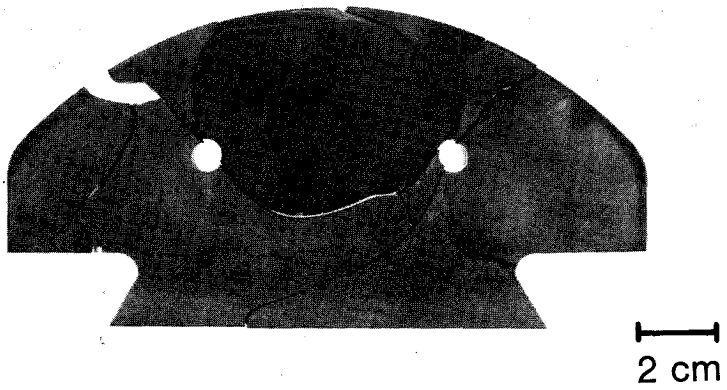

Fig. 2.2, a,b: Disintegration of two ceramic sandwich discs (below and above a metal disc) in the sandwich limiter in TEXTOR (a), obviously by a deep-ranging energy deposition by run-away electrons

Fig. 2.2 b: Macrograph of one of the two disintegrated sandwiches of fig. 2.2 a

During normal plasma operation, the plasma wall interaction deposites energy to the first wall /30,31,32/ in the surface near area few micrometer to few hundred micrometer thick. The energy deposition is pulsed with a pulse length equal to that of the burning plasma. The energy is deposited with a power density of approximately 0,1 MW m^{-2} during pulse durations of typically

2 s (TEXTOR), 20 s (JET), 200 s (NET).

These values are valid for those parts of the first wall which achieve only a low loading by the plasma. They make up to 70 - 80 % of the total first wall surface. The highly loaded first wall components receive energy with a power density in the order of magnitude of 5 MW m^{-2}.

The pulse durations are as just mentioned. These loading conditions are valid for armor tiles, limiters, in particular their leading edges, and divertors.

The number of pulses or plasma discharges which the first wall has to survive should be as large as possible - for example 10^5 plasma discharges lifetime for the first wall of NET - to avoid a frequent, complicated exchange of first wall components.

During unstable plasma conditions the energy deposition to the limiters by plasma disruptions and/or run away electrons can reach huge values. Characteristic numbers of power density are

$$50...2000 \text{ MW m}^{-2}.$$

The deposition periods are reported to be

$$10 \text{ µs up to } 100 \text{ ms}.$$

Short deposition times are valid for run away electrons, whereas the disruption durations are reported to be between 2 and about 100 ms.
Similar values should be also true for the neutral beam shine-through during neutral beam injection heating.

Finally, the first wall loading by arcing shall be mentioned. If conclusions are drawn from the material damage caused by arcs one should assume that the conditions in an arc are similar to that during disruptions concerning the power density, but showing very short burning times and very small affected wall areas:

$$50...2000 \text{ MW m}^{-2},$$

burning time per crater some µs to some 10 µs, chains of craters, fig. 2.3,

each crater having a diameter of typically 1...10 µm and a depth of the same order of magnitude.

The just mentioned loading parameters are graphically summarized in fig. 2.4.

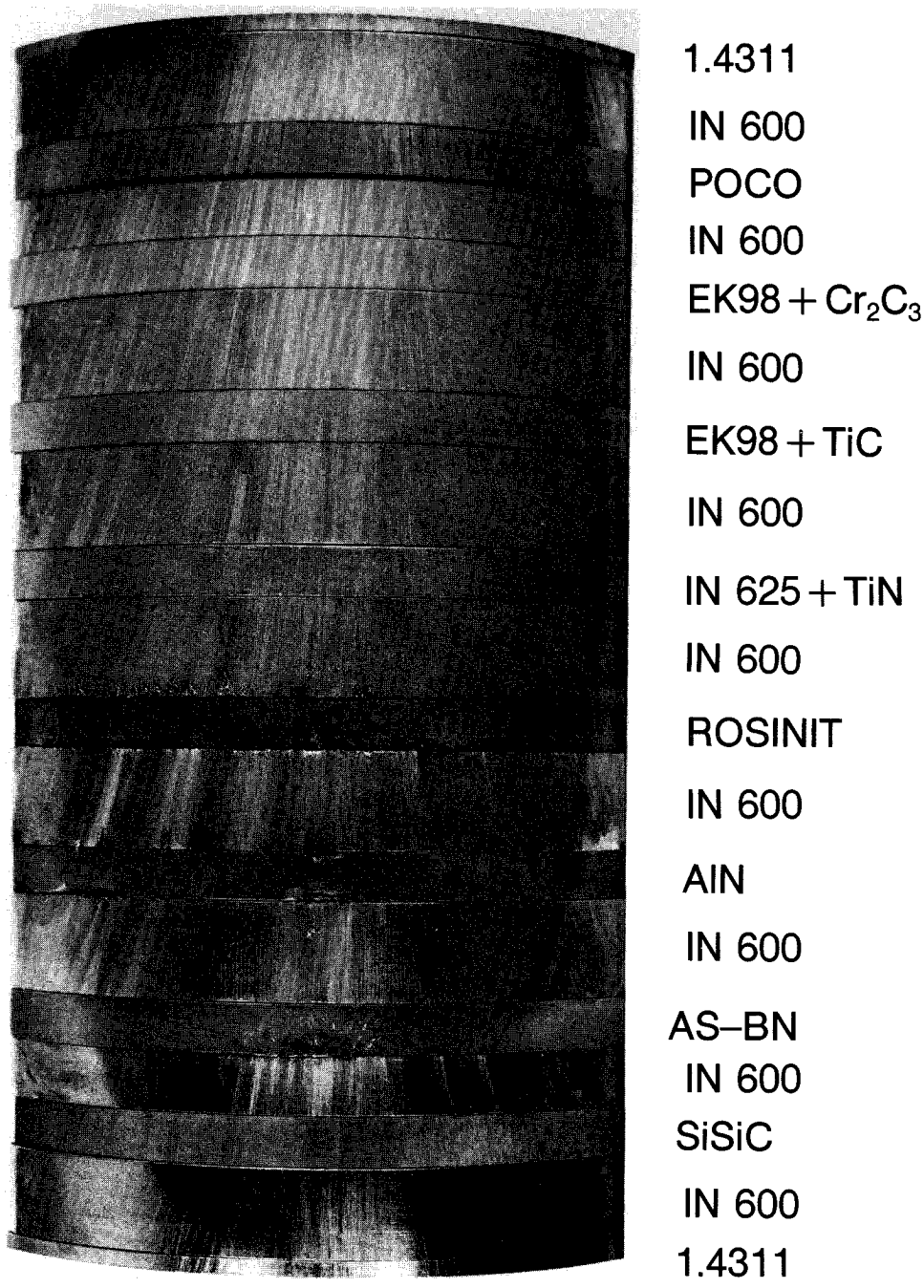

Fig. 2.3, a,b: Chains of arcing craters running in preferentially vertical direction across the surface of a sandwich limiter after plasma exposure in TEXTOR (a), and some arcing craters at higher, magnification (b)

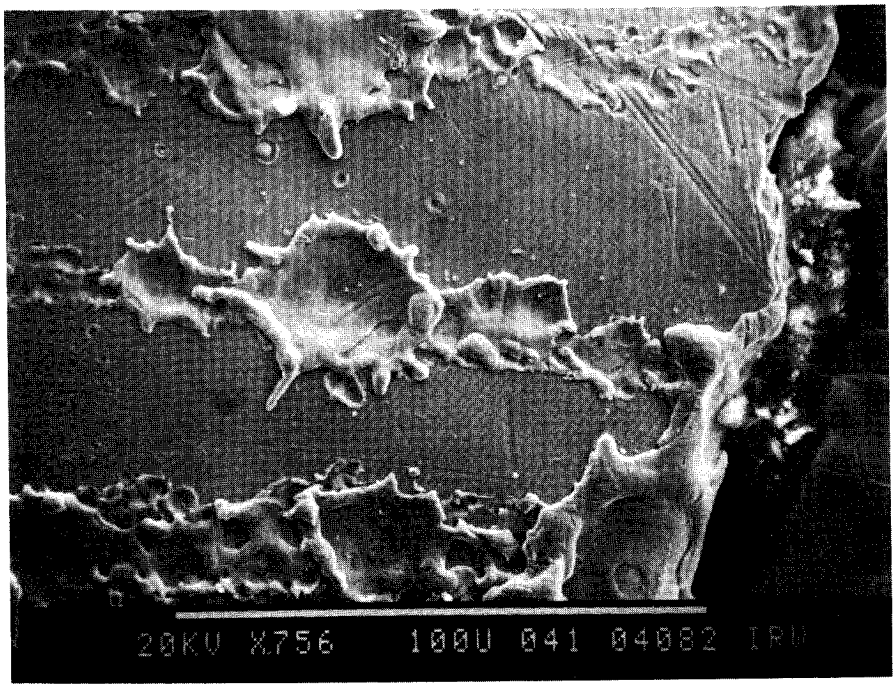

Fig. 2.3 b: see fig. 2.3, a,b.

3. Plasma Induced Effects on First Wall Materials

The plasma wall interaction as being described before affects the first wall of the plasma chamber and its materials, resp. The depth of the attack, the depth of the energy deposition and the kind of damage caused by the plasma wall interaction depend on the type of the sub-process being essential operative. Thus, the different kinds of plasma induced material defects, their relation to plasma wall interaction and the role they play as life-limiting effects for the first wall and their components have to be looked at in detail.

3.1 Thermal Fatigue

Two sub-processes of plasma wall interaction are running to a certain extent directly coupled to the burning plasma, namely thermal fatigue and erosion. Thermal fatigue is of course operative only as far as plasma machines are regarded with pulsed plasma operation.

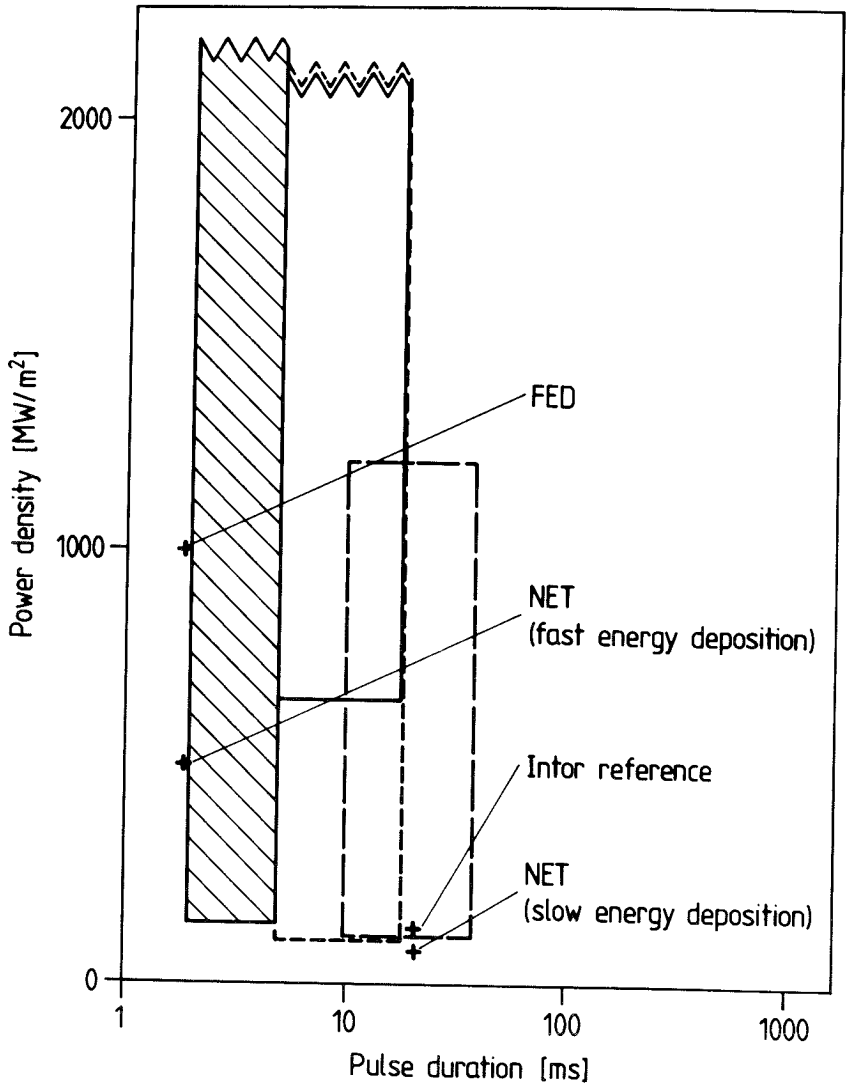

Fig. 2.4: Loading parameters for different fusion reactor designs: power density as a function of energy deposition duration

The process of thermal fatigue /33,34/ is caused by the energy flux from the hot plasma through the surface of the first wall to the cooling system. The term energy flux summarizes from this point of view all plasma born processes which ultimately result in the deposition of thermal energy and thus in a temperature rise in the first wall. All further effects, e.g. particle erosion from the first wall by particle flux from the plasma, and processes which occur only occasionally like plasma disruptions are not regarded. In this sense, four processes contribute to the continuous energy deposition in the first wall: the flux of electrons and the flux of ions - hydrogen-isotropes, helium -, which leave the plasma tube but still follow the magnetic field lines on helical orbits, neutrals which arise by charge exchange in the plasma boundary layer, and electro-magnetic radiation from the excitation states of the ions in the plasma.

During regular plasma discharges the total energy flux from the plasma to the first wall is provided by these processes. Of course this is only true for the existing plasma machines and may be for those of the next generation, i.e. for plasma machines in which real fusion processes occur only occasionally. Otherwise the fusion neutrons transport about 80 % of the total energy flux. Neutrons and their effects on first wall material are not regarded in this presentation.

Since the first wall components directly facing the plasma are not subjected to high, long ranging mechanical stresses, the influence of thermal fatigue on the first wall material is actually a mainly thermal one, caused primarily by the pulsed flux of thermal energy through the first wall. The phenomenon of affection of the structure of alloys by pure thermal processing at temperatures far below the melting point is well known, e.g. recrystallisation /35/, aging /36/, or thermal etching /37,38/. Whether thermal fatigue - in the sense ment here - could have life-limiting effects on the first wall material strongly dependent on the base temperature and on the temperature variation therefore has to be investigated.

Whether or not thermal fatigue will limit the lifetime of first wall materials will be in any case strongly controlled by the actual thermal load. As has been mentioned already, the major part of the first wall remains at medium temperatures of few hundred ^{o}C - somewhere between $300^{o}C$ and $500^{o}C$ -, superimposed by a temperature variation of only few degrees, caused by the plasma discharges. As long as chemical processes are not regarded - e.g. between the metallic first wall and a surface layer deposited to reduce erosion - the just mentioned thermal conditions should not give rise to any problems like thermal fatigue.

This is no longer true in the case of the high heat flux components. Here, the steady-state temperature may reach values well above $1000^{o}C$, superimposed by a temperature variation by the plasma discharges of some hundred degrees. The total thermal load is equivalent to about 5 to 10 MW m^{-2}, as has been mentioned already. These conditions may indeed not be sufficient to cause instantaneously serious material damage like cracking or melting. But they are far above those which are found usually in conventional techniques, e.g. the wall loading of the walls of the combustion chamber of an automobile engine with 1 MW m^{-2} on an average. So it can be expected that under these conditions thermal fatigue could play an important role among

the life-limiting processes although the investigations of first wall samples from real, operating plasma machines (e.g. TEXTOR, TFTR, PDX, JET) did not yield any structural changes that could be interpreted as thermal fatigue. But this may be due to the fact that these machines are small compared with the NET to which the mentioned data are devoted, and may be due to relatively small values of wall loading and small numbers of plasma discharges during the operation period of the resp. component.

A similar problem may arise with the material in the low loaded area of the first wall when a first wall concept /39/ is realized in which graphitic or ceramic tiles are "curtained" between the cooled metallic wall and the plasma, and the energy transfer from the ceramic "curtain" to the wall is realized just by radiation. These tiles are fixed in a metallic lattice at a distance of few mm in front of the actual first wall, the lattice hanging on the metallic first wall in spacers. Depending on the respective input data the temperature of the tiles in the plasma facing side is calculated to be some 1500 to 1800°C with a temperature gradient along the thickness of the tile of few 10 degrees per cm. In this first wall concept thermal fatigue may not play a really important role, but corrosion problems may come up in the areas where the graphitic or ceramic tiles are in direct contact with the metallic lattice. This problem is not subject of this presentation.

Thermal fatigue, the structural changes caused by this process in the first wall material, and their dependence on the load conditions are subject of one of the following chapters.

3.2 Thermal Shocks

During unstable plasma states or plasma states with low particle density two sub-processes of plasma wall interaction can occur which can cause severe material damage, namely plasma disruptions and run-away electron events. The conditions under which the one or the other process or both processes arise cannot be discussed here. Important, from the standpoint of life-limiting effects in the first wall material, is the fact that plasma disruptions and run-away electrons can deposit huge amounts of energy to the protective components of the first wall.

Applying the design data of JET /40/ in its basic version: plasma current for D-shape plasma close to 4 MA and a circumferential voltage of about 2 V, one finds a total power input into the plasma of about 8 MW without additional heating. Additional heating may contribute with some 10 MW. Assuming a plasma disruption deposits the total plasma energy to a surface area of about 100 cm^2 the maximum power density that has to be expected can reach the already mentioned value of about 2000 MW m^{-2}.

Run away electrons which may reach energies up to some 10 MeV may deposit their energy with similar power densities but higher penetration depths.

It is commonly accepted that there exists no material that could survive under these conditions. Due to the short energy deposition duration of 0.01 to 100 ms these plasma wall interactions cause severe thermal shock loadings of the first wall material, even under the assumption that typical disruption and run away electron events deposit their energy with a power density about a factor of ten lower than the mentioned maximum one.

In metallic alloys, the thermal shock loading can cause large area melting, surface cracking of the material and recrystallisation/remelting of the material, fig. 3.1. When during operation of a first wall protective compo-

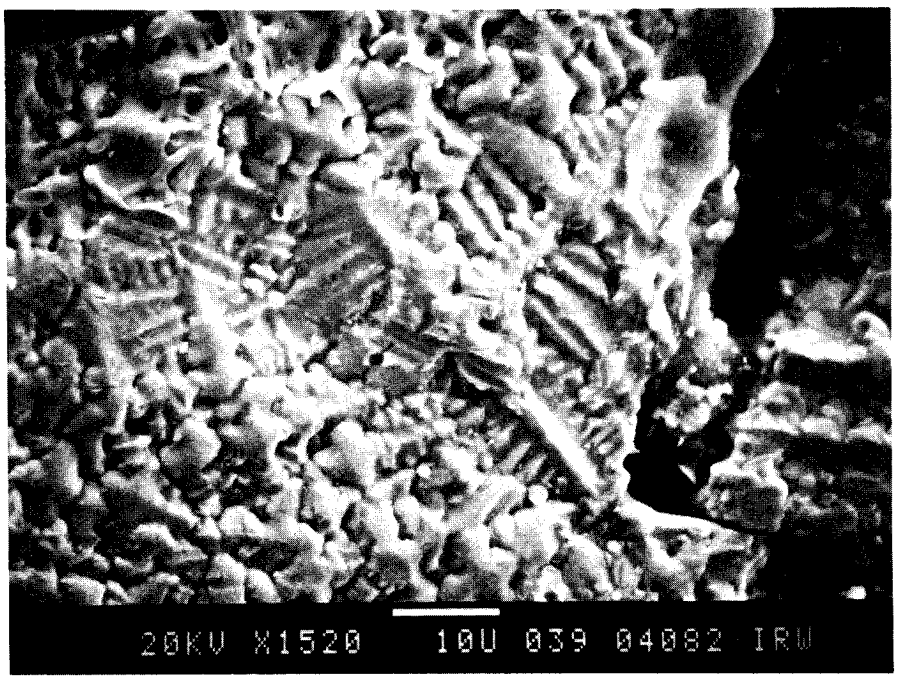

Fig. 3.1: Thermal crack and recrystallized, dendritic material in the surface of an INCONEL 600 limiter after a thermal shock event in TEXTOR

nent some plasma disruptions "land" consecutively on the very same area multi layer remelt zones can be generated, fig. 3.2 which then can reach large depth values up to some 100 micrometer. The size and the depth of the melted and cracked area depend on the actual thermal shock loading of the material.

Under thermal shock loading ceramics behave still worse than metallic alloys. Brittle ceramics like for example SiC can be destroyed, that means completely disintegrated by one single thermal shock. First experimental results, fig. 2.2, can be obviously interpreted in that sense, that run away electrons deposit their energy in the material deep below the surface. This can cause an explosive disintergration of a material.

As far as life limitations of first wall material are concerned cracking and to a smaller extend melting are the most dangerous effects of thermal shock especially when surface-parallel cracks are generated. These can cause a rapid "peeling" of the material, fig. 3.3.

Thermal shock loading in the discussed meaning, the induced melting and cracking are one important aspect of the suceeding chapters.

3.3 Erosion

The bombardment of the first wall material with ions, neutrons and electrons removes material form the surface, fig. 3.4. This material can be directly redeposited or can enter the plasma, move along some distance and then be redeposited somewhere in the vacuum vessel /41,42/. A similar process happens to material that is evaporated by arcing, during plasma disruptions or run-away electron events. The last-mentioned plasma wall interaction processes can also produce material droplets /43/ which may be splashed to the surface of the first wall in the very neighborhood of the touch down area of the disruption or of the run away electrons.

The material erosion by particle bombardment may be enhanced by additional chemical processes between the first wall material and the bombarding particles. The simultaneous flux of energetic particles and electrons to the first wall surface can also cause an enhanced sputtering by synergistic effects /44/. Chemical sputtering /45/ and synergestic effects are not investigated in the frame of the work discussed here.

Fig. 3.2: Multi layer remelting zone in the surface of a TEXTOR limiter part, made of the Fe-base alloy 1.4311

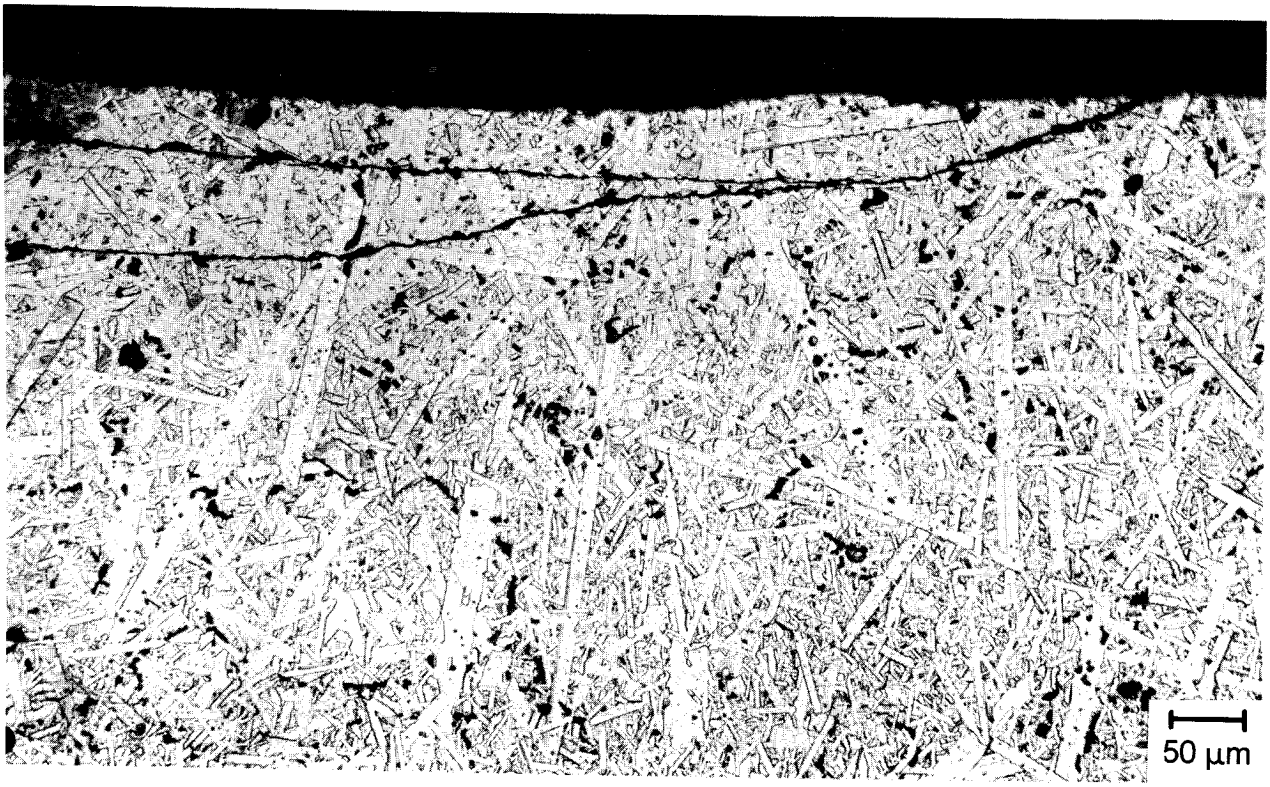

Fig. 3.3: Long-ranging surface-parallel cracks in a SiC-sample after a thermal shock experiment cause rapid sample "peeling".

Erosion in the sense of removement of first wall material by plasma born particles or electrons is reported only incidentally. Material erosion by evaporation and splashing of molten material (metallic alloys) or by sublimation and removement of larger fragments of the first wall material, e.g. grains (ceramics), on the other hand, is an important measure for the quantification of plasma induced material damage by thermal shock load.

3.4 Simulation Experiments for Plasma Wall Interaction Processes

Aside from a pure theoretical analysis e.g. by time dependent temperature/stress analysis, there exist two different ways of investigating plasma wall interaction experimentally: the first and most realistic way is to expose material samples to a near-fusion plasma in one of the existing, large Tokamaks, the second way is to test materials in convenient laboratory experiments.

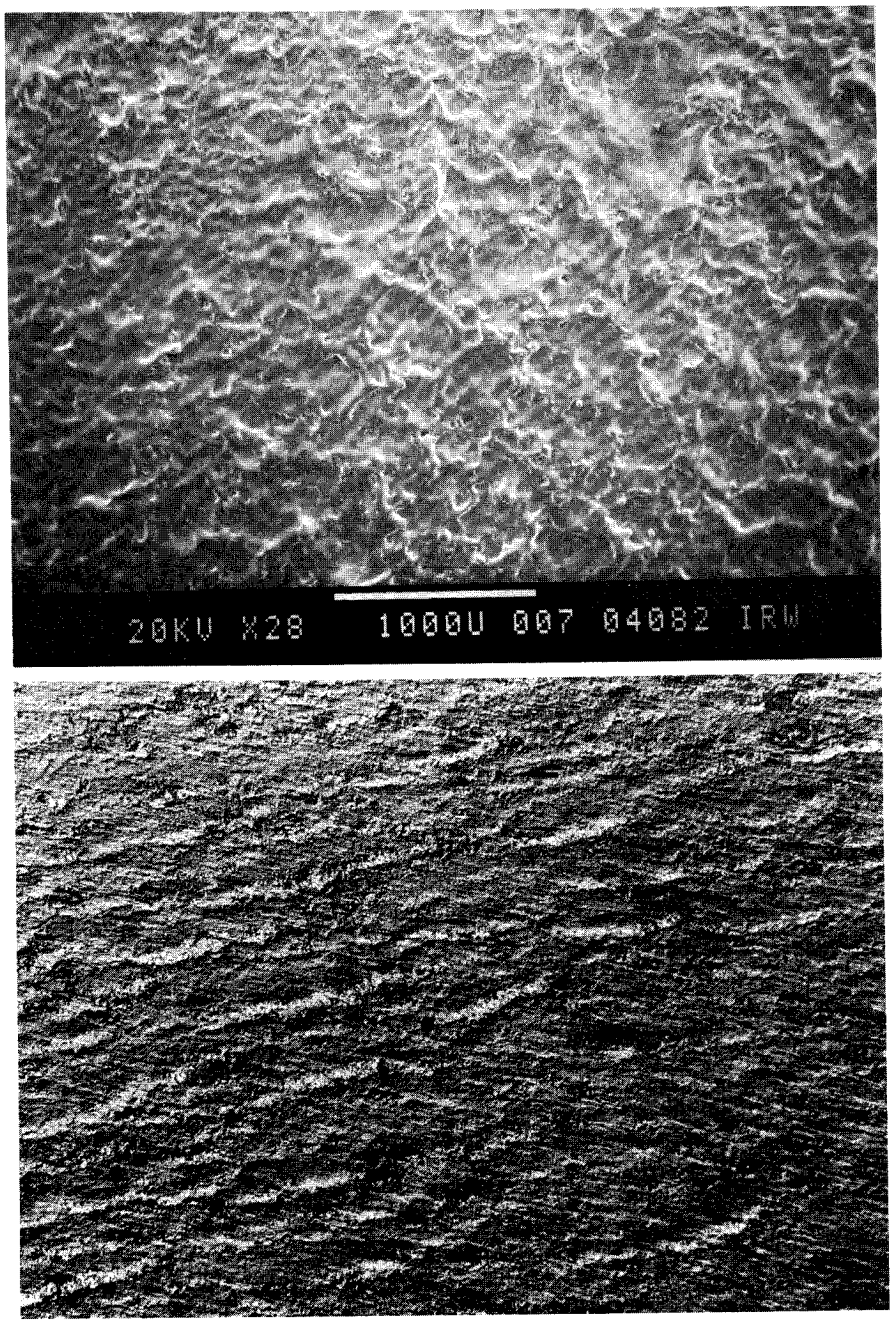

Fig. 3.4: Material erosion from the surface of a TEXTOR rail limiter, made of the Fe-base alloy 1.4311;
top: erosion on the electron drift side
bottom: erosion on the ion drift side

Extensive, systematic material tests in operating Tokamaks are not possible at present, since the plasma machines are designed primarily for other purposes, e.g. investigation of plasma physics, plasma diagnostics etc.. Nevertheless it is indispensable to fall back also on Tokamak in-pile material tests within the development of improved first wall materials, e.g. for the intense studies of the material damage caused by the real, complex system of plasma wall interaction, for the adjustment of experimental parameters in simulation experiments, and for finally decisive material tests. A plasma machine which is well equipped also for material tests in the Tokamak TEXTOR /46/ in the Nuclear Research Center (KFA) Jülich. First results of such in-pile material tests are reported elsewhere /47/.

The systematic series of material tests with a broad variation of material candidates and loading parameters have to be executed in simulating laboratory experiments /48, 49/. There are some conditions that have to be satisfied in order to carry out realistic laboratory experiments:

1. The loading process should be related as close as possible to one of the sub-processes of the real plasma wall interaction:
   a) neutral/ion beam,
   b) electron beam,
   c) electromagnetic radiation,
   d) electric arc.

2. The experimental test parameters have to cover the real loading parameters with respect to power density during loading event, loading time duration, deposition depth of deposited energy, and relation of pulse to interrupt duration. The data and parameter values that have to be taken into account have been discussed already in a preceding chapter.

3. The total number of applied load pulses has to be large enough to allow an extrapolation to the planned lifetime of a fusion reactor.

4. The sample size has to be large enough to give a realistic information as compared with the real first wall component. In a progressed state of material tests the sample shape has to be approximated to the resp. real first wall component.

Material testing in simulating laboratory experiments seems to be the most significant indication of the present state of material development for the first wall of fusion reactors. One common procedure is the investigation of candidate first wall materials in electron beam test devices /50,51/.

4. Electron Beam Tests

The electron beam tests for simulation of plasma wall interaction cover at a first sight the sub-process of electron - material - interaction in a plasma machine. But the information content of a properly planned experiment comprises, at least with a sufficiently high precision, the total, complex effects of plasma wall interaction, may be without the results of the two sub-processes arcing and electromagnetic radiation. These two interaction mechanisms should be excluded from this considerations: arcing affects only very small areas, the area of impact is in the order of $(\mu m)^2$, and the burning time per impact is very short, it may be well below microseconds; electromagnetic radiation may actually penetrate the surface of the first wall material to a depth of approx. one wavelength of the radiation, when metallic alloys and graphites are concerned, thus producing real surface effects. This might not be true for "transparent" ceramics. In any case: the effects of the mentioned two sub-processes should be investigated separately.

So, drawing the conclusion, electron beam tests are well convenient for systematic tests of the material behaviour /52,53/ under thermal shock load and thermal fatigue, caused by the pulsed plasma operation of a tokamak and by uncontrolled plasma termination and run away electrons, resp..

4.1 Test Facility

The electron beam simulation tests are carried out in an electron beam welding machine*). Their nominal layout data are:

---

*) The authors cordially thank Dr. R. Lison and Mr. E. Sigismund from the Central Devision for General Technology (Zentralabteilung für Allgemeine Technologie) of KFA for implementing the material tests in their electron beam welding machine.

accelerating voltage	150 kV,
beam current max.	100 mA,
pulse duration min.	10 ms,
beam rise time max.	0.2 ms.

The electron beam is passing in vertical direction, the sample being below the electron gun. The samples are fixed to a copper base plate by clips to give a sufficiently good thermal contact to the heat sink. An active cooling is not provided at present. Some experiments are carried out whith a glass or copper collector probe next to the loaded material sample to allow the investigation of the chemical composition of the eroded/evaporated material.

The electron beam can be applied in defocused or poorly focused mode or can be focused to values in the order of 0.1 mm. This possibility of focusing the electron beam together with the variation of the beam current allow the necessary variation of the beam power density - or energy deposition density - corresponding to the requirements of the specific test program.

It is well known that even at the relatively high energy of the electrons an appreciably high amount of electrons is backscattered (or reflected) by the sample, depositing only a fraction of their energy in the sample. The amount of backscattered electrons /54,55/ can vary from few % in graphite to almost 40 % in tungsten. At present, this energy loss - which in principle has to be taken into consideration when making extended quantitative calculations of the resulting material defects - is partly omitted.

Another remark has to be devoted to the acceleration voltage. The range of electrons with an energy of 150 keV in bulk, solid material reaches from more than 200 µm in graphite to about 50 - 60 µm in Ni- or Fe-base alloys and about 25 µm in W /56,57/. The range of electrons depends on their energy following - for the resp. material - a law of the type /58/

$$R = A \; E^B \quad ([E] = \text{KeV}; \; [R] = \mu\text{g cm}^{-2}) \qquad (4.1)$$

where A is in the order 10, depending on the resp. author, and B is in many cases specified from 1.3 to 1.7. So, the calculation of the electron range in a special material gives results which lie in a relatively broad scatter band. Additionally one has to take into account that the generated material

damage is a function of four parameters: acceleration voltage, beam current, pulse length, and heat sink, of course not regarding the important role of the material itself..

Inspite of these uncertainties, the simulation of plasma disruptions and the induced material defects caused by the momentary contact of the first wall with the hot central plasma with particle and electron temperatures in the order of some 10 keV seems to be quite realistic. A lot of experimental results confirms this assumption.

On the contrary, the pure run-away electron damage in ceramic material can be simulated in the mentioned electron beam welding machine only very limited: Because of the strong increase of the range of electrons with their increasing energy the run-away electrons with energies up to some 10 MeV penetrate into ceramic or graphitic material to a depth in the order of cm. That means, that also the energy deposition and thus the area of damage generation will lie in that distance below the material surface. Also this fact seems to be confirmed by experimental results, fig. 2.2.

In the case of metallic alloys this problem is not so aggravating, since the values of the electron range, e.g. in Fe- or Ni-base alloys, are about 50 - 60 µm in the case of 150 kV accelerating voltage and in the order of 1 mm, when the accelerating voltage is 10 MeV.

The simulation of thermal fatigue by 150 keV electrons seems to be really doubtful. In this case, the first wall material interacts with the relatively "cold" plasma boundary layer at plasma temperatures of few 10 eV. Quantitative conclusions should be drawn only with particular care. But also here, such experiments should give useful informations, may be on a very conservative scale, on the thermal fatigue behaviour of the material.

Finally, it has to be pointed out that the power distribution along the cross section of the electron beam is not homogeneous, fig. 4.1. It rather shows a distribution which at a first glance looks like a Gaussian one with a nearly radial symmetry. Moreover it has to be added that the nominally circular area loaded by the electron beam actually is roughly elliptic, fig. 4.2. The authors believe that these facts affect the information content of the electron beam experiments only in a tolerable extent.

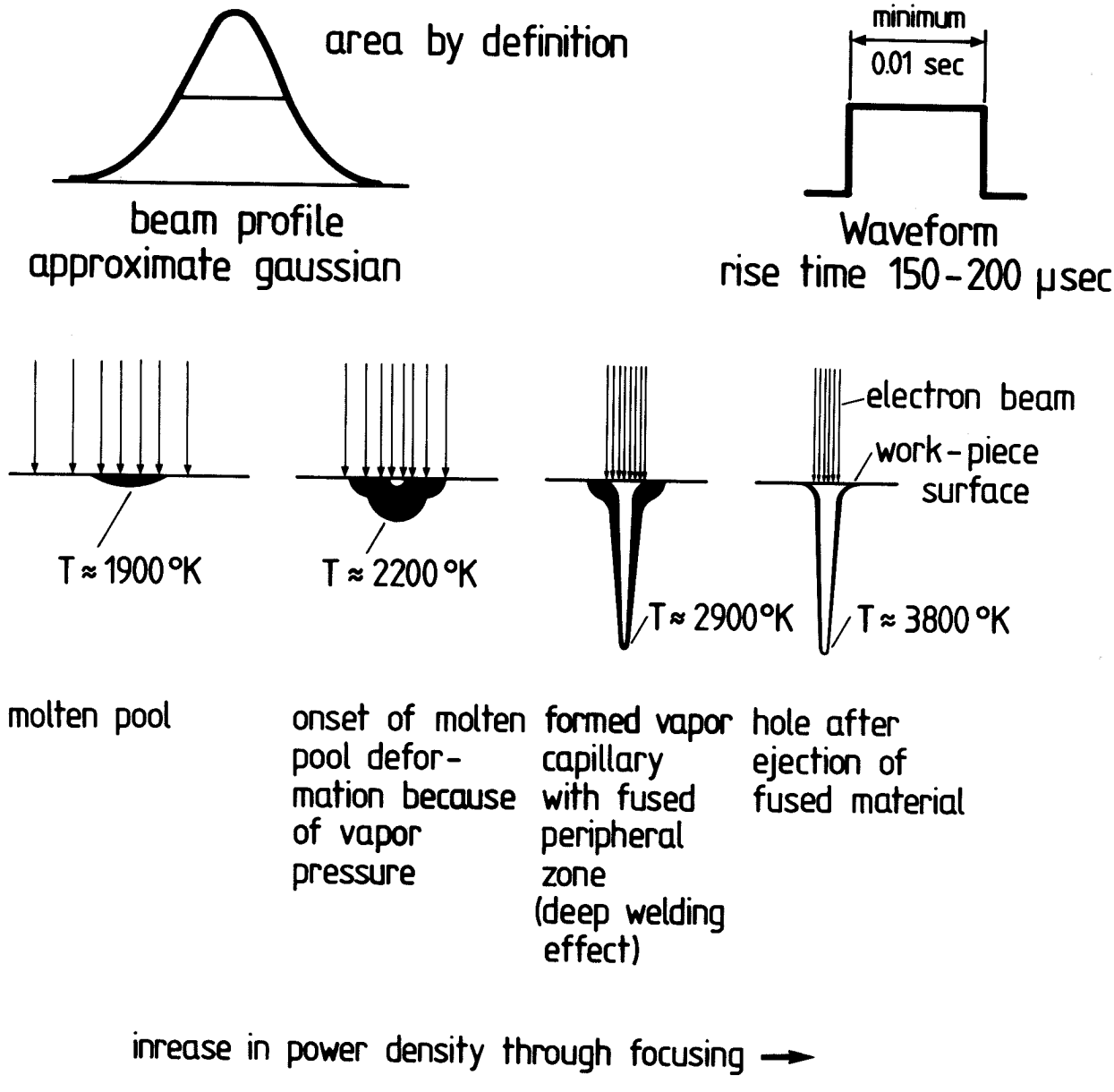

Fig. 4.1: Approximated gaussian intensity distribution of the electron beam in materials tests (top left) and idealized distribution form (top right); variation of crater geometry at constant beam power but decreasing beam cross section (bottom)

4.2 Thermal Fatigue

The necessary experimental data for the simulation of thermal fatigue by a pure electron loading have to meet the following values:

The thermal load deposited by the electron beam has to be equivalent to 0.1 MW m^{-2}. This is a very low value, and one can assume that with relatively small numbers of pulses no effects might arise. Thus, experiments are

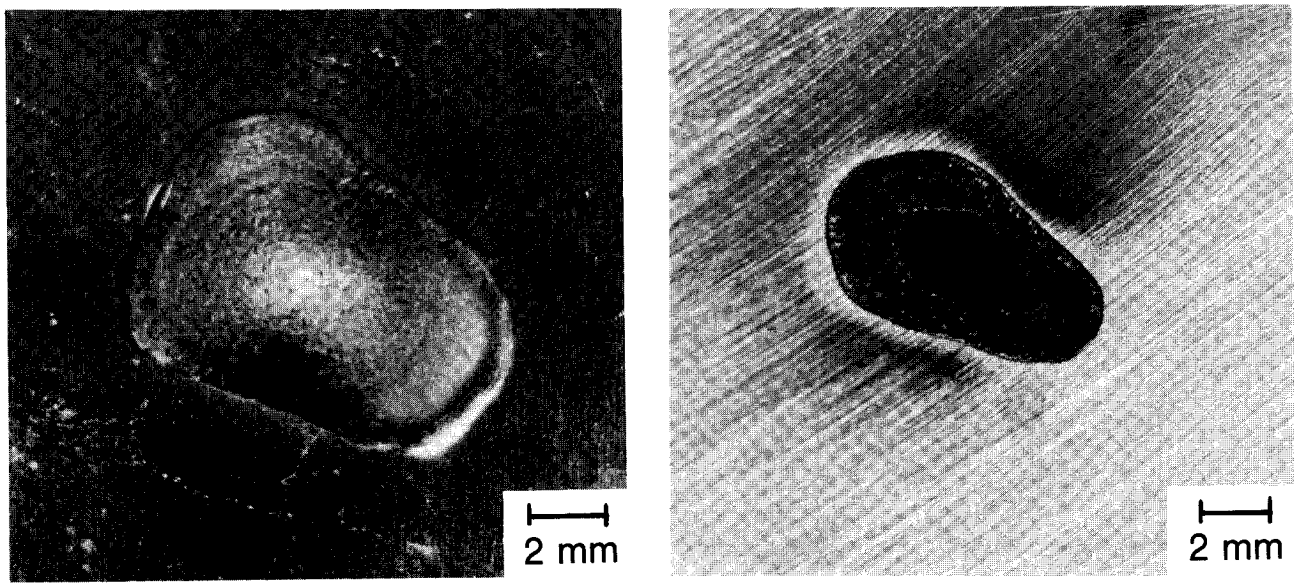

Fig. 4.2: More or less "elliptic" crater shape after electron beam test: INCONEL 600 (left); 1.4311 (right)

started with the beam power density between 5 and 30 MW m^{-2}, that means far above the desired value for the low-loaded parts of the first wall. On the other hand, this power density has to be compared with the thermal fatigue loading of the high heat flux components of the first wall which is about 500 Wcm^{-2} corresponding to 5 WM m^{-2}. The mentioned starting value thus gives a fairly good approach to the thermal fatigue loading of the high heat flux components. Consecutive experiments have to be carried out with decreasing power density.

The pulse duration for the first experiments is 1 s, the pulse numbers are 1, 10, 100, and 1000 pulses. In further experiments the pulse durations have to be extended up to values realistic for NET, i.e. 200 s.

Another important parameter is the keying ratio, that is the ratio of the "pulse on"-time and and the "pulse off"-time. For the existing plasma machines this ratio is well below "1", i.e. "pulse on"-time is much shorter than the "pulse off"-time or the time interval between two pulses. The discussed experiments are carried out with a "pulse off"-time of 9 s.

Additionally some experiments with refractory alloys have been carried out applying power densities up to 5 kW cm^{-2} corresponding to 50 MW m^{-2} to the material sample also in thermal fatigue experiments in order to produce visible material damage.

4.3 Thermal Shock

The thermal shock parameters to be looked at have been discussed already:

The power density lies above the upper limit of thermal fatigue, i.e. above 50 MW m^{-2}, and can reach more than 2000 MW m^{-2}. The loading time should vary between 10 µs and 100 ms. Two typical pairs of parameter values, valid for the present NET-concept, are

500 MW m^{-2} during 2 ms and
75 MW m^{-2} during 20 ms.

The first set of parameter values is denoted "fast energy deposition" and the second one the "slow energy deposition". Each sample is loaded by one single beam pulse. The mentioned extreme conditions cannot be fulfilled with the available experimental device: Neither can a power density of more than 200 MW m^{-2} be realized, at least not with a sufficiently large loaded area, nor a pulse length shorter than 1 ms.

The impossibility to reach power densities higher than 200 MW m^{-2} is so far meaningless, since the materials available at present are destructed already at 200 MW m^{-2} even during the shortest shock loadings. Nevertheless it is absolutely necessary for future thermal shock experiments to include shorter pulse lengths and higher power densities to realize the very fast energy deposition situation.

The experiments discussed in this presentation are carried out with the loading conditions:

electron beam power density between 20 MW m^{-2} and 200 MW m^{-2}
pulse duration between 0,01 s and 1 s.

5.. Selection of Test Material

The thermal shock and thermal fatigue simulation experiments by electron beam loading are carried out under two aspects: the first one - and at least at present the principal one - is to investigate systematically the plasma induced material damage in the first wall of the plasma chamber and

to find the critical heat loadings as represented by resp. pairs of beam power density - pulse duration values. The second aspect covers consecutively the tests of alternative and hopefully improved first wall materials with loading parameters determined quantitatively during the test series discussed here.

Thus, the materials selected for the simulation experiments so far cover the four "conventional" materials groups applied for plasma facing components in the first wall of operating plasma machines:

graphites and ceramics,
Ni- and Fe-base alloys,
coated systems,
refractory metals and their alloys.

A certain exception in this series represents the last group. Because of their high Z-values refractory metals are not used so far as plasma facing materials. The first wall of the big Japanese Tokamak JT 60, /59/, for example, has been manufactured of molybdenum but has subsequently been covered with TiC-tiles to protect the plasma from high Z-impurities eroded from the wall. But one must not ignore that refractory metals have decisive benefits compared to other first wall materials, namely their probably low erosion rate and - in the case of Mo and W - the very high acceptable surface heat flux under steady state loading.

The experiments discussed in the following chapters have been carried out with

- Tungsten (W)
- Tungsten alloyed with 26 % Rhenium (W 26 Re)
- Tantalum (Ta)
- Niobium alloyed with 1 % Zirconium (Nb 1 Zr)
- Molybdenum (Mo)
- Molybdenum alloyed with 0,5 % Titanium and 0,08 % Zirconium (TZM)
- Molybdenum, CVD-coated with 5 µm TiC (Mo + TiC)
- Molybdenum, CVD-coated with 5 µm TiN (Mo + TiN)
- bulk Titanium Carbide (TiC)
- bulk Titanium Nitride (TiN)
- Nickel-base alloy INCONEL 600 (Ni Cr 15 Fe)
- Iron-base alloy 1.4311 (X2 Cr Ni N 18 10).

6. Tests of Refractory Metals

Only few data on the behaviour of refractory metals during thermal shock loading are already available in the scientific literature. The important data are summarized in fig. 6.1 and fig. 6.2, fig. 6.1 giving "absolute"

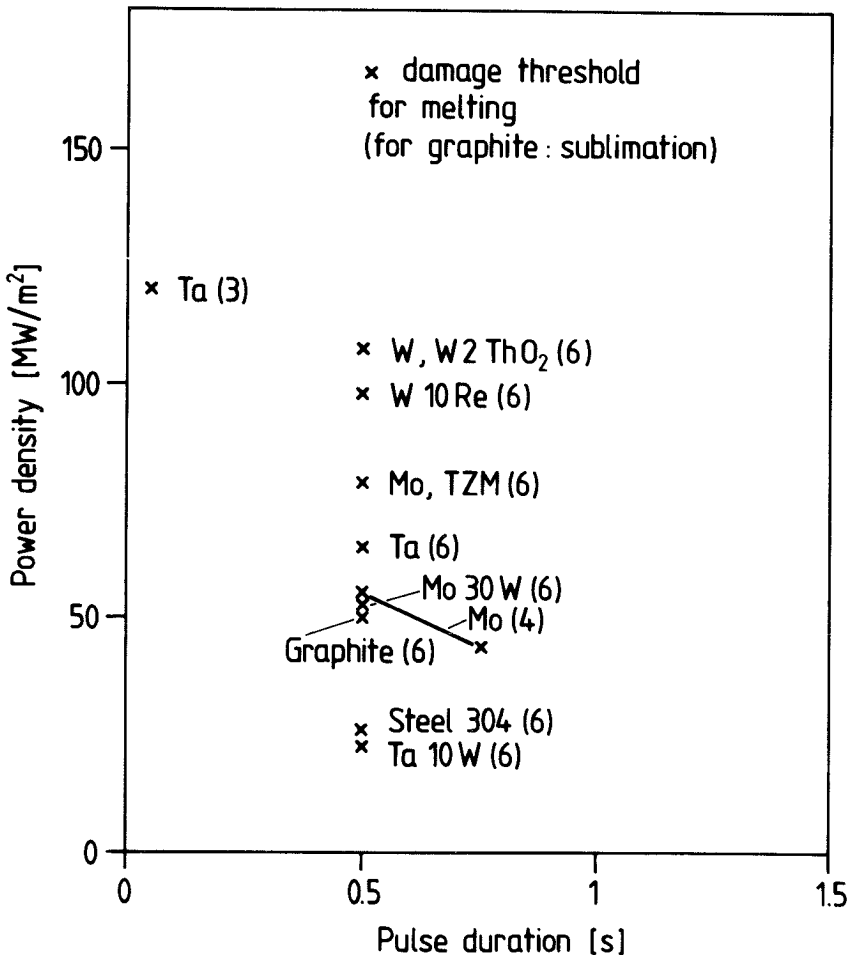

Fig. 6.1: Summary of results of electron beam disruption simulation experiments available in the literature
(3: Summary of the IAEA Workshop, 1983 - 1985, INTOR-Group, Nuclear Fusion, 25, 1985, 12;
4: de Coninck, R.; A. Gijs, A, Suijkers: Rev. Int. Hautes Temp. Refract. 16, 1979, 294;
6: Ulrickson, M: J. Nucl. Mat. 85 + 86, 1979, 231)

experimental results of material behaviour as a function of deposited electron beam power density and pulse duration, fig. 6.2 allowing an extrapolation to short loading times aiming at realistic disruption and arcing conditions.

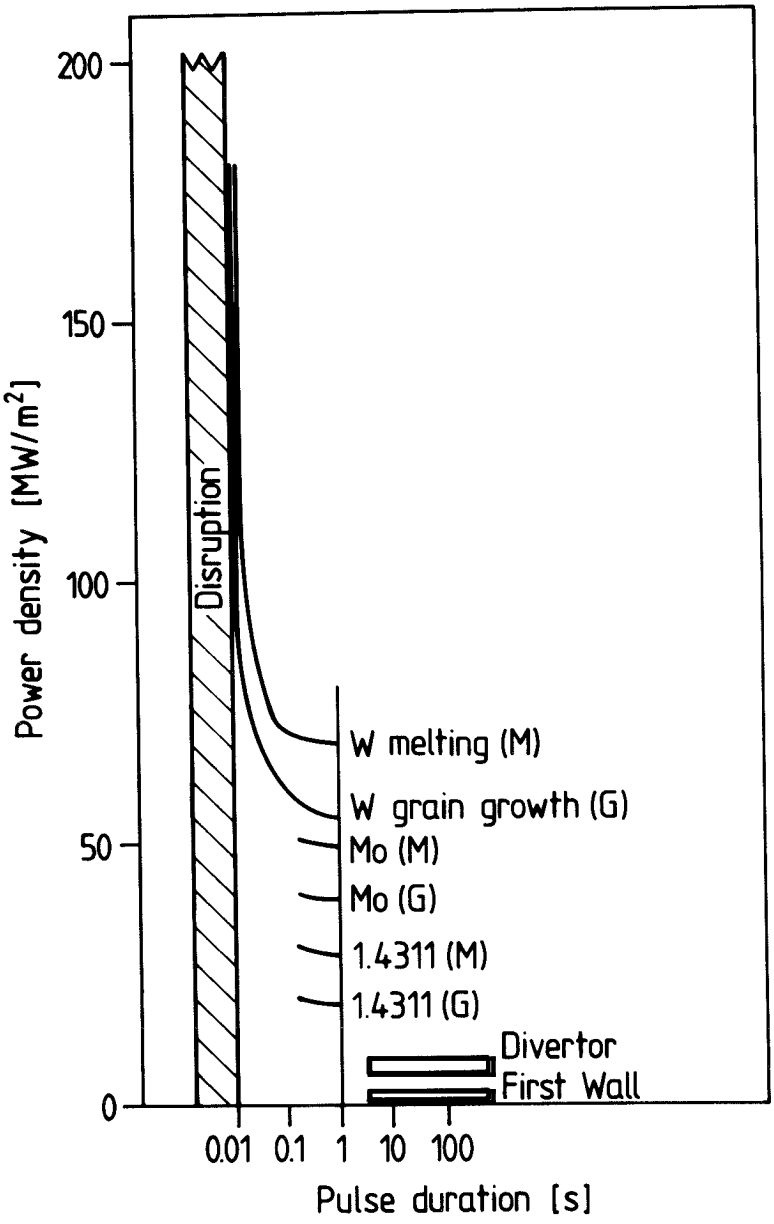

Fig. 6.2: Thermal loading of materials in a nuclear fusion reactor; vertical axis: expected power density; horizontal axis: loading pulse duration

The materials investigated in the following experiments which belong to the group of refractory metals are listed in Tab. 1. All materials and samples have been manufactured and have been made available for the tests by Metallwerk Plansee*). Fig. 6.3 shows metallographic sections of some of the tested materials. Except for TiC, TiN, W 26 Re, and Graphite, the materials show a fully dense structure.

*) Metallwerk Plansee GmbH, A-6600 Reutte/Tirol, Austria

	Cold worked	Grain orientation to electron beam	remarks
W	60-80 %	perpendicular	sintered
W	60-80 %	parallel	
Mo	60-80 %	parallel	
TZM	60-80 %	parallel	
Nb	60-80 %	parallel	
Nb1Zr	60-80 %	parallel	
Ta	60-80 %	parallel	
Mo + 5 µm TiC (CVD)	60-80 %	parallel	
Mo + 5 µm TiN (CVD)	60-80 %	parallel	
2 mm graphite on Mo (Ag-Cu-Ti solder)	-	-	graphite S+E/ FE 159
2mm graphite on Mo (Zr solder)	-	-	graphite S+E/ FE 159
TiC sintered	-	-	
TiN sintered	-	-	

Tab. 1: Materials investigated in electron beam disruption simulation experiments

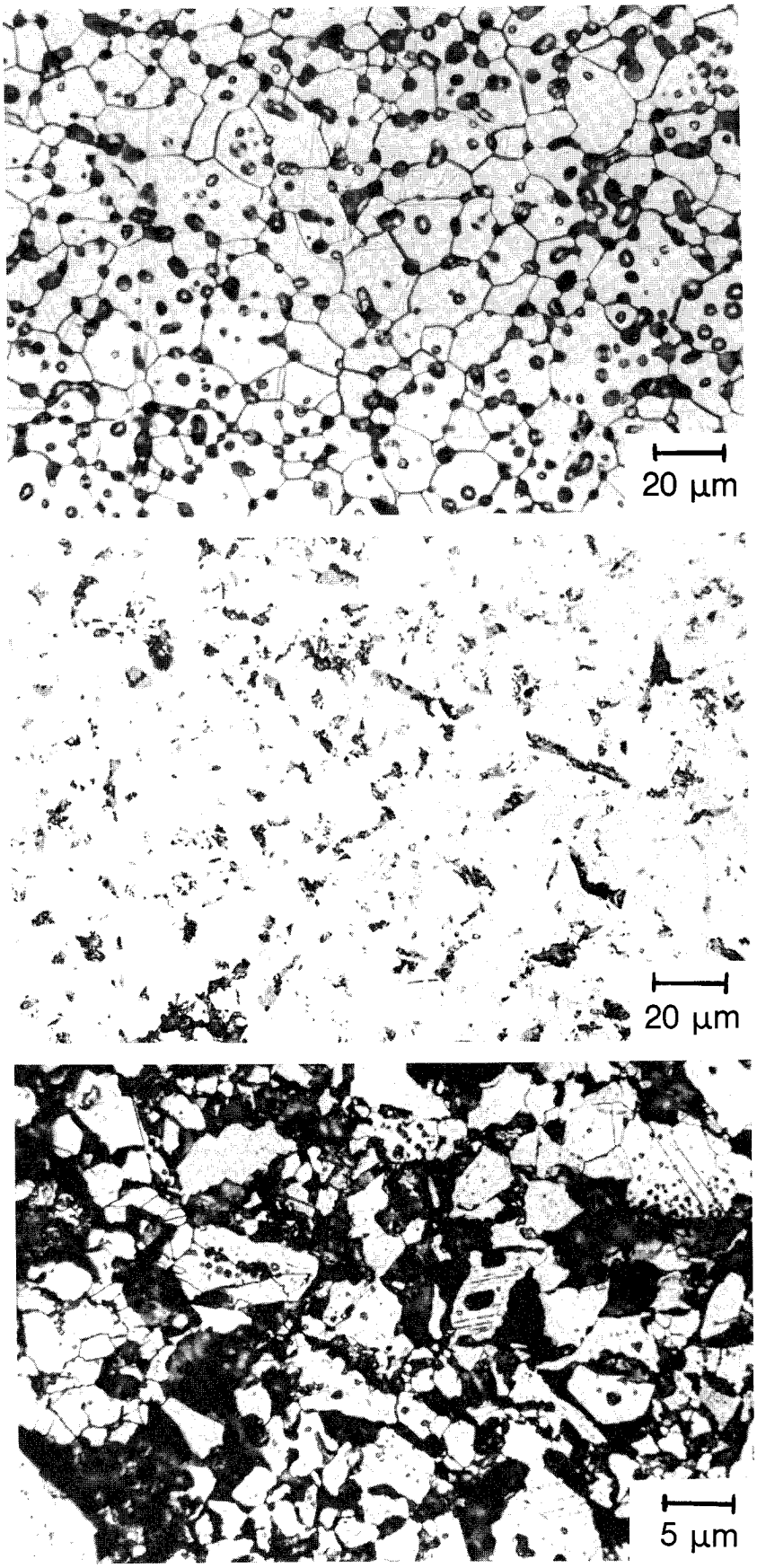

Fig. 6.3: Metallographic sections of some of the tested materials

The cold-worked materials have been oriented in such a way that the grain orientation was vertical to the loaded surface, fig. 6.4. This experimental condition uses the refractory metals in the direction of their poorest thermal-mechanical properties. The samples with a thickness of 10 mm are cut from a bar with a diameter of 25 mm. The side facing the electron beam is metallographically polished with the finishing step with 3 µm diamond compound. For tests with the grain orientation parallel to the loaded surface - that means vertical to the incident beam direction - the samples were cut from a sheet with 10 mm thickness, the samples having square shape with an edge length of 25 mm.

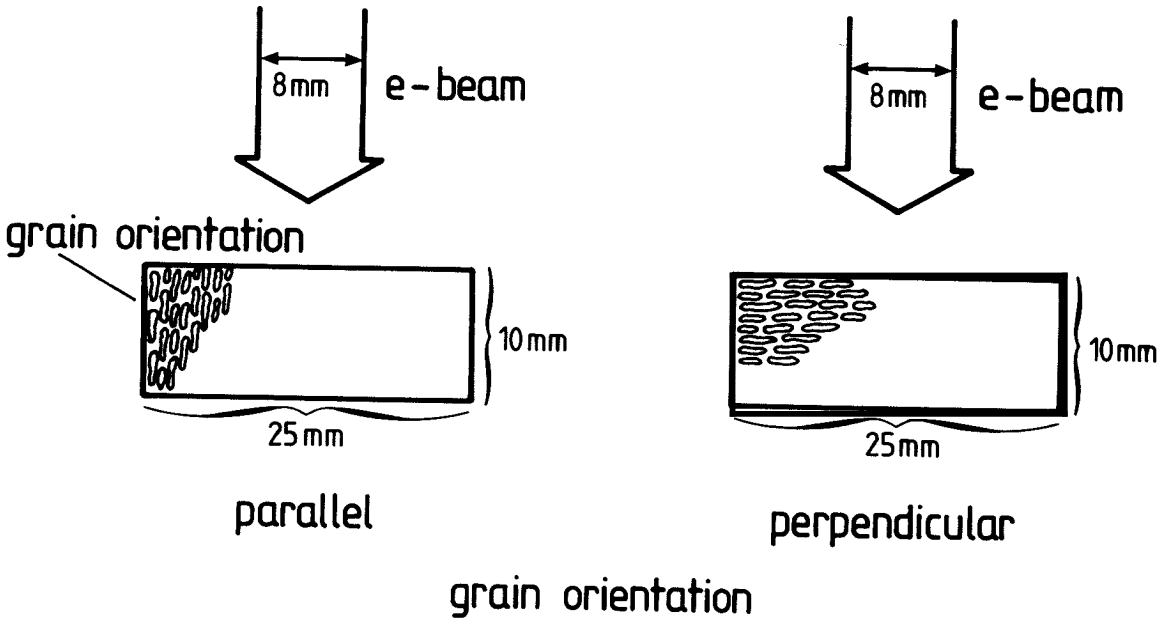

Fig. 6.4: Schematic representation of grain orientation in the samples of refractory alloys with respect to the incidence direction of the electron beam

The loaded area had a size of approximately 80 mm^2 - assuming an approximately circular beam focus with 10 mm diameter -. The deposited beam power was calculated from the constant accelerating voltage with 150 kV and the variable beam current, the primary data not being corrected for energy loss by backscattered electrons (this phenomenon has been discussed in chapter 4.1). For the respective individual test series, the beam current, too, has been kept constant.

6.1 Erosion

During disruption experiments with refractory metals also erosion of the material occurs by

- evaporation,
- ejection of liquid metal droplets, and
- ejection of solid metal particles.

The evaporated and ejected material has been collected on a glass collector probe. As an example, fig. 6.5 shows evaporated molybdenum which has re-

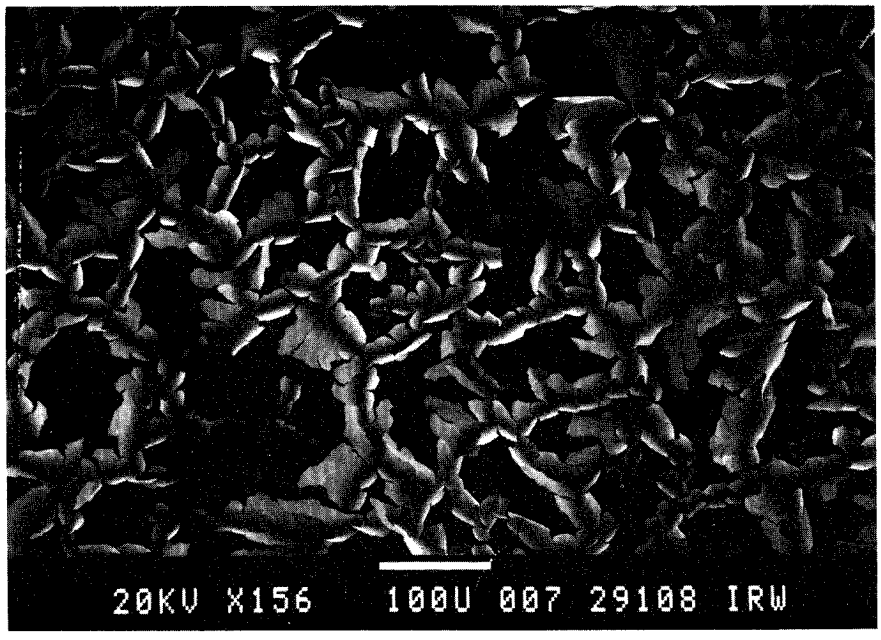

Fig. 6.5: SEM-micrograph of evaporated Mo after electron beam test, trapped on a glass collector probe adjacent to the loaded sample

crystallized on the glass collector. The evaporated material can penetrate into the plasma, can be directly ionized and be transported in the torus thus contaminating and cooling down the plasma.

The material ejected in solid or liquid state apparently carries an appreciable amount of the deposited energy, in the form of kinetic and/or thermal energy. In a Tokamak, such droplets and particles are redeposited in the very neighborhood of the loaded area or can fall down to the bottom of the torus vessel. A secondary and very intense energetic interaction would be required to ionize this material. Fig. 6.6 shows a molybdenum particle collected by the glass probe. When striking it, it has cracked the glass. A small area below the particle has been molten.

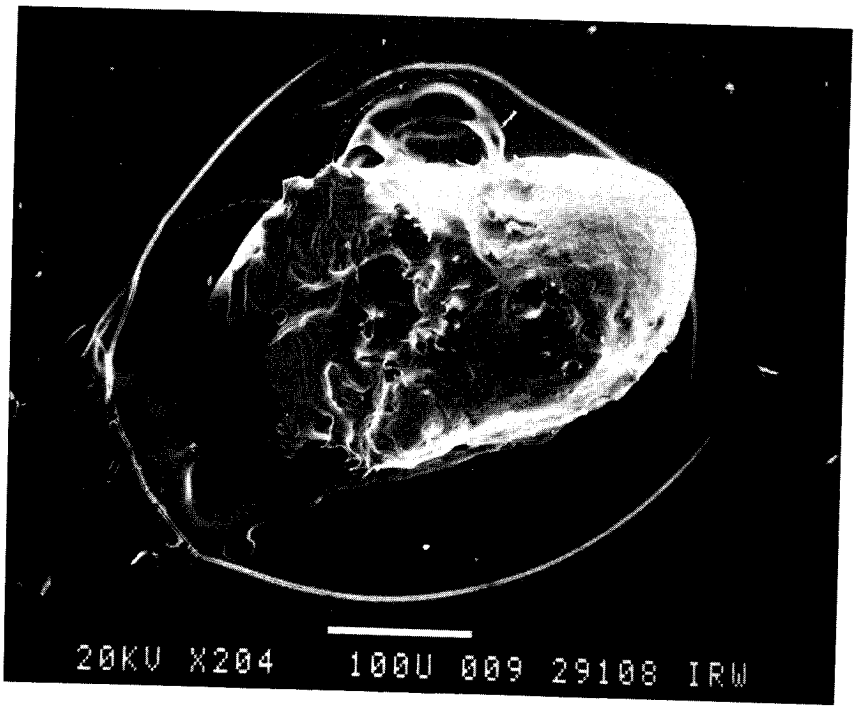

Fig. 6.6: SEM-micrograph of an ejected Mo-particle after electron beam test, trapped on a glass collector probe; secondary electron image

Since the experimental setup was too simple, it was not possible to split up the total weight loss of the sample into evaporated material, solid and liquid particles. The weight loss of samples shown in fig. 6.7 and fig. 6.8 for molybdenum and tungsten samples represents therefore the sum of all three processes. A threshold line - the solid line in fig. 6.7 and 6.8 -

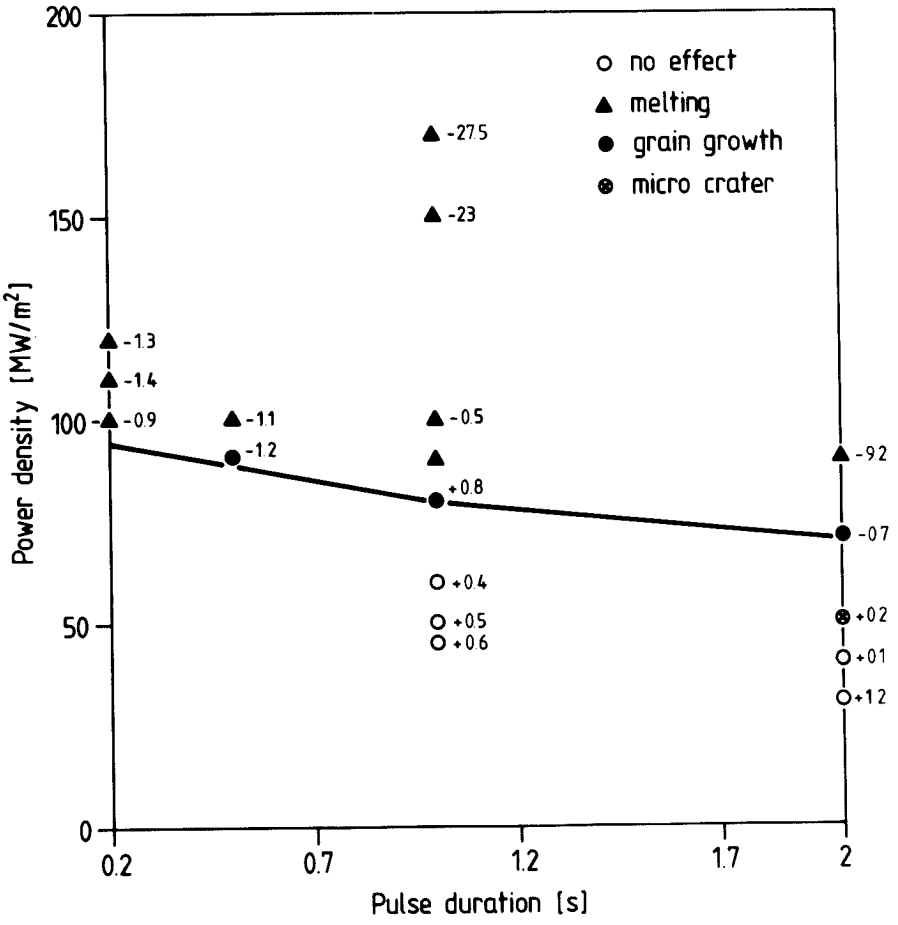

Fig. 6.7: Weight loss in mg for W-samples - indicated at each individual measuring point - after different single shot electron beam tests (beam power density as a function of pulse duration); the solid line represents the empirically evaluated damage threshold line

has been evaluated empirically by visual inspection of the loaded samples in an optical microscope. It is important to note that below the threshold line for material damage (melting and/or recrystallization) no weight loss in detectable. Below the threshold line no appreciable material erosion is therefore expected to occur. At or above this threshold recrystallization and, at sufficiently high thermal loads, finally melting of the sample materials appear. Fig. 6.9 shows a micrograph of the surface of a molybdenum sample with a melt crater, fig. 6.10 presents a metallographic section through this crater. The typical coarse-grained dendritic quench structure can be seen, together with some included gas bubbles. Because of the high melting point of the refractory metals many of the precipitations and impurities should have volatilized or evaporated. This should be true especially for interstitial oxygen and metal oxides. It has to be remarked

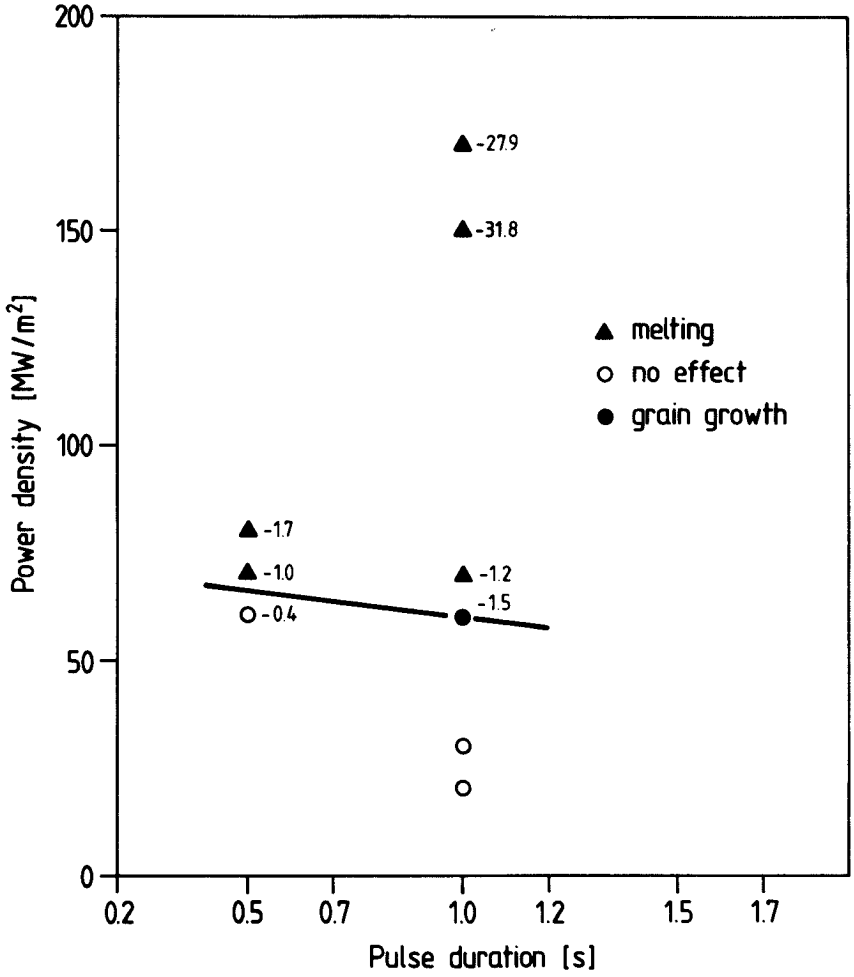

Fig. 6.8: The same as for fig. 6.7, but for Mo-samples.

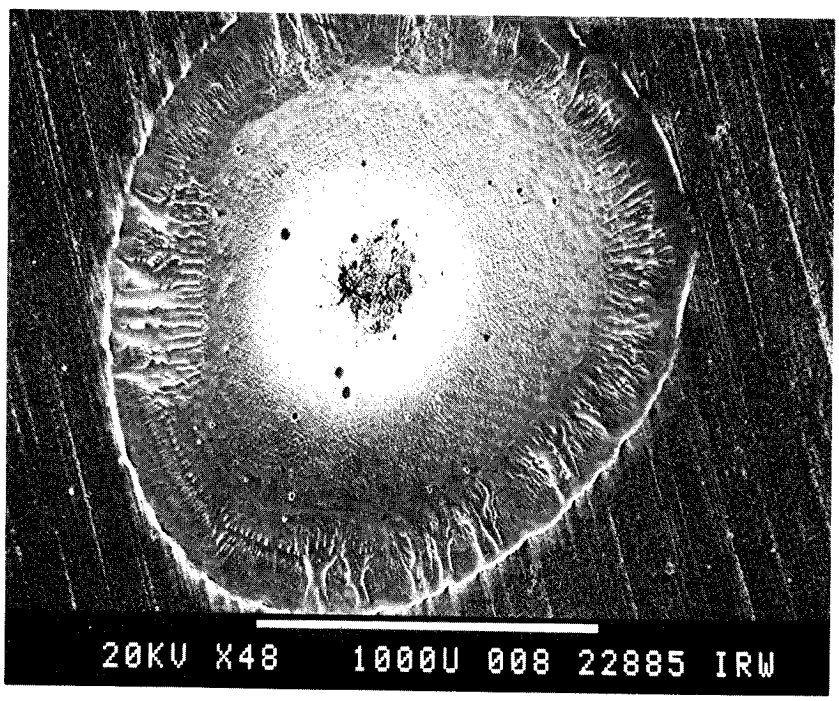

Fig. 6.9: Melt crater in the surface of a Mo sample after electron beam thermal shock test; 50 MW m^{-2}, 1 s pulse length; SEM micrograph

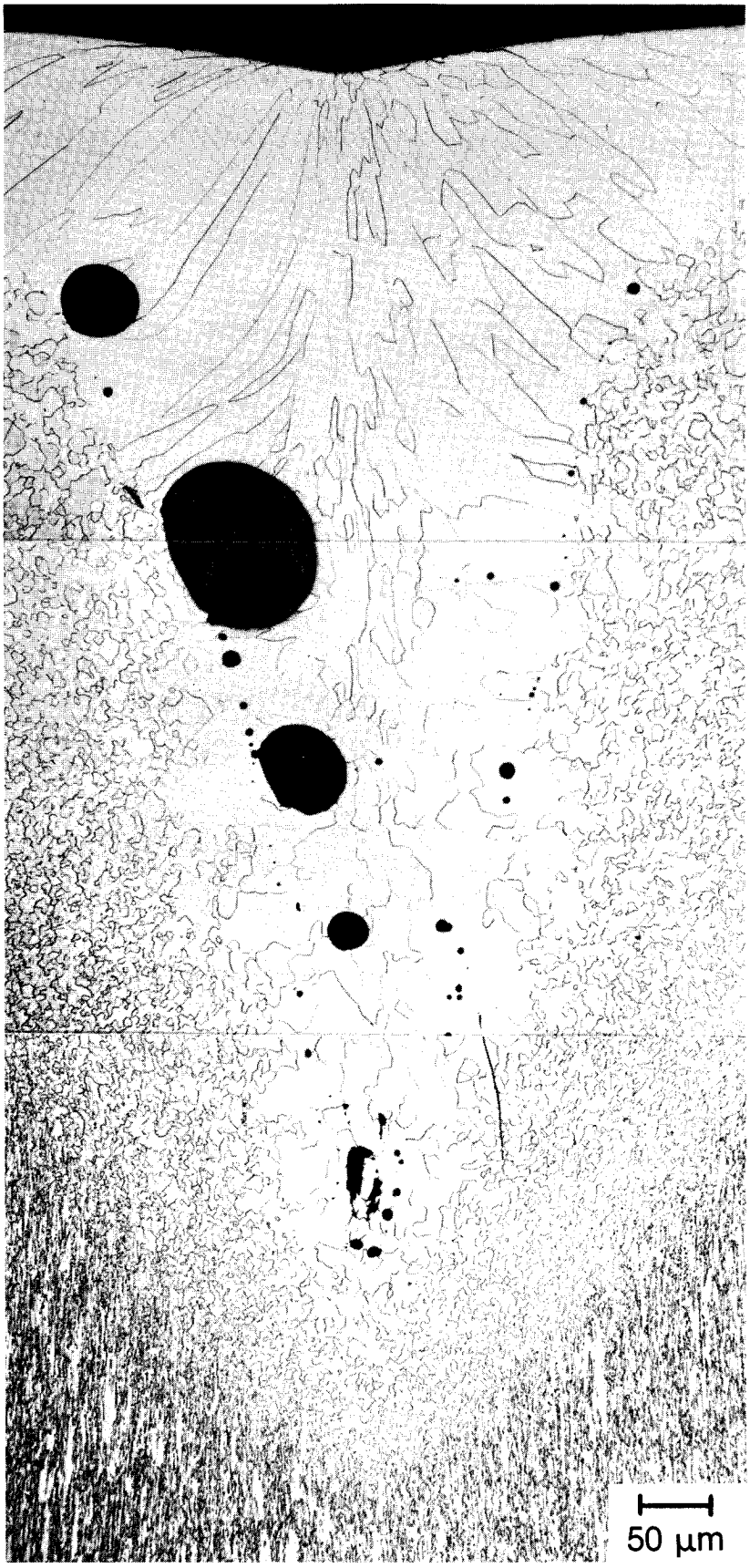

Fig. 6.10: Metallographic section through a melt crater in the surface of a Mo sample after electron beam thermal shock test; 100 MW m^{-2}, 2 s pulse length

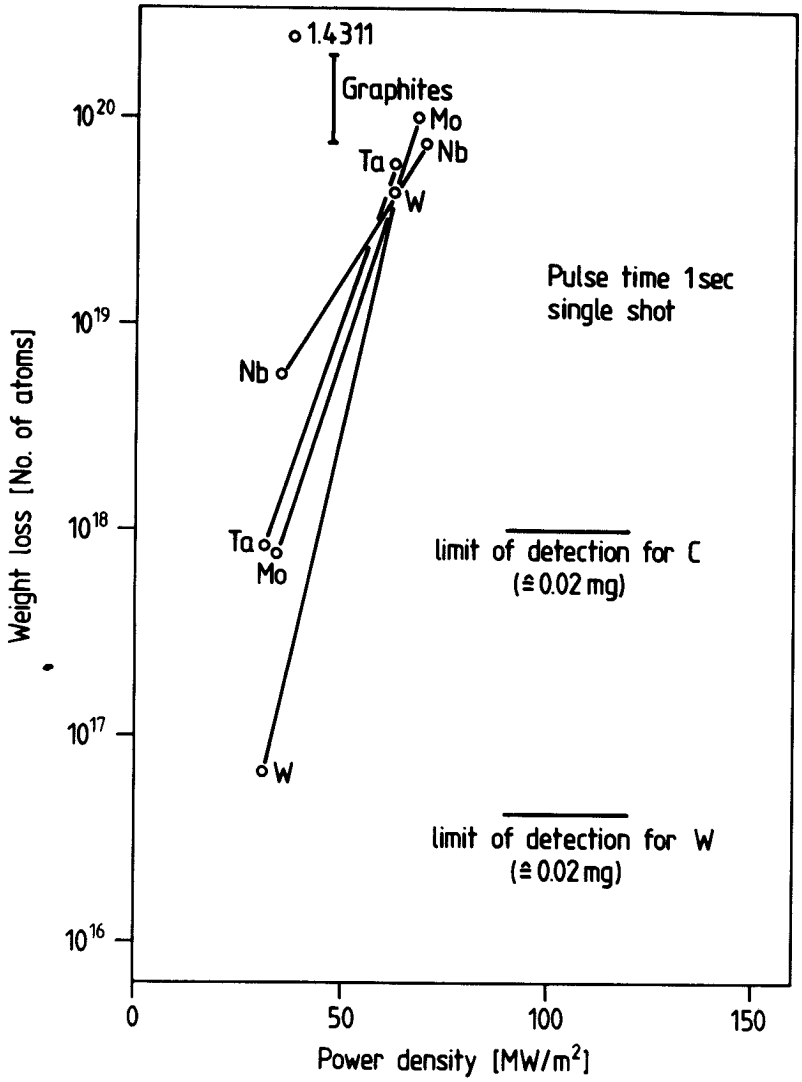

Fig. 6.11: Weight loss of refractory metals in electron beam thermal shock tests (disruption simulation experiments); graphite and the alloy 1.4311 are indicated as references; power density is corrected for energy losses by backscattered electrons

the oxygen contents of the resp. materials were 10 ppm for Mo and 8 ppm for TZM, with H and N being below 5 ppm each.

Gas bubbles are visible mainly in Mo and TZM, thus being in conformity with the fact that Mo oxides rapidly evaporate at temperatures near or even above 1000°C /60/. In the transition zone between the melting crater and the unaffected material considerable grain growth is visible.

With respect to weigth loss tungsten ranks best as compared with the other materials, fig. 6.11. 1.4311 in contrast shows the greatest values of re-

movel. This property of W is surely attributed to its high melting point and the large amount of backscattered electrons which eliminate a larger portion of the total, nominal energy input than for example in the case of 1.4311. At constant beam power the weight loss increases, of course, with increasing pulse length or disruption time very rapidly, fig. 6.12. Again W has a great advantage compared with the other alloys, in particular with respect to the short energy deposition times during a real plasma disruption.

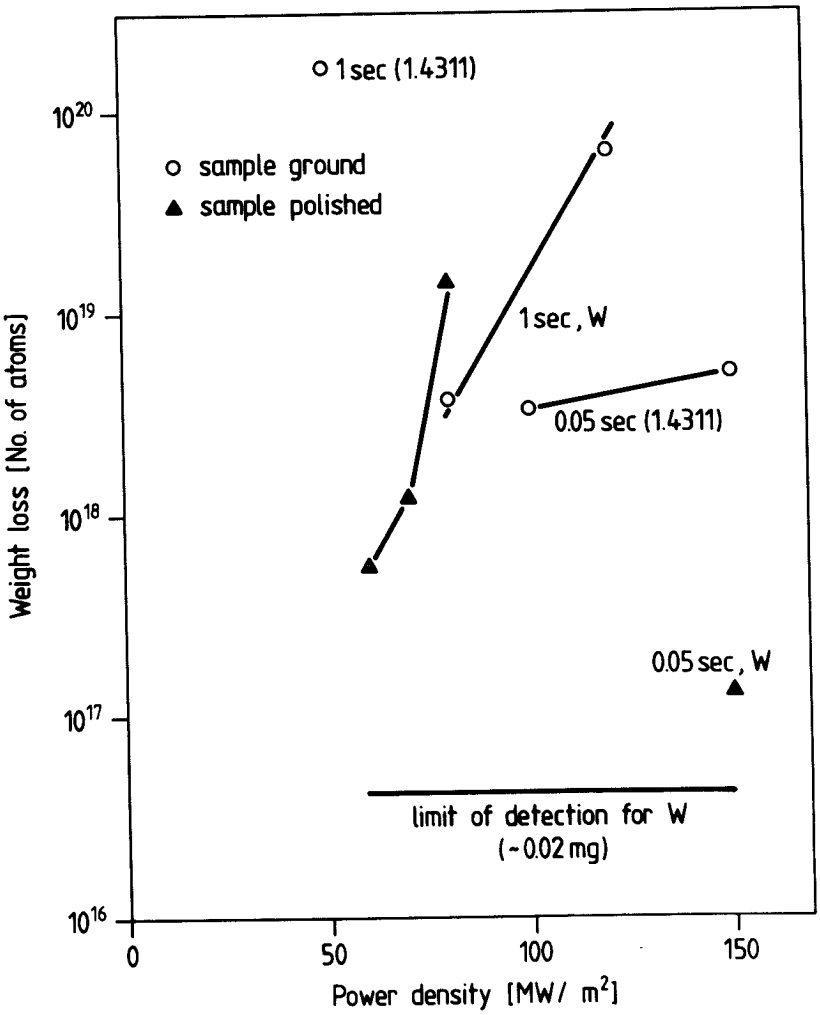

Fig. 6.12: Weight loss of W and alloy 1.4311 in electron beam thermal shock tests as a function of beam power density; variable parameters are pulse duration and sample surface condition

6.2 Thermal Shock

The thermal shock behaviour of the refractory metals was estimated by investigating the samples in the vicinity of the empirically determined damage threshold line mentioned in chapter 6.1. The samples were controlled by visual microscopic inspection of the exposed polished surfaces. Depending on beam power density and pulse duration the following phenomena were observed:

- recrystallization without melting,
- surface melting,
- formation of cracks.

The results are graphically summarized in the fig. 6.13 through 6.15 for the bulk materials Mo, TZM, W, W 26 Re, Ta, and Nb 1 Zr. Again, the damage

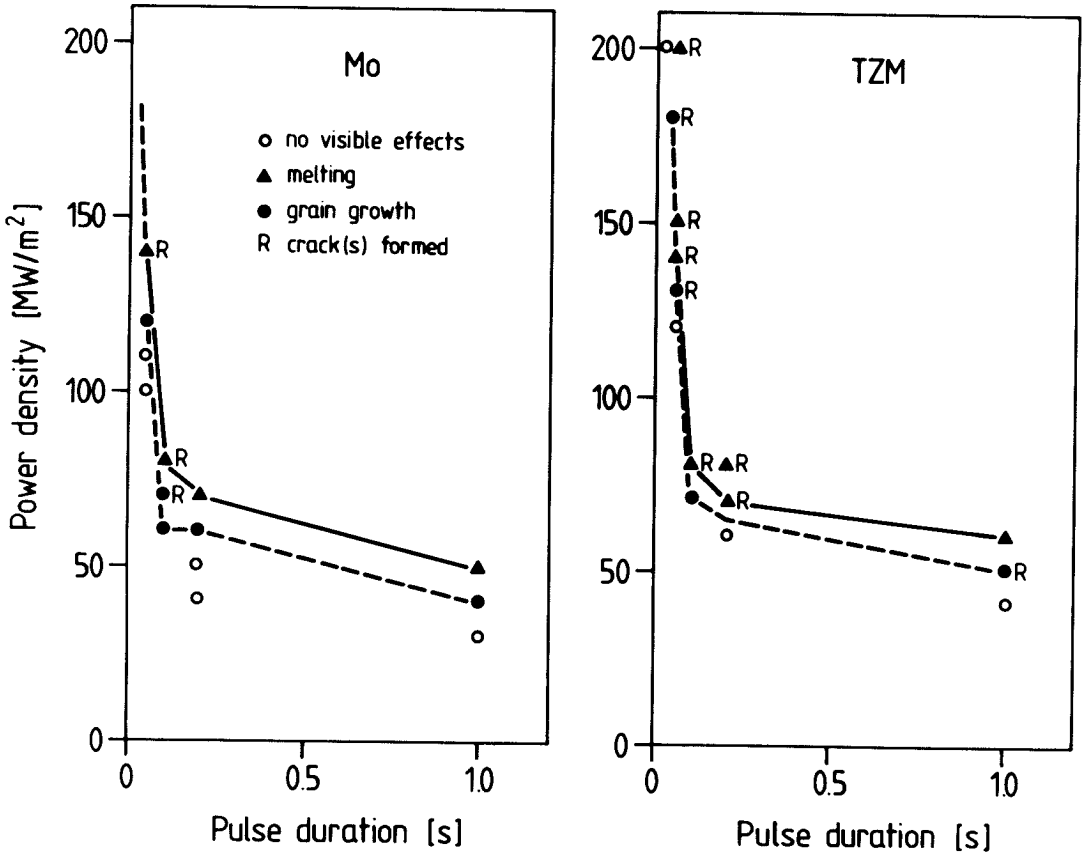

Fig. 6.13: Results of thermal shock experiments for Mo and TZM by electron beam disruption simulation; electron beam power density as a function of beam pulse duration; solid line: damage threshold for melting, dashed line: damage threshold for grain growth.

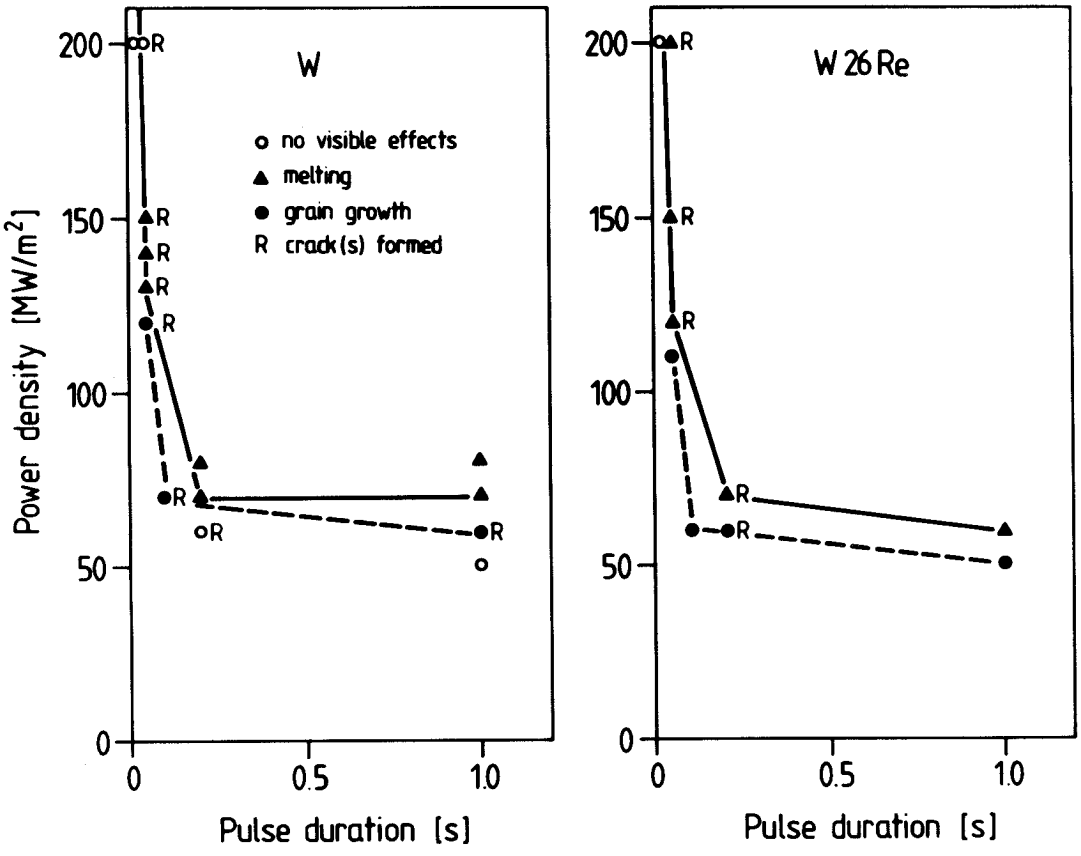

Fig. 6.14: Same as fig. 6.13, but for W and W 26 Re

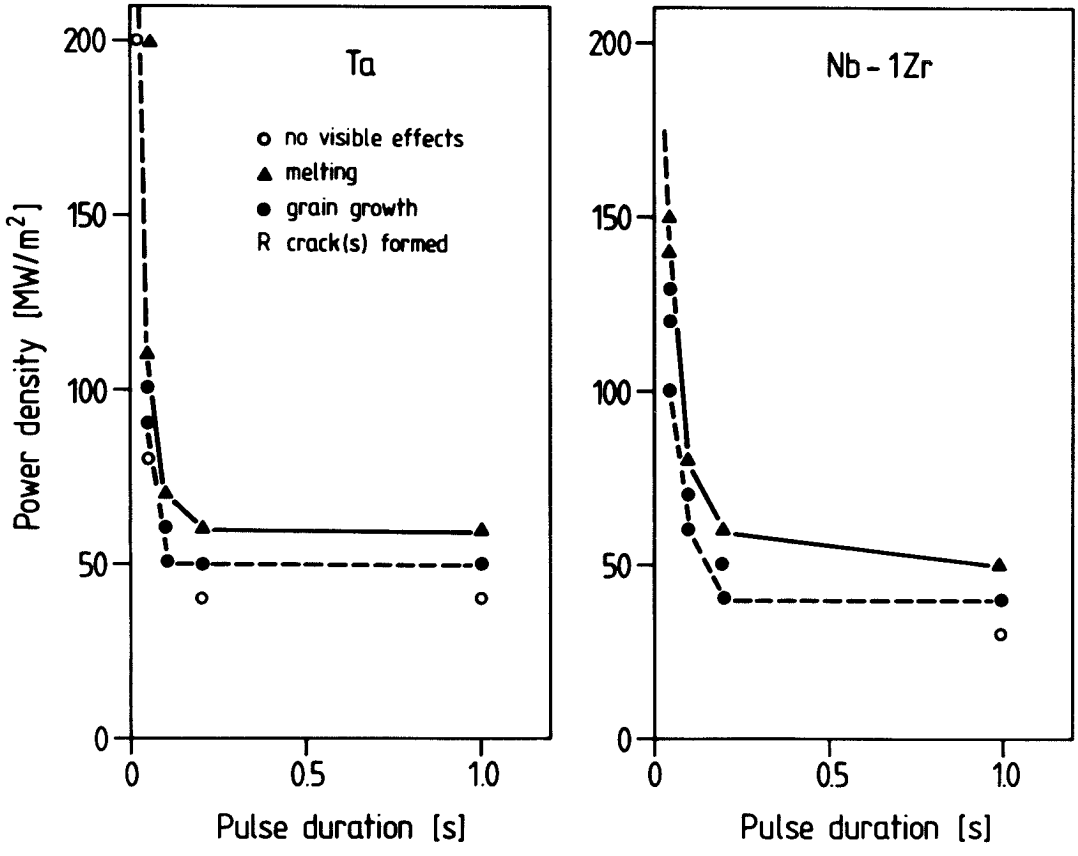

Fig. 6.15: Same as fig. 6.13, but for Ta and Nb1Zr

threshold lines are entered into the figures. In the case of Mo (and TZM) radial cracks appear which seem to originate in the heat affected area, fig. 6.16.

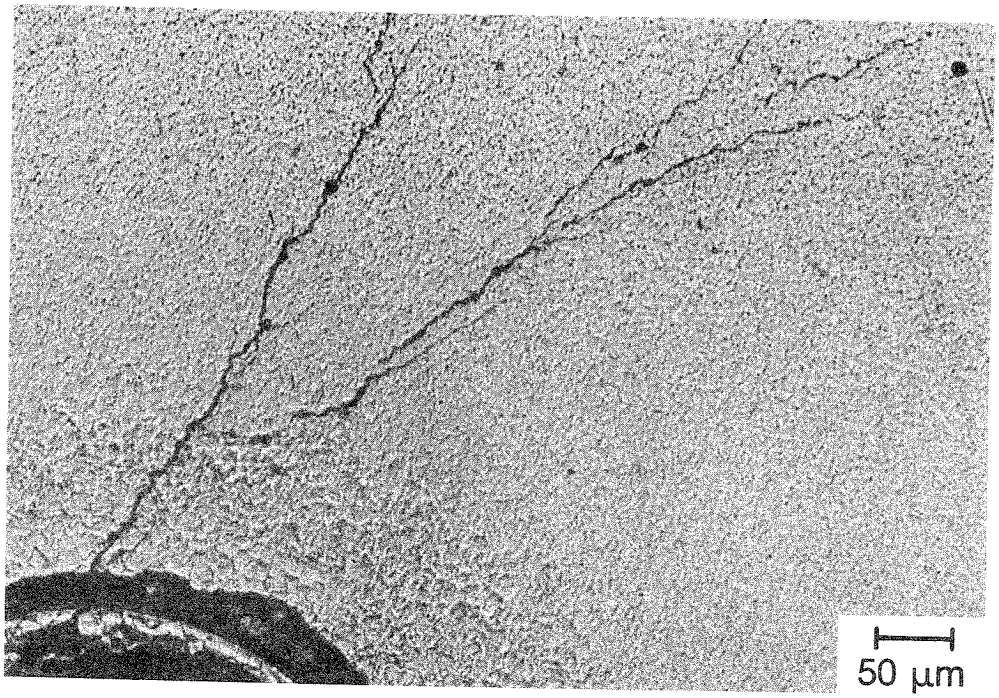

Fig. 6.16: Cracks in the surface of a Mo-sample, initiated in an electron beam thermal shock experiment (140 MW m^{-2}, 50 ms); the cracks obviously start in the heat-affected area

TiC and TiN coatings, each 5 µm thick and deposited on Mo substrate by CVD were tested, too. As long as the substrate does not melt, the coatings seem to withstand the - relatively low - shock loading. When the thermal load is high enough to melt the substrate material the coating is distroyed, too. So the conclusion may be drawn that thin layers cannot protect the base material. The results of these tests are given in fig. 6.17.

Pure TiC and TiN samples show the brittle behaviour as is expected for this type of ceramic, fig. 6.18. From the thermal-mechanical data of these materials it could be concluded that TiN tolerates higher thermal loads than TiC. This assumption is confirmed by the results in fig. 6.18.

Thick layers - 2 mm layer thickness - of graphite brazed to a Mo substrate with a Zr-solder show on the contrary only an tolerable erosion, fig. 6.19. Even at thermal loads as high as 100 MW m^{-2} and pulse durations up to 2 s the brazing zone and thus also the substrate remained unaffected.

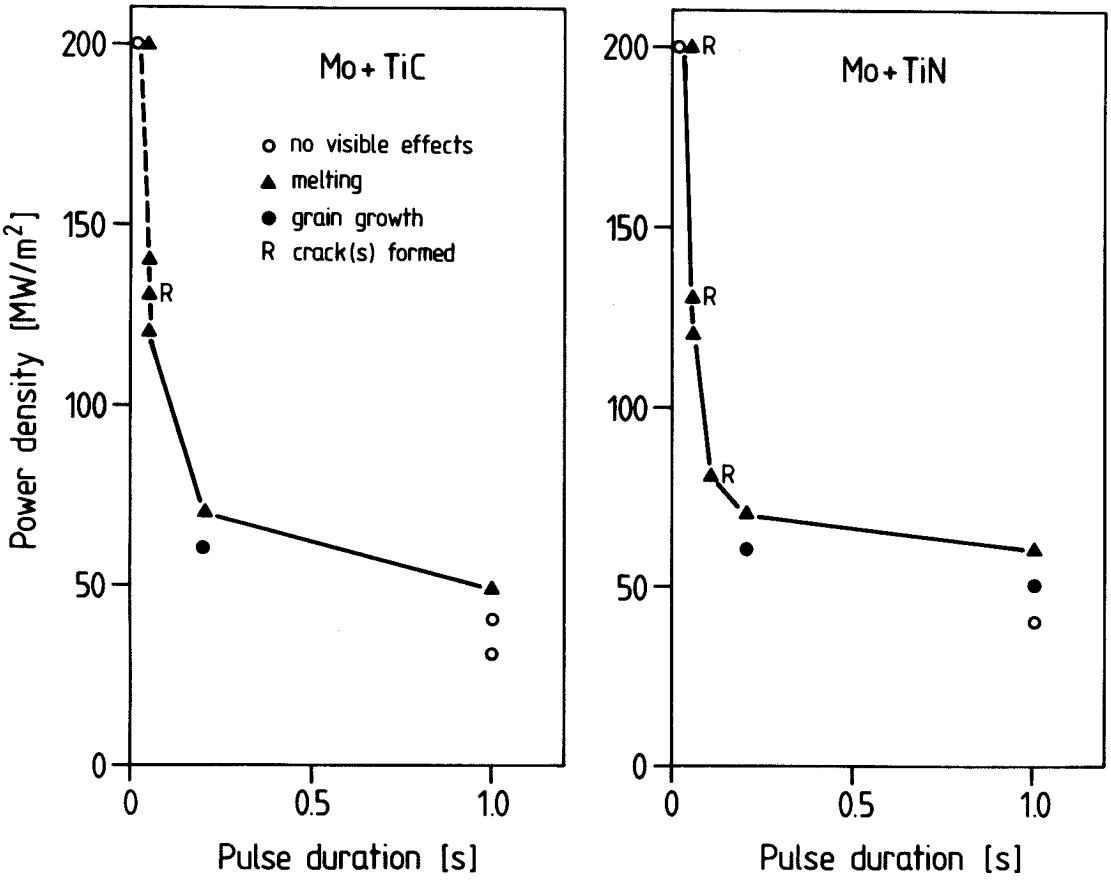

Fig. 6.17: Results of thermal shock experiments for Mo-samples, coated with 5 µm TiC and TiN, resp., by electron beam disruption simulation; electron beam power density as a function of beam pulse duration; solid line: damage threshold for melting

The behaviour of materials under very high, but short-term thermal loading - 190 MW m^{-2} nominal, pulse durations 10 to 50 ms - is presented in fig. 6.20. All tested materials, Mo with TiC and TiN coatings included, survive these thermal shocks if the pulse duration is sufficiently short, that means 30 ms or shorter, except Ta and, as a reference material, 1.4311. Ta and 1.4311 show grain growth already at 30 ms-pulses. For the next generation Tokamak INTOR, a reference disruption /61,62/ is defined with the parameters power density = 115 MW m^{-2} and duration of disruption = 20 ms. All tested materials could therfore survive this type of reference disruption and, of course, also the disruption type denoted the NET-"slow energy deposition" (chapter 4.3).

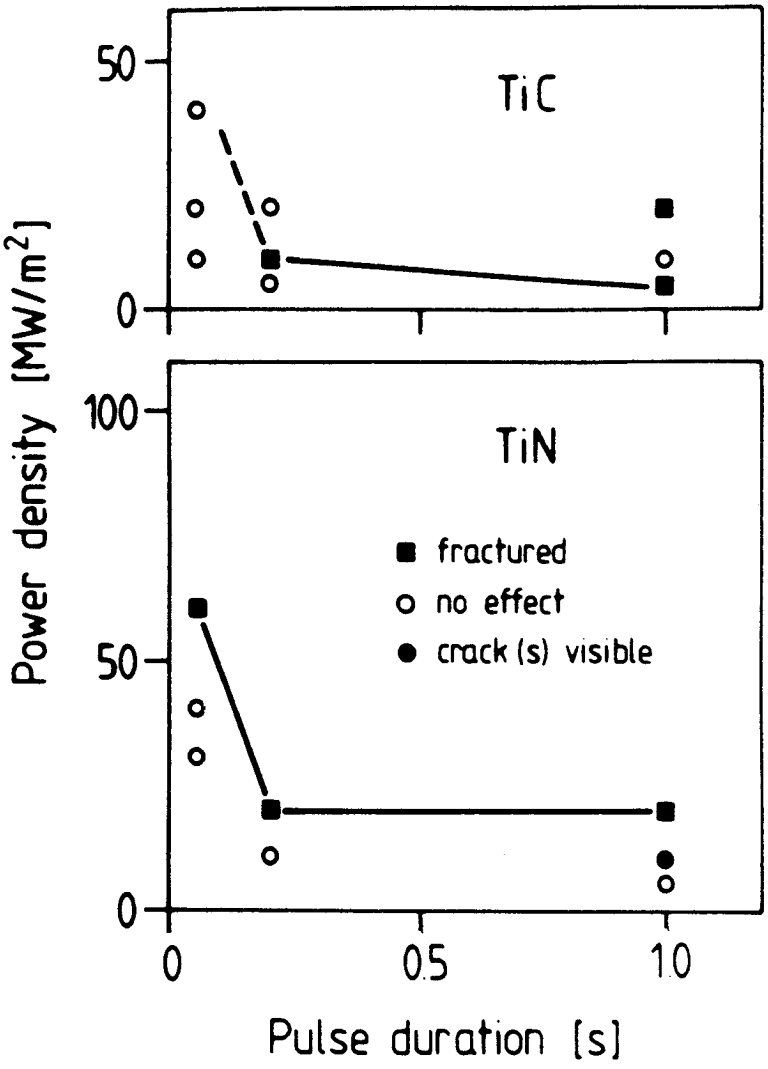

Fig. 6.18: Same as fig. 6.17, but for bulk TiC and TiN; the less brittle behaviour of TiN as compared with TiC is clearly visible

All experimental data for the longer beam pulses discussed so far are presented in fig. 6.21 for refractory metals and alloys. Added are two data points of bulk chromium and, as a reference, 1.4311. It is obvious that all data lie in a relatively narrow (scatter-) band with a strong ascent to higher tolerable power densities with decreasing pulse durations.

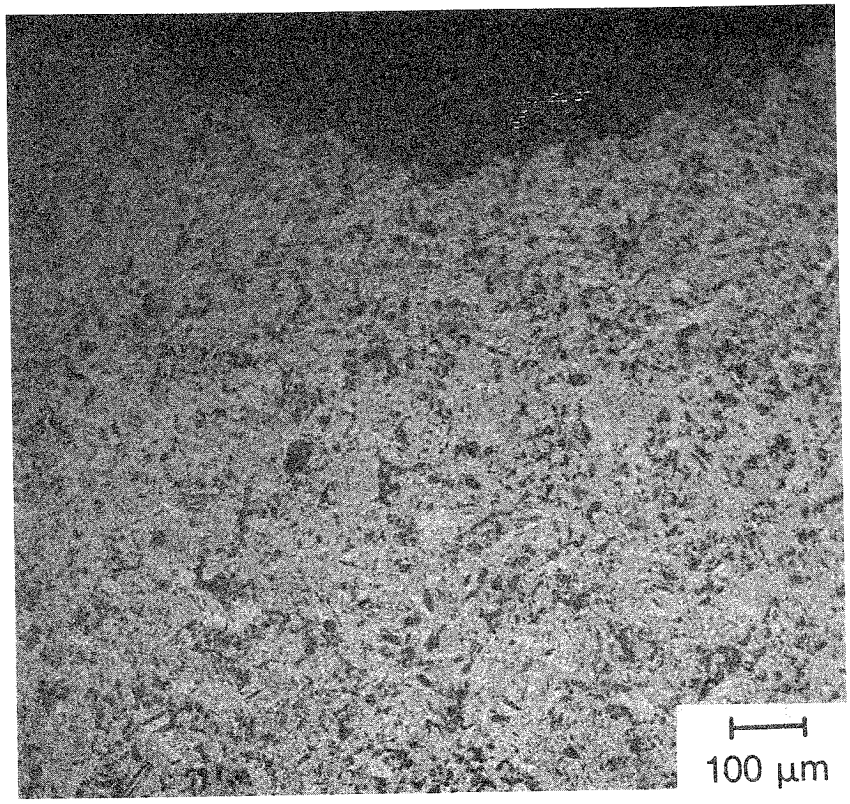

Fig. 6.19: Graphite layer, 2 mm thick, on Mo substrate after electron beam thermal shock experiment; 50 MW m^{-2}, 2 s; the graphite is eroded but shows no cracks

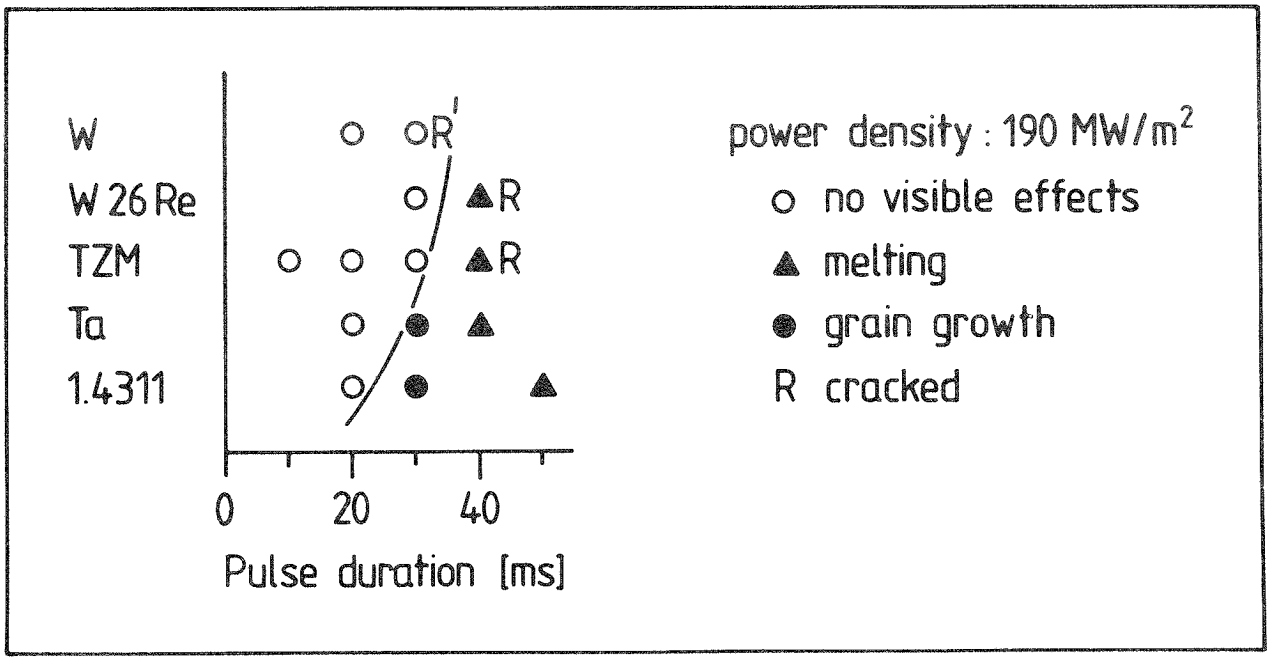

Fig. 6.20: Summary of short-pulse electron beam thermal shock experiments at a constant power density of 190 MW m^{-2} but varying beam pulse durations; solid line: damage threshold for melting and grain growth

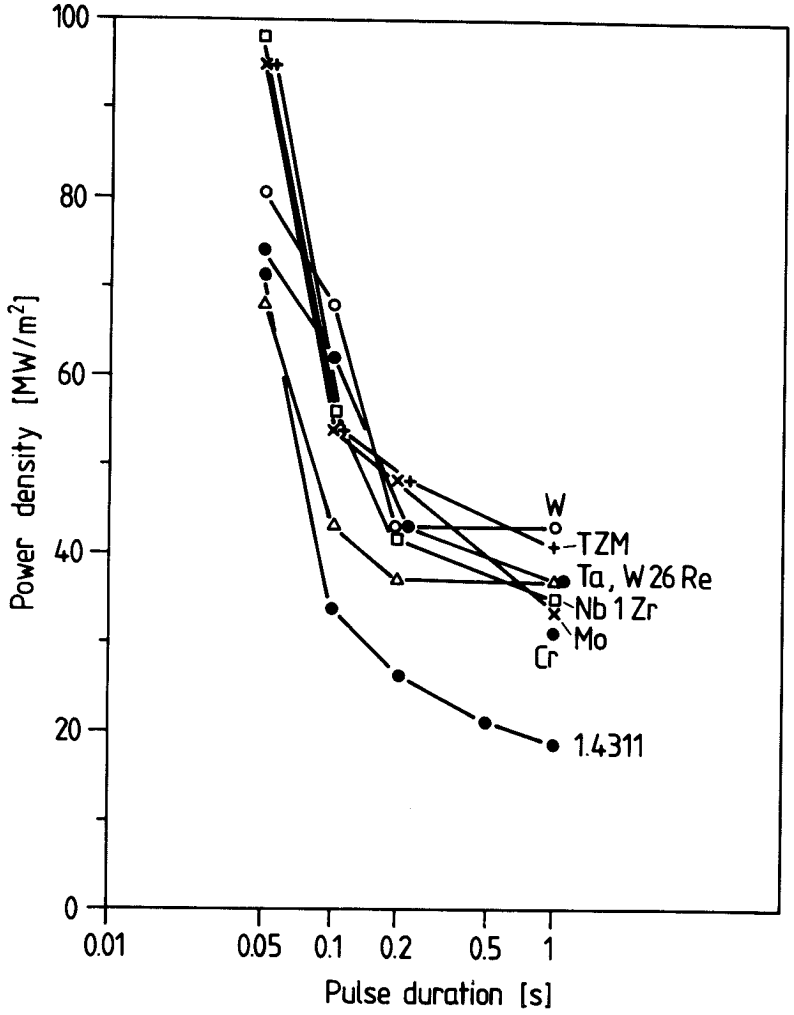

Fig. 6.21: Summary of "medium"- and "long"-pulse electron beam thermal shock experiments; electron beam power density as a function of beam power duration; the power density has been corrected for energy losses by backscattered electrons

6.3 Influence of Grain Orientation and Substrate Temperature on Thermal Shock Behaviour

The refractory metal samples tested so far have been used in a cold worked state with the grain orientation parallel to the electron beam incidence, that is vertical to the loaded sample surface. The temperature of the samples at the beginning of the experiments was in general at ambient level. The ductile to brittle transition temperature (DBTT), that is the temperature (range) below which the material behave brittle, and above which the materials behave ductile, is below $0^{o}C$ for V, Nb, and Ta, and near or above

room temperature for Cr, Mo, and W. So one may assume that the experimental base temperature has a strong influence on the fracture behaviour of the refractory metals during thermal shock tests. The same may be true for the role of grain orientation, because grain orientation also influences strongly the DBTT.

The results of thermal shock experiments with W samples and grain orientation parallel to the sample surface are shown in fig. 6.22. The strong influence of grain orientation is clearly visible when comparing these data with those presented earlier in fig. 6.14: Here, only 1 of 14 tested samples shows cracks, while with grain orientation vertical to the sample surface, fig. 6.14, 8 of 14 tested samples were cracked. The different position of the damage threshold line in both figures may have its reason in slightly different test parameters, e.g. electron beam focus.

The W test samples with grain orientation parallel to the sample surface were also used to examine the influence of an elevated base temperature on crack formation. For that purpose the samples were heated to approximately 330°C before carrying out the electron beam thermal shock test, fig. 6.23. No sample cracking is visible. The same positive result is found with W samples with grain orientation vertical to the sample surface, fig. 6.24: When the sample base temperature rises above 250°C, no fracture of the samples occurs during the thermal shock tests. This critical temperature is even lower for Mo than for W. Some results yield the surprising conclusion that with respect to the critical temperature TZM behaves similar to W but not to Mo. An explanation for this result cannot be given so far.

6.4 Thermal Fatigue

As has been pointed out fatigue should play an important role only for the materials of the highly loaded first wall components. The experimental conditions have therefore to cover the correct parameter ranges as they have been discussed earlier.

It is well known that thermal cycling can fatigue a material under conditions which do not affect it during one single shot. This fact is illustrated in fig. 6.25. For that experiment the test parameters have been chosen to be 20 MW m^{-2} electron beam power density and 1 s pulse duration with 9 s

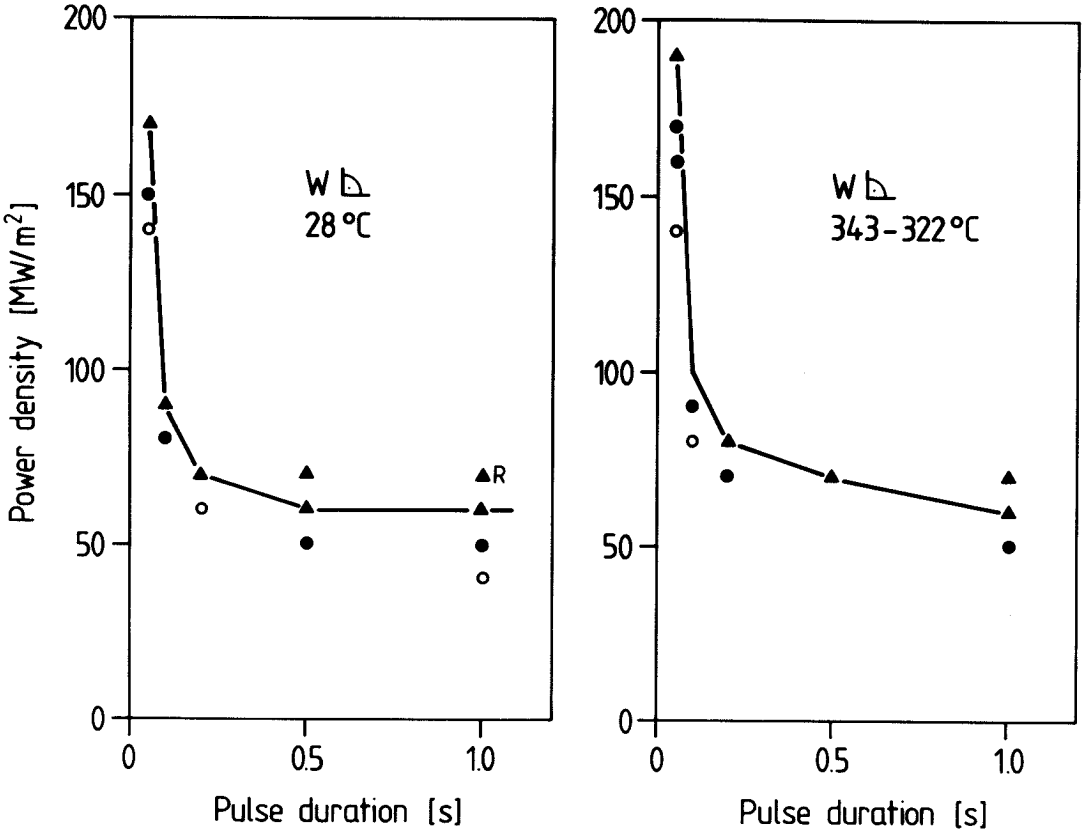

Fig. 6.22/6.23: Thermal shock behaviour of W-samples in electron beam experiments, grain orientation parallel to the sample surface, that is vertical to the incident beam: with sample base temperature at room temperature only one sample showed thermal shock cracks, with base temperature raised to about 330°C no sample cracking occurs.

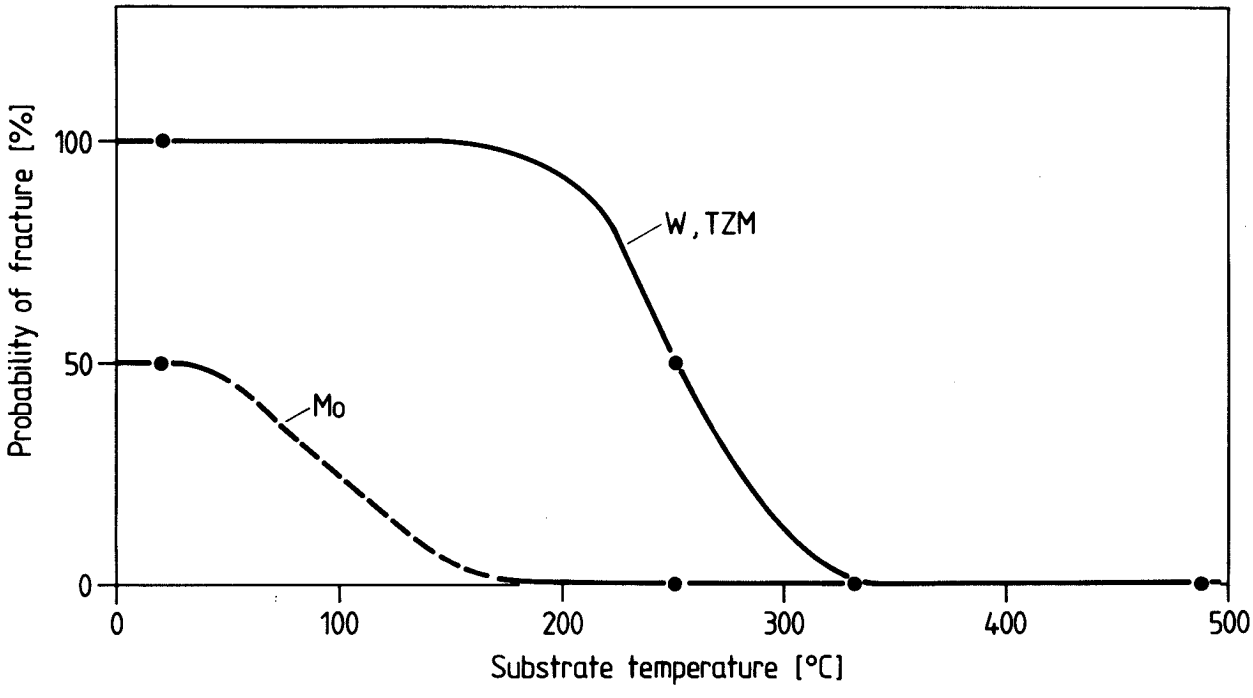

Fig. 6.24: Influence of sample base temperature (x-axis) on the fracture behaviour of Mo-, W-, TZM-samples

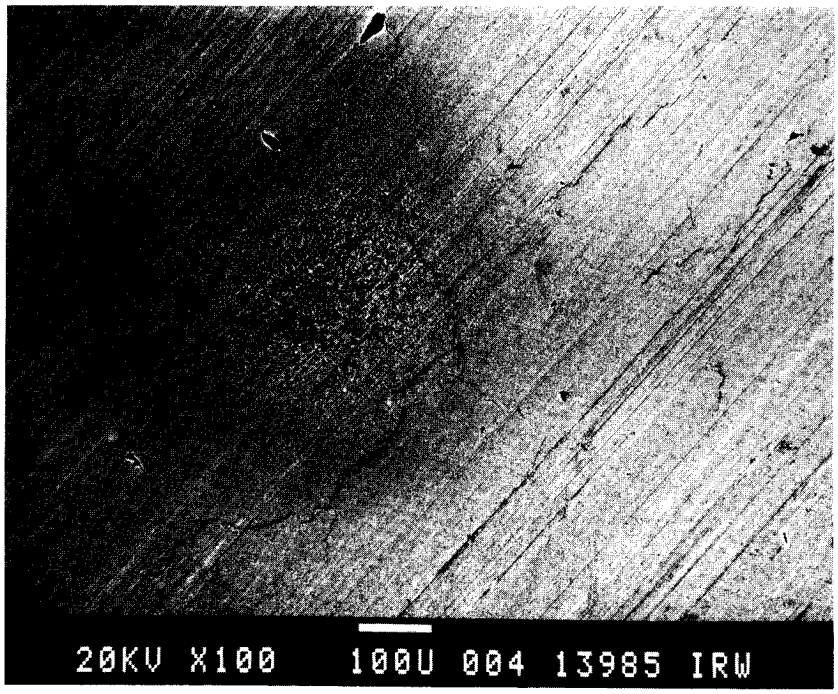

Fig. 6.25: Cracks in the surface of a W-sample; the sample has been loaded in an electron beam thermal fatigue experiment; 20 MW m^{-2}, 100 pulses, pulse duration 1 s, interval time 9 s; SEM micrograph

interval time. These values cause no effect on W in single shot (thermal shock) experiments, fig. 6.14. After 100 pulses "landing" successively on the same area severe cracking occurs in the sample surface.

The results of thermal fatigue experiments are presented in fig. 6.26 for W and W 26 Re, in fig. 6.27 for Mo and TZM, and in fig. 6.28 for Ta. With the applied loading conditions fatigue cracking occurs in W 26 Re, Mo, and Ta at loads of 50 MW m^{-2} and 100 pulses. For TZM this limit is somewhat lower at 40 MW m^{-2}, whereas W shows cracking already at 10 MW m^{-2} and 100 pulses. So the conclusion should be valid that - may be except for pure W - refractory metals can very well withstand the thermal fatigue conditions even for the highly loaded first wall components at least for low and medium amounts of discharges. This is especially true for the Tokamak NET, in which these components will be loaded with nominal 5 MW m^{-2} to 10 MW m^{-2}, depending on the resp. technical concept.

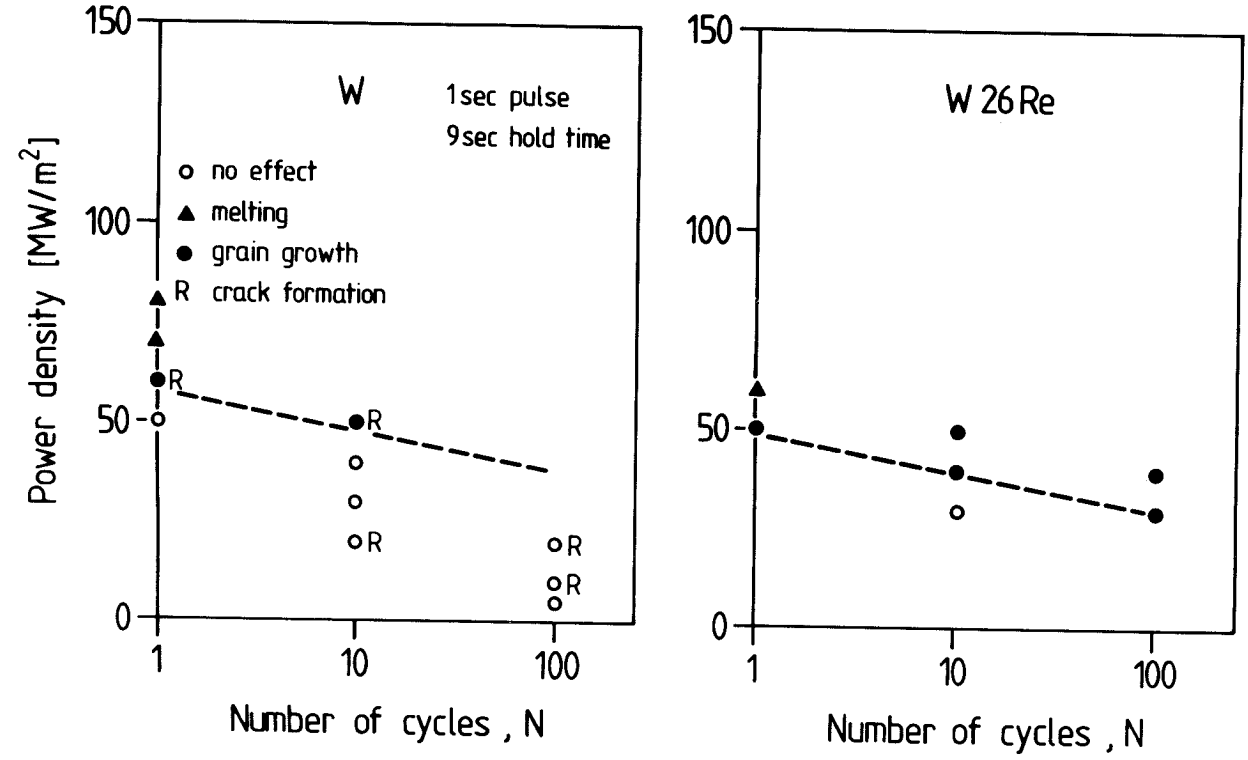

Fig. 6.26: Results of electron beam thermal fatigue experiments for W and W 26 Re; solid line: damage threshold for melting; dashed line: damage threshold for grain growth

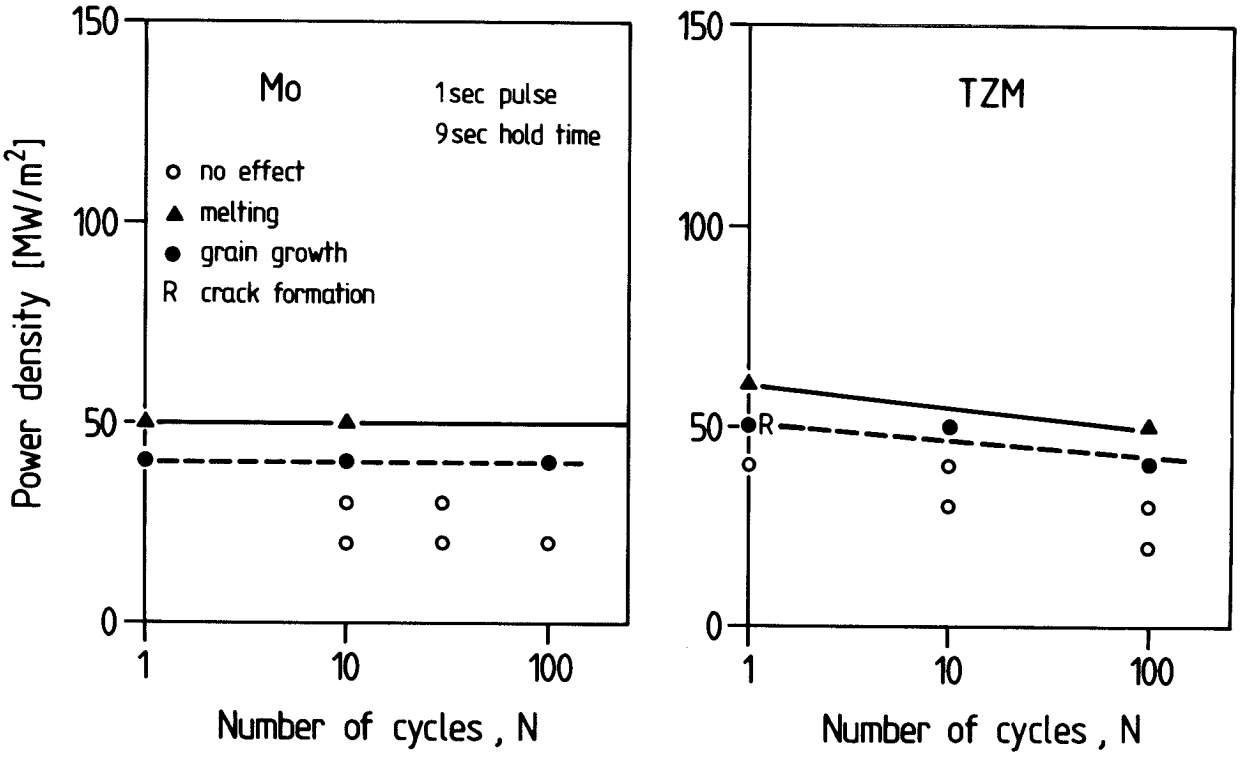

Fig. 6.27: Same as fig. 6.26, but for Mo and TZM

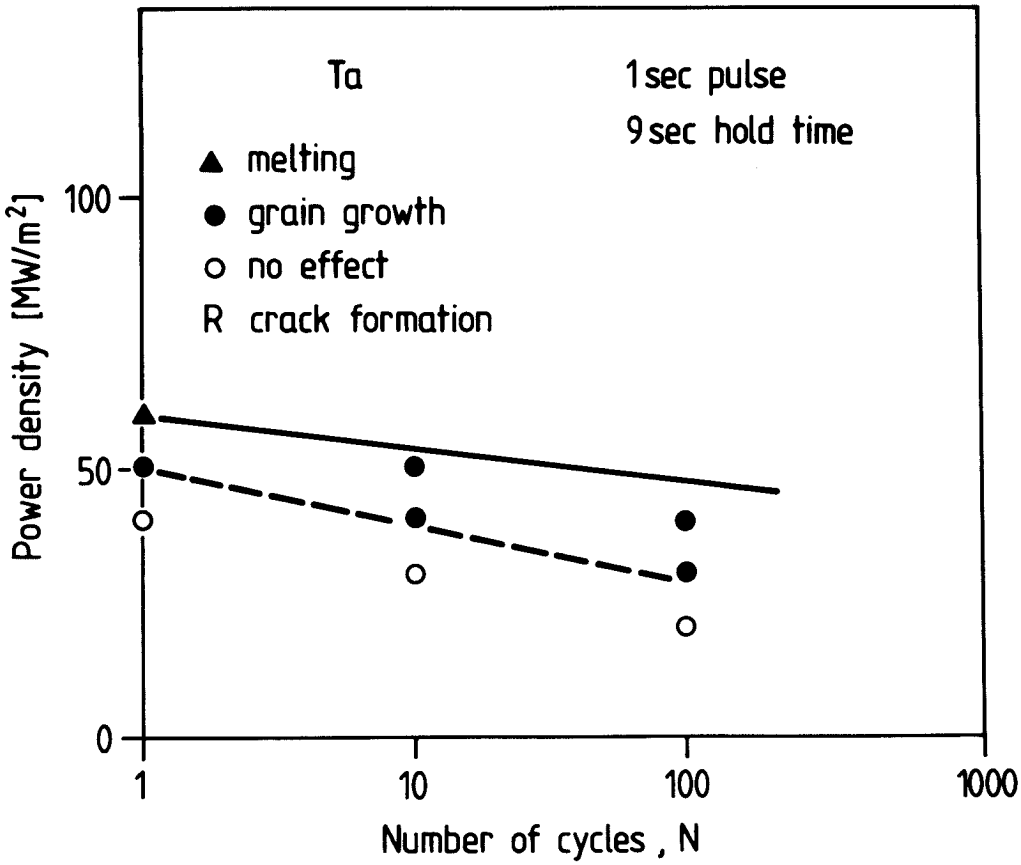

Fig. 6.28: Same as fig. 6.26, but for Ta

6.5 Discussion

For an acceptable mutual comparison of the investigated materials it is necessary to consider the reduction of energy deposition by backscattered electrons. Since other contributions to this energy loss than by backscattered electrons - e.g. by secondary electrons, X-rays, thermal radiation - can be neglected, it depends on the atomic number Z of the resp. element, Tab. 2. The correction for the energy loss has already been taken into account in fig. 6.11 and 6.21: It is obvious that on the experimental conditions applied during the discussed tests all refractory metals behave similar, and appreciably better than Fe-Ni-base alloys. The loading threshold for surface melting for refractory metals in roughly 50 % higher than for 1.4311.

The tendency for crack formation below and above the melting threshold is quantified in Tab. 3. The general conclusion is that crack formation is significantly lower when the material remains in the solid state during thermal shock loading. The only exception seems to be W but there is obviously no definite explanation for this behaviour. This is confirmed by the W samples with the grain orientation parallel to be loaded surface (vertical to the incident electron beam): at sample temperatures of about 330°C no cracks at all were forming. The conclusion should be allowed that the other refractory metals, too, might show a similar reduced crack tendency at elevated base temperatures. Finally it shall be pointed out, that pure Mo behaves significantly better than TZM under thermal shock loads, and that Ta and Nb 1 Zr showed no cracking at all, neither below nor above the melting threshold.

The following conclusions might summarize the experimental results presented so far:

- The total weight loss by erosion is least for W followed by Mo, TZM, Ta and Nb. The weight loss of W is three orders of magnitude lower than for 1.4311, and 1.5 orders of magnitude lower than for graphite.

- The loading thresholds for recrystallization and melting differ not very much from one-another in the group of refractory metals and are significantly higher than for Ni-Fe-base alloys represented by 1.4311.

- Thin layers of TiN and TiC cannot protect the refractory metals against thermal shock.

- Thick layers of graphite brazed to a support of refractory metals are an effective protection for the metal from plasma attack as well as for the plasma against potential contaminations by high Z material.

- The resistance against crack formation depends on the material, the grain orientation, and whether or not the energy deposition is high enough to introduce melting of the material: Below melting threshold the crack resistance is highest for Nb, Ta, and W with grain orientation parallel to the sample surface, above melting threshold for Nb, Ta, and W again with grain orientation parallel to the sample surface, but here only when the sample base temperature exceeds 300°C.

material	atomic number	backscattered power
graphite	6	6 %
Cr	24	23 %
1.4311	26	25 %
Nb	41	30 %
Mo, TZM	42	32 %
Ta	73	38 %
W, W26Re	74	38 %

Tab. 2:

Ratio of backscattered power P_R to irradiated power P_o for normal beam incidence on a plane target (Lit. 62) for electron beam experiments

	No. of samples cracked	total No. of experiments	%
	Base temperature above damage threshold for melting		
Mo	1	17	6
TZM	3	14	21
W	10	14	71
W26Re	2	10	20
Ta	0	16	0
Nb-1Zr	0	9	0
W /RT	0	7	0
W /330°C	0	7	0
	Base temperature below damage threshold for melting		
Mo	2	5	40
TZM	7	8	87
W	3	7	43
W26Re	4	5	80
Ta	0	5	0
Nb-1Zr	0	5	0
W /RT	1	7	14
W /330°C	0	5	0

Tab. 3: Crack formation in refractory alloys and metals; cumulative results of single shot and thermal fatigue experiments

- It seems reasonable to conclude that grain orientation effects similar to those with W will also occur in the case of Mo and TZM. Increasing the substrate temperature in experiments with Mo and TZM causes a strong reduction of crack formation tendency, at elevated temperatures no crack formation could be found during the experiments. This temperature is higher for TZM than for Mo.

- Marked grain growth occurs for all refractory metals in the molten zone and in the surrounding recrystallization area as soon as the energy deposition exceeds the melting threshold.

- Assuming that the already discussed generalization may be acceptable one can conclude that surface cracking of the refractory metals does not occur when the sample base temperature exceeds considerably room temperatur. The necessary base temperature depends on the resp. material. Whether or not it is strongly correlated to the DBTT cannot be derived from the experiments performed so far.

7. Tests of Medium-Z Alloys

Medium-Z alloys are the commonly used plasma facing materials in the first wall of todays tokamaks. Two typical representatives for this material group are the alloys

1.4311 - CRONIFER 18 10 - X 2 Cr Ni N 18 10 and
2.4816 - INCONEL 600 - Ni Cr 15 Fe.

The alloy 1.4311 is Fe-based, the alloy 2.4816 is Ni-based. Their alloying constituents are listed in Tab. 4, together with the relevant material properties. The structure of these two alloys is shown in fig. 7.1.

The shape of the samples exposed to the electron beam was square with an edge length of 25 mm and - in some cases - 50 mm and a thickness of 10 mm. The loaded area again was roughly circular with a diameter of about 10 mm, that is equal to the conditions mentioned introductory to chapter 6. The accelerating voltage was kept constant at 150 kV. The already discussed energy loss due to the backscattered electrons was normally not taken into account.

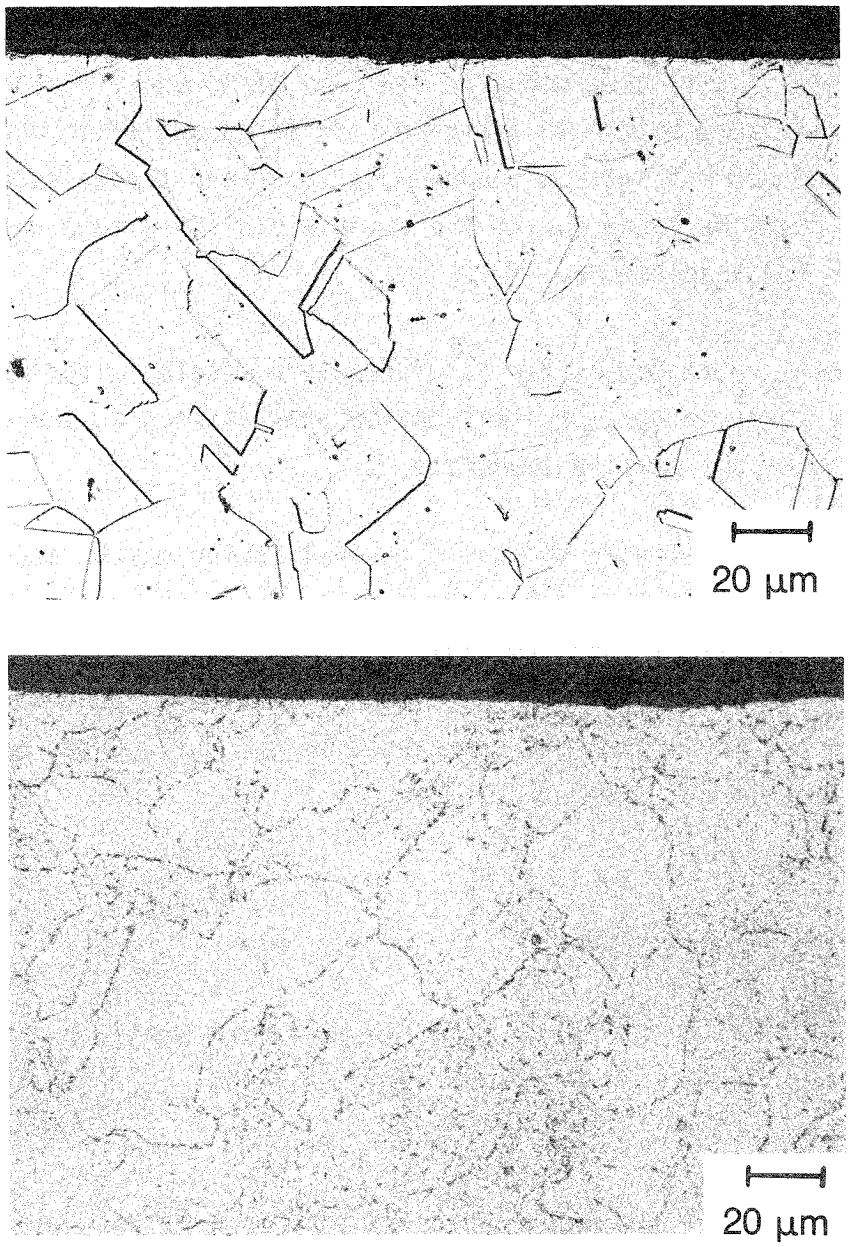

Fig. 7.1: Metallurgical structure of the two alloys 1.4311 - CRONIFER 1810 - (top) and 2.4816 - INCONEL 600 - (bottom); metallographic section, grain boundary etched

7.1 Thermal Shock

The thermal shock experiments are single shot material tests. The loading parameters are

beam power density	20 MW m^{-2}	to 170 MW m^{-2},
pulse duration	50 ms	to 1000 ms.

The phenomena examined for the estimation of the thermal shock behaviour of the alloys 1.4311 and 2.4816 are

- grain boundary step development,
- surface melting,
- crack formation,
- weight loss, and
- microhardness.

The results of the materials tests with respect to grain boundary step development and surface melting are summarized in fig. 7.2. The damage

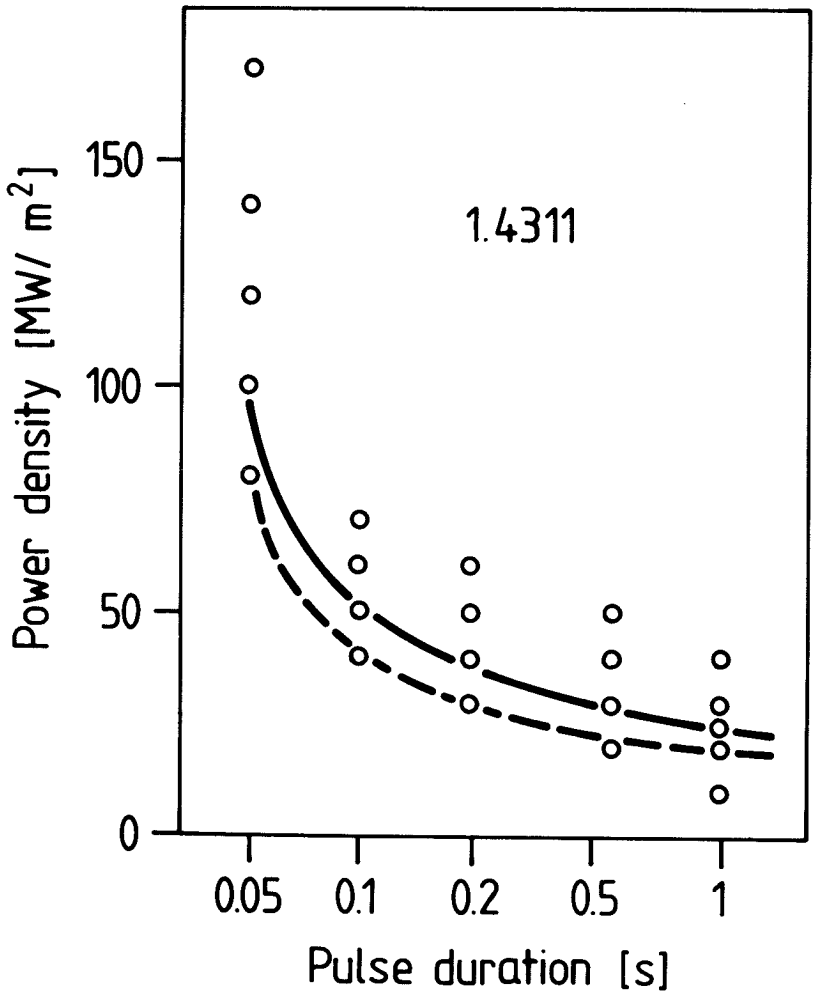

Fig. 7.2, a,b: Experimental condition of electron beam thermal shock experiments with the alloys 1.4311 (a) and 2.4816 (b); beam power density as a function of beam pulse duration; solid line: damage threshold for melting; dashed line: damage threshold for grain boundary step development

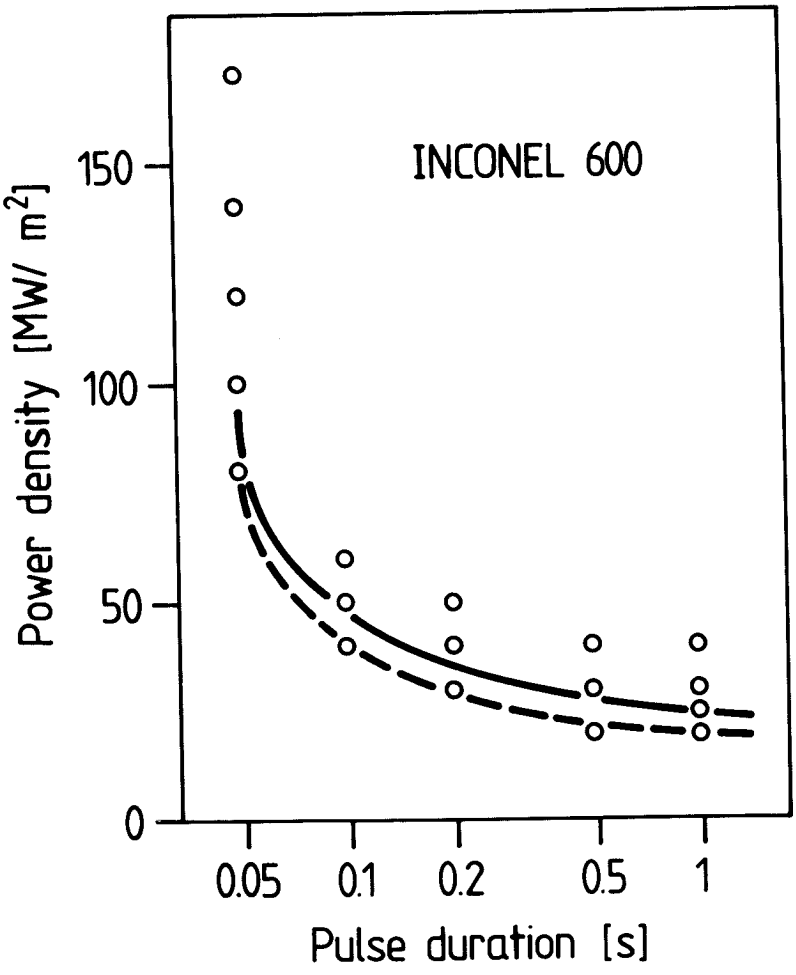

Fig. 7.2, b: see fig. 7.2, a, b.

threshold lines for these two types of material attack are entered into the figures. It is obvious that the alloys 1.4311 and 2.4816 behave very similar to one-another. Consequently, most of the following discussions are dedicated to the alloy 1.4311 only.

The volume of the material melted during the thermal shock load is approximated under the assumption that the melted area has the shape of a cup of a sphere. Thus the volume of the originally melted material is calculated by

$$V_{melt} = \pi/6 \cdot h \cdot (3\,(d/2)^2 + h^2) \qquad (7.1)$$

were

$$d = (4 \cdot A/\pi)^{1/2} \text{ and}$$

A = surface area of the molten zone,

h = depth of the molten zone in the center of the crater.

Loss of material, e.g. by evaporation, is not regarded in this context. The calculated values are presented in fig. 7.3, at which A and h have been determined microscopically from the microscopic plain views and from the metallographic sections of the loaded samples, resp. Additionally, the data are listed in Tab. 5. When the pulse duration is sufficiently long - above 100 ms - the melted volume increases rapidly with increasing power density as soon as the threshold load for melting is clearly exceeded. At short pulse durations - 100 ms or shorter - this rise is considerably smaller even with a strong increase of the deposited energy.

The same result is found when the thermal shock induced material loss Δ G is examined. Δ G summarizes the material removal by all contributing processes like erosion, evaporation and/or splashing. Δ G is determined by measuring the sample weigth before and after thermal shock test on a micro balance. The data are presented in fig. 7.4 and Tab. 6, here only for the alloy 1.4311.

The threshold value for the loading power density to cause surface melting of the material has been calculated by a one-dimensional computation, using the equation /19-21, 31, 51, 63, 64/

$$\frac{P}{A} = \frac{T_S - T_O}{2} \quad \frac{(\pi \cdot \varrho \cdot c \cdot k)^{1/2}}{t} \tag{7.2}$$

with the symbols having the following meaning:

T_O = steady state, base temperature in the sample surface
T_S = the melting temperature of the investigated material which has to be reached by the calculated deposited energy $P \cdot t$

In the case examined here, T_O is essentially the room temperature, T_S is the melting temperature of the alloy 1.4311, namely 1425°C.

ϱ = material density, here 7,86 g cm^{-3}
C = thermal capacity, here 0,17 cal $\cdot g^{-1} \cdot K^{-1}$ or
0,69 J $\cdot g^{-1} \cdot K^{-1}$, and

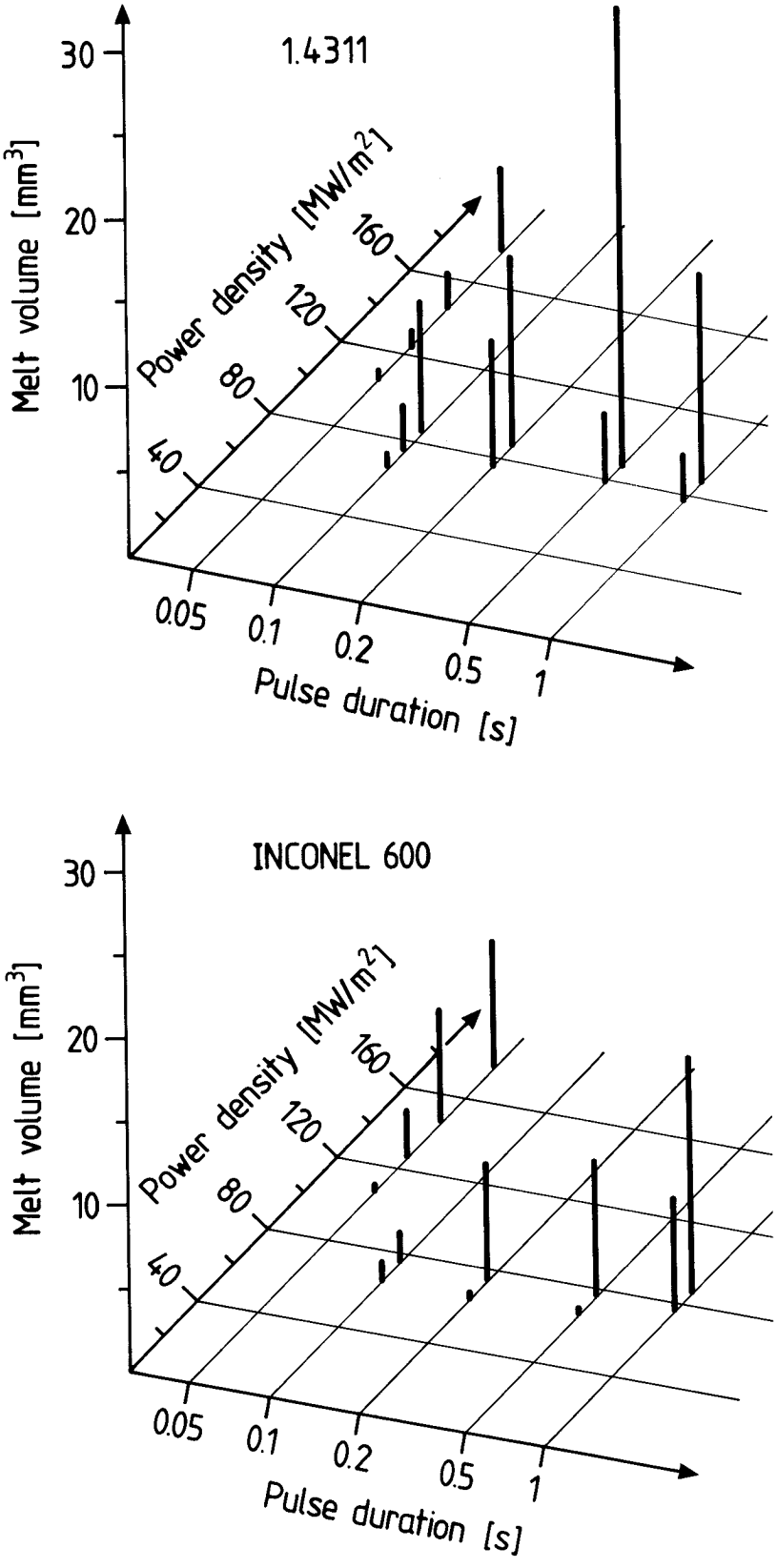

Fig. 7.3: Melt volume in the crater after electron beam thermal shock experiments, in the surface of the alloy 1.4311 (top) and of the alloy 2.4816 (bottom); calculated following eq. 7.1

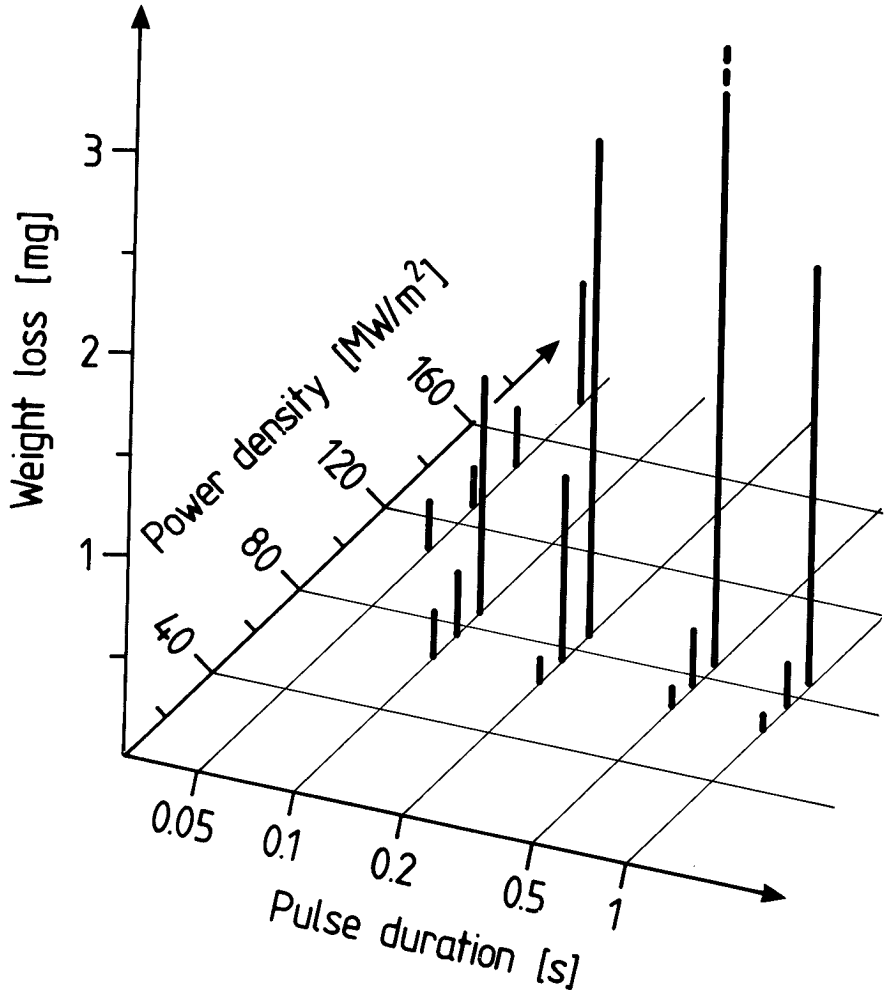

Fig. 7.4: Material loss (expressed by the weight loss) in alloy 1.4311 samples after electron beam thermal shock experiments

k = thermal conductivity, here 6 cal · m^{-1} · s^{-1} · K^{-1} or
27 W · m^{-1} · K^{-1}, for a
sample temperature of about
1000°C or more.

The calculated graph of the power density as a function of deposition time or pulse length is plotted in fig. 7.5, together with the experimentally determined threshold line for melting. The correlation of these two graphs is obviously quite good. A discussion of the differences between the graphs on the basis of the available data seems too risky.

Material	Constituents (W %)							
	Fe	Ni	Cr	C	Si	Mn	N	Cu
1.4311 (CRONIFER 1810)	Bal.	10	18	0,03	1,0	2,0	0,2	-
2.4816 (INCONEL 600)	8,0	Bal.	15,5	0,15	0,5 max.	1,0	-	0,5 max.

Tab. 4: Chemical composition of the investigated materials

t_H (s)	P/A (kW/cm^2)	V_{melt} (mm^3) (1.4311)	V_{melt} (mm^3) (INCONEL 600)
0.05	10	0.3	0.3
0.05	12	0.5	2.6
0.05	14	1.9	6.6
0.05	17	4.9	7.5
0.1	5	0.7	1.2
0.1	6	2.5	1.7
0.1	7	7.6	-
0.2	4	-	0.3
0.2	5	7.4	6.9
0.2	6	11.3	-
0.5	3	-	0.3
0.5	4	4.1	8.0
0.5	5	27.1	-
1	3	2.7	6.8
1	4	12.3	14.2

Tab. 5: Melt volumes in the craters of samples of the alloys 1.4311 and 2.4816 (INCONEL 600) after electron beam thermal shock tests (see also fig. 7.3).

t_H (s)	P/A (kW/cm^2)	ΔG (mg)
0.05	10	0.23
0.05	12	0.21
0.05	14	0.29
0.05	17	0.61
0.1	5	0.23
0.1	6	0.32
0.1	7	1.18
0.2	4	0.13
0.2	5	0.92
0.2	6	2.46
0.5	3	0.09
0.5	4	0.28
0.5	5	6.16
1	2	0.1
1	3	0.22
1	4	2.28

Tab. 6: Weight loss G of samples of alloy 1.4311 after electron beam thermal shock experiments (see also fig. 7.4)

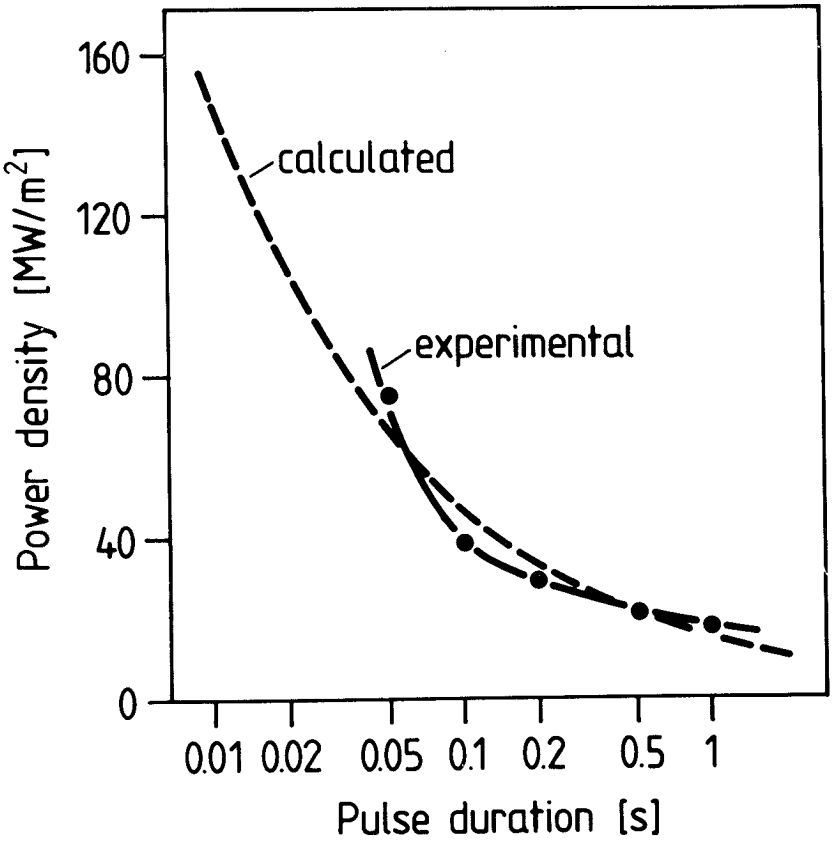

Fig. 7.5: Threshold lines for material melting by electron beam thermal shock experiments for the alloy 1.4311; solid line: experimental data; dashed line: one-dimensional calculation; the experimental values are corrected for 25 % energy loss by backscattered electrons

7.2 Thermal Behaviour of the Materials

To obtain reliable values of the maximum surface temperature of the samples when loaded with the electron beam finite elements calculations have been carried out*). For this task the computer program TWODEPEP has been used which also allows to take into account the energy losses due to radiation and vaporisation during the loading process.

The radiated energy is calculated with the equation /64, 65, 66/

$$F_{rad}\,(T_V) = \varepsilon \cdot \sigma \cdot (T_V^4 - T_O^4) \cdot A \qquad (7.3)$$

with:

ε = emissivity, for the alloy 1.4311 = 0,3,

σ = Boltzmann constant = $5{,}67 \cdot 10^{-8}$ W $\cdot$ m^{-2} $\cdot$ K^{-4},

T_0 = steady state first wall temperature, for a first approximation equal to room temperature, thus T_0 = 293 K,

T_V = surface temperature of the loaded area,

A = heated, i.e. radiation emitting area, here $0.8 \cdot 10^{-4}$ m^2.

Radiation loss is negligible near or below the melting temperature. At the melting point of the alloy 1.4311, that is at $T_V = T_m$ = 1698 K, the radiated power during electron beam experiments is just about

$$F_{rad}\ (T_m) = 12\ W,$$

but as can be seem from equ. 7.3, increases rapidly with increasing temperature T_V.

The energy loss due to absorption by eroded and already evaporated sample material is considered by the equation

$$F_{vap}\ (T_V) = \frac{\dot{n}}{N_0}\ H_{vap} \tag{7.4}$$

$$\text{and } \dot{n}\ (T_V) = 3{,}5 \cdot 10^{22}\ p\ (T_V) \cdot (M \cdot T_V)^{1/2} \cdot A, \tag{7.5}$$

with

$\dot{n}$ = evaporated atoms per second,

N_0 = Avogadro-number = $6 \cdot 10^{23}$ mol^{-1},

H_{vap} = heat of evaporation = 349,6 kJ $\cdot$ mol^{-1} for Fe,

$p\ (T_V)$ = vapor pressure of the sample material at the resp. surface temperature; for Fe at the melting point of the alloy 1.4311 $p\ (T_m)$ = 1,0 Pa,

M = atomic mass; for Fe M = 55,85, the alloy 1.4311 may be approximated with M = 56.

Also energy loss due to vaporisation can be neglected at temperatures below or near the melting point. At $T_V = T_m$ this contribution to the total energy loss is for the alloy 1.4311 about

---

*) The authors cordially thank Mr. B. Brandt from the Institut für Plasmaphysik, Kernforschungsanlage Jülich, for performing these finite elements calculations.

$$F_{vap}\ (T_m) = 0{,}5\ W$$

and then slowly increasing with increasing temperature T_v.

With the equations 7.2 through 7.4, the sample surface temperature is calculated for the alloy 1.4311, under the assumption that the sample is loaded with an electron beam pulse of 30 MW m^{-2} for a pulse duration of 1000 ms. The nominal power is corrected for 25 % energy loss due to backscattered electrons, so that the calculations have been performed with a power input of 22,5 MW m^{-2}. Moreover it is assumed that the energy is deposited in flat distribution, the loaded area being circular with a diameter of 10 mm. The result is plotted in fig. 7.6, with and without consideration of energy losses. It is obvious that the surface temperature reaches the melting point already after 0.3 s and approaches or even exceeds 2000°C at the end of the loading beam pulse.

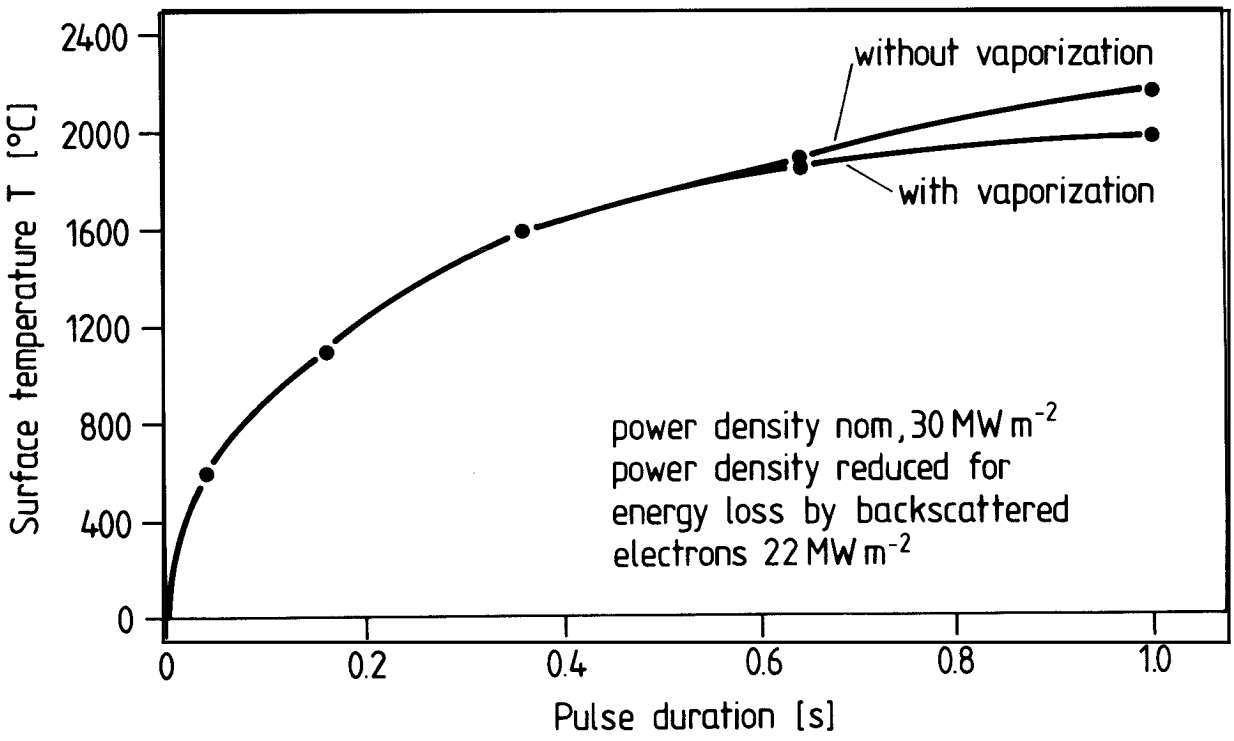

Fig. 7.6: Surface temperature of a sample of alloy 1.4311 during an electron beam shot: nominal beam power density 30 MW m^{-2}, corrected for 25 % energy loss by backscattered electrons, pulse duration 1000 ms; two-dimensional calculation

This result confirms the good correlation between calculated and meaursed data in fig. 7.5 and also the data in fig. 7.2, after which melting should be reached in about less than 0.5 s for a pulse with 30 MW m^{-2} nominal power density.

The weight loss by vaporization can be calculated using equation 7.5. This has been done for the just mentioned conditions, i.e. a one-second electron beam pulse of 22,5 MW m^{-2} real power density. The result is shown in Tab. 7:

time step ms	40	160	360	640	1000
surface temperature ^{o}C	605	1080	1493	1834	2007
Weight loss mg	$0,24\ 10^{-13}$	$0,51\ 10^{-6}$	$0,94\ 10^{-3}$	0,06	0,35

Tab. 7: Peak surface temperature and weight loss due to evaporation by an electron beam pulse of nominal 30 MW m^{-2}, real 22,5 MW m^{-2}, and 1000 ms pulse length; two-dim. calculation, loaded area circular with 10 mm diameter

At the end of the pulse, i.e. after 1000 ms, a total amount of 0.35 mg should have been evaporated. This is in quite good agreement with the experimental data in fig. 7.4 and Tab. 6, resp. where 0.22 mg have been eroded from the sample.

A comparative calculation with a slightly reduced beam power density of nominal P/A = 26.7 MW m^{-2}, that is real 20 MW m^{-2} brings a theoretical weigth loss of about 0.1 mg. That means, that a power decrease of about 10 % results in a decrease of the evaporated material of about 70 %. This is again in very good correlation with the experimental data in fig. 7.4 and Tab. 6, which show a very rapid increase of eroded material as soon as the melting point of the material is exceeded.

7.3 Microhardness and Crack Formation

Two additional parameters have been examined in the loaded material samples, again presented for the alloy 1.4311, namely the microhardness and the crack behaviour.

The microhardness has been measured on metallographic sections, going vertical through the exposed surface of the samples and through the center of the recrystallized/molten crater, fig. 7.7. The measurements have been per-

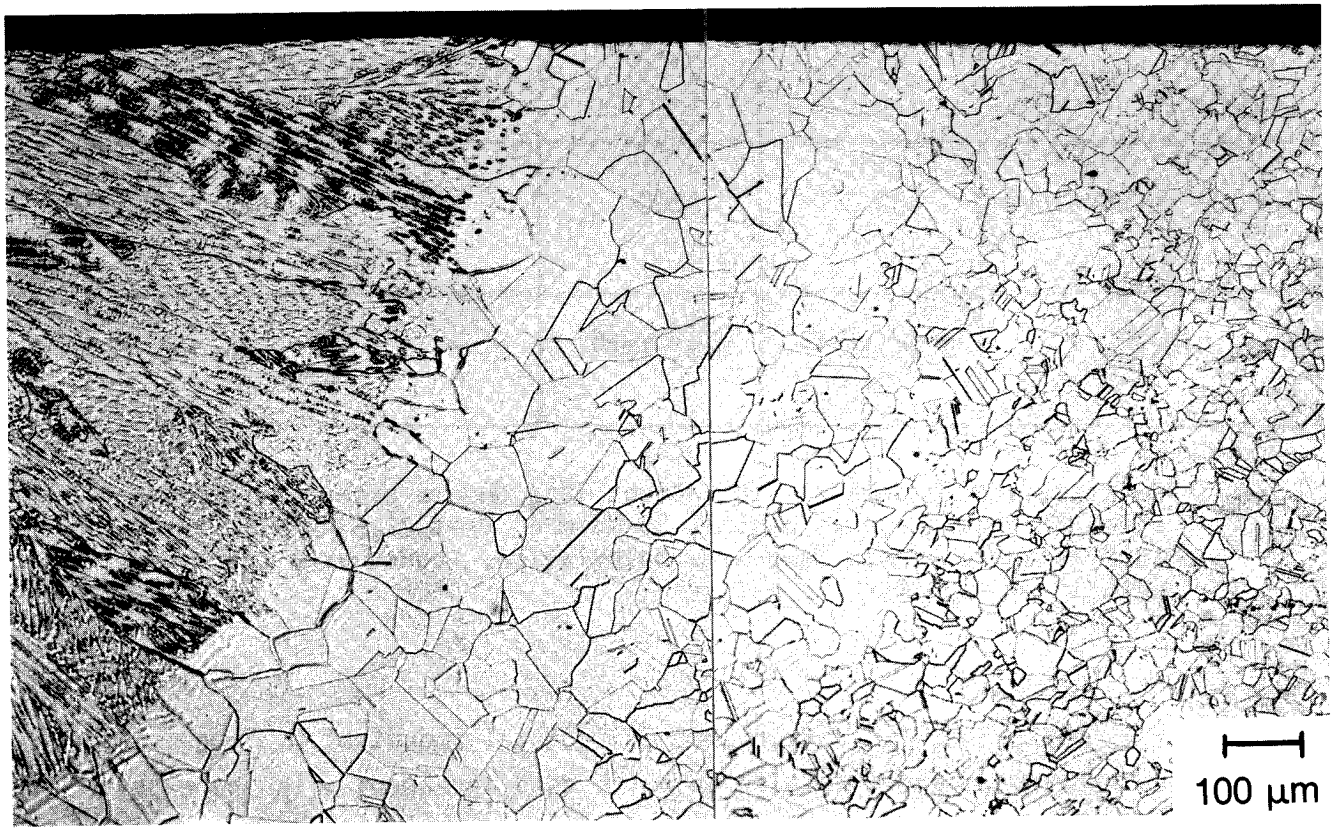

Fig. 7.7: Metallographic section through the melting crater (left), the transition zone (center) and the unaffected structure of the alloy 2.4816 (INCONEL 600) after an electron beam thermal shock test.

formed with a Vickers hardness measuring device, with a load G = 250 N and an effective induction period of 10 s per measuring spot. In each sample the microhardness has been measured along a line from the (molten) surface through the center of the crater and the crystalline transition zone to the unaffected material. The distance between two measuring points was 50 µm.

The results of the determination of microhardness are shown in fig. 7.8. The symbol "S" characterizes the last measuring point in the boundary molten zone/transition zone, "F" marks the first measuring point in the transition zone. The microhardness in the molten zone, that means in the recrystallized area is on an average about 15 % to 20 % lower than in the unaffected material. This result is in very good accordance with the general difference of microhardness between an initial alloy structure (without special hardening procedures) and the recrystallized, molten structure.

All material samples were examined for cracks that might have formed during the electron beam thermal shock tests. Only those cracks were considered which were visible in optical microscopy, that means microcracks and even the transition range of crack size between optical-microscopical visibility and microcracks remained unconsidered. Again, the experimental results of the alloys 1.4311 and 2.4816 are almost identical with one another so that the results are exemplified with the alloy 1.4311.

In all tests cracks occured only when the material had been melted during the tests. Most cracks are localized to the molten area and propagate to the original material only in exceptional cases.

Quantification of crack formation is realized by two parameters, namely

- the crack density in the loaded sample surface:

$$n_S = \frac{N_S}{A_S}$$

  with N_S being the absolute number of cracks in the examined area A_S, A_S being coincident with the molten surface area,

- the crack density in the molten volume, expressed by the crack density in a metallographic section through the center of the molten crater:

$$n_C = \frac{N_C}{A_C}$$

  with N_C and A_C defined corresponding to N_S and A_S.

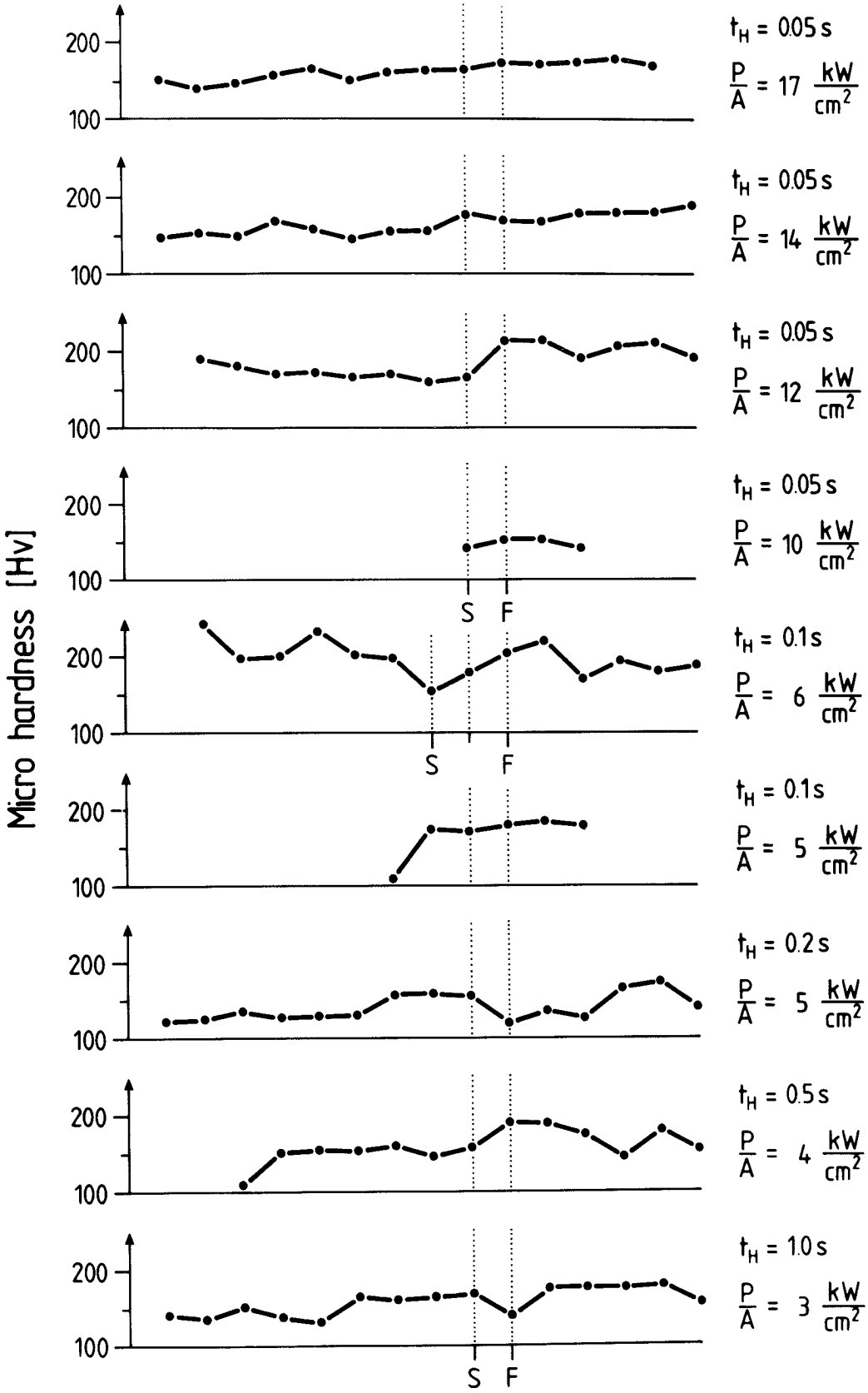

Fig. 7.8: Microhardness profiles of the alloy 1.4311 after electron beam thermal shock experiments, left hand side of the x-axis: measuring points in the molten, recrystallized zone, S: transient molten/transition zone, F: transition zone

In a quite analogous way the two parameters l_s and l_c for the specific crack length are defined, namely

- the specific crack length in the molten surface:

$$l_s = \frac{L_s}{A_s}$$

- and the specific crack length in a cross-sectional plane through the molten crater:

$$l_c = \frac{L_c}{A_c}$$

with L_s and L_c being the total or absolute crack length in the surface plane or cross sectional plane, resp.: $L_{s,c} = (\Sigma L_i)_{s,c}$

The results are summarized in fig. 7.9 and 7.10 and Tab. 8. From these pre-

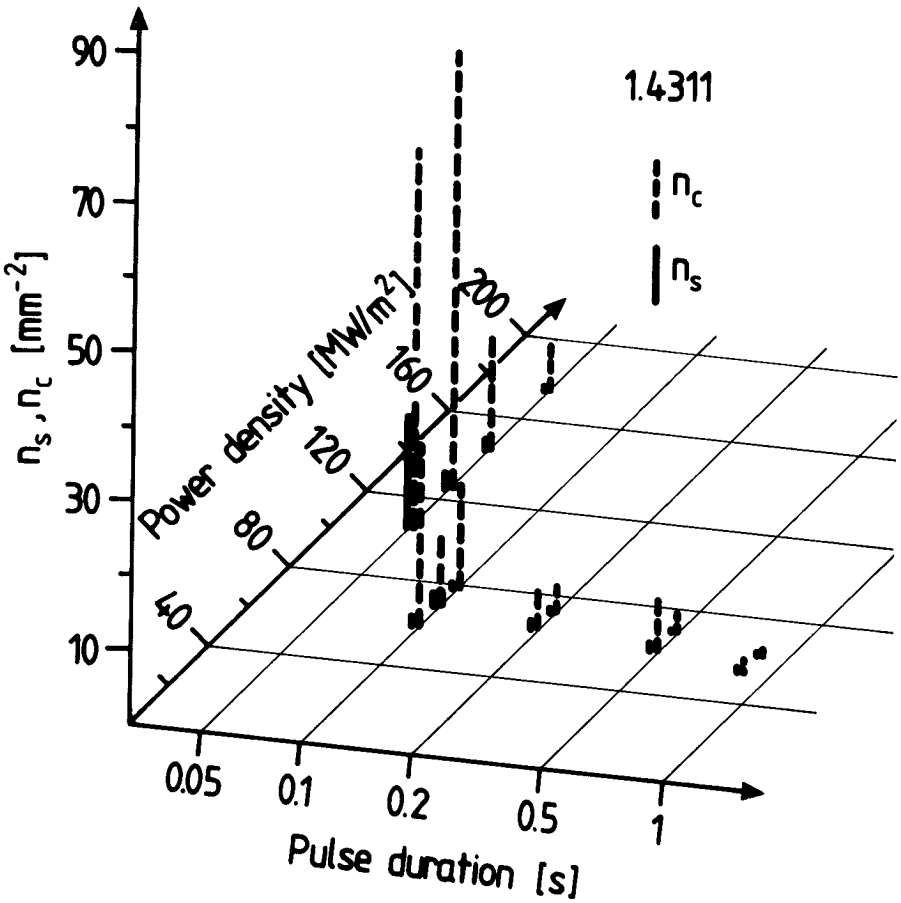

Fig. 7.9: Crack density n_s in the sample surface and n_c in the molten volume in alloy 1.4311-samples after electron beam thermal shock tests

Crack parameters of 1.4311					
t_H (s)	P/A (kW/cm^2)	n_S (mm^{-2})	n_C (mm^{-2})	l_S (mm^{-1})	l_C (mm^{-1})
0.05	10	15.1	50.0	1.1	2.2
0.05	12	2.4	80.0	0.2	6.9
0.05	14	1.7	15.9	0.2	1.5
0.05	17	0.7	6.3	0.1	0.8
0.1	5	1.4	24.0	0.1	2.3
0.1	6	2.3	9.7	0.2	0.4
0.1	7	0.8	13.8	0.1	1.5
0.2	5	1.0	5.5	0.2	0.5
0.2	6	0.7	3.1	0.2	0.5
0.5	4	1.5	7.5	0.2	0.5
0.5	5	0.3	2.6	0.1	0.4
1	3	0.8	1.5	0.1	0.2
1	4	0.3	0.8	0.1	0.1
Crack parameters of INCONEL 600 (2.4816)					
t_H (s)	P/A (kW/cm^2)	n_S (mm^{-2})	n_C (mm^{-2})	l_S (mm^{-1})	l_C (mm^{-1})
0.05	10	7.7	2.5	0.7	2.9
0.05	12	2.4	7.0	0.5	1.8
0.05	14	2.0	9.3	0.5	1.9
0.05	17	2.8	10.6	0.6	1.5
0.1	5	3.6	36.0	0.6	4.9
0.1	6	1.3	16.2	0.1	2.3
0.2	4	2.2	56.3	0.34	6.7
0.2	5	2.6	2.2	0.24	0.2
0.5	3	8.4	15.4	0.7	1.7
0.5	4	0.5	2.7	0.1	0.6
1	3	0.3	3.2	0.1	1.1
1	4	0.2	0.9	0.0	0.2

Tab. 8: Results of crack quantification measurements
crack density parameters n_C, n_S of 1.4311 (top)
crack length/area parameters l_C, l_S of 2.4816 (bottom)

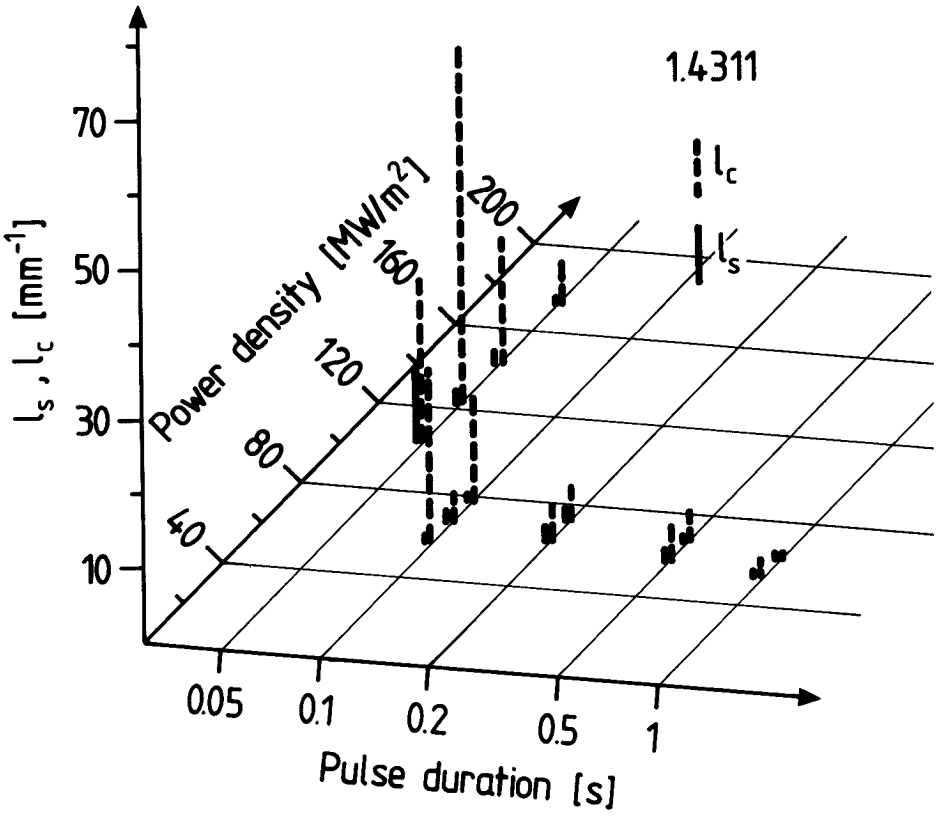

Fig. 7.10: Specific crack length l_s in the sample surface and l_c in the molten volume in alloy 1.4311-samples after electron beam thermal shock tests

sentations, it is obvious that crack density n_c and specific crack length l_c drastically increase with decreasing pulse length, but slowly decrease at short pulse lengths when the power density is increased.

7.4 Thermal Fatigue

Thermal fatigue of the alloys 1.4311 and INCONEL 600 was tested in multiple shot electron beam experiments. The parameter variations were

power density	from	5 MW m^{-2} to 30 MW m^{-2}		
pulse duration	1 s			
interval time	9 s			
pulse number	1	10	100	1000

The results which again nearly coincide for the two alloys are presented in fig. 7.11. With increasing pulse number the threshold load for surface melt-

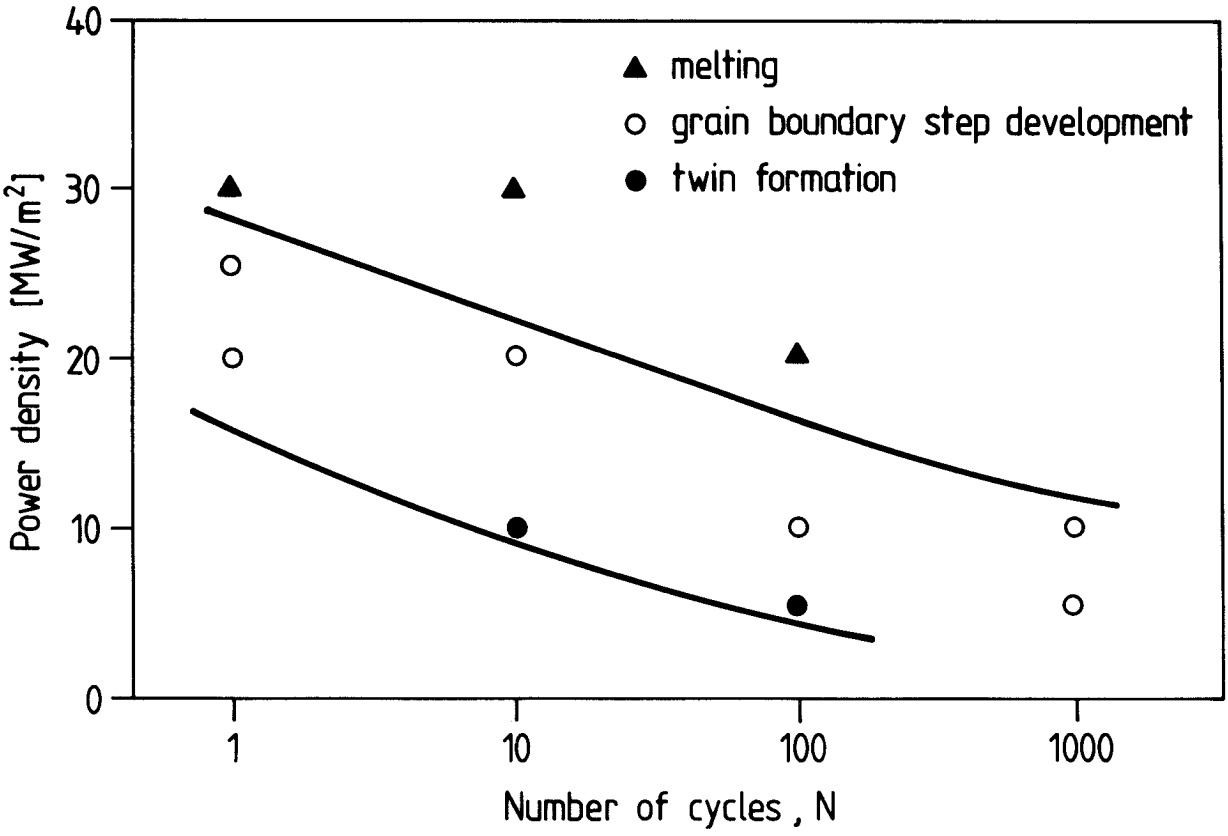

Fig. 7.11: Thermal fatigue experiments in an electron beam device; pulse duration for all experiments 1 s, interval time 9 s; the curves indicate the damage thresholds for melting (upper curve) and for twin formation (lower curve)

ing decreases. This may be at least partly caused by the base temperature which increases during the first some 10 beam pulses since the 9 s interval time are obviously not sufficient for an entire loss of the energy deposited during each pulse in the sample. This fact is expressed for example by the "steady state" temperature on rear side of the samples which increases from room temperature up to 400°C after about 40 pulses with a power density of 20 MW m^{-2} and then remains more or less constant during the further course of the experiments.

The structure of the alloys is changed during thermal fatigue tests already well below the melting threshold. The load limit above which such structural changes in the solid phase occur is also marked in fig. 7.11. The process which is responsible for the structural changes can be denoted grain boundary step development. Fig. 7.12 shows this fatigue phenomenon in top view, fig. 7.13 shows the surface and surface - near structure of the sample after 1000 electron beam pulses in a metallographic section after chemical etching (grain boundary etching). The phenomenon which causes this effect is essentially the process of surface diffusion /67, 68/.

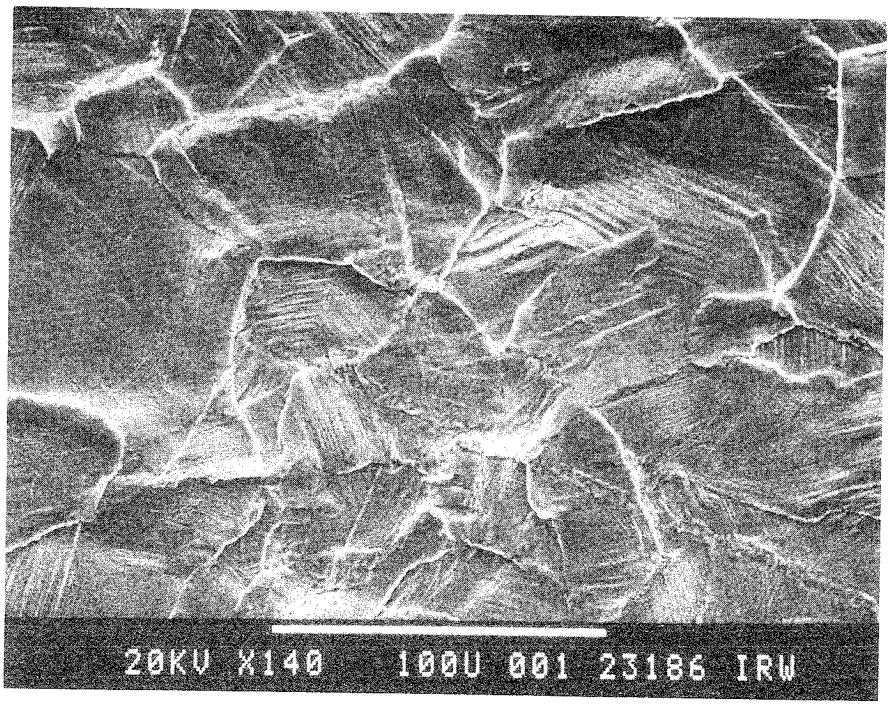

Fig. 7.12: SEM micrograph of the surface of an alloy 1.4311 sample after an electron beam fatigue experiment; beam power density 10 MW m^{-2}, pulse duration 1 s, interval time 9 s, 1000 pulses; grain boundary step development and twin formation are visible

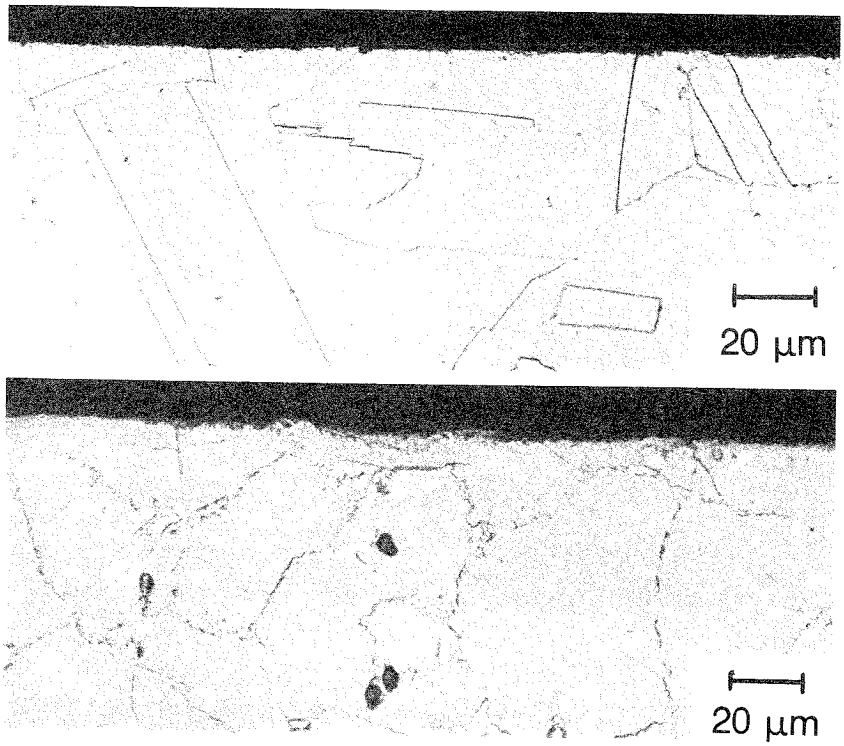

Fig. 7.13: Sample of alloy 1.4311 before (top) and after (bottom) electron beam fatigue experiment (process data as mentioned in fig. 7.12); the grain boundary step development by the fatigue process is clearly to be seen

The conclusion may be valid that this phenomenon of thermal fatigue by itself should not be life-limiting, even in the case of high-heat-flux components, especially when one takes into account that the applied electron beam power density is a factor of 2 higher than the target value (10 MW m^{-2} instead of 5 MW m^{-2}). But it must be considered that the pronounced roughening of the material surface may considerably increase arcing and erosion of the first wall components.

Another important effect of thermal fatigue which occurs already at low cycle numbers is twin formation in the loaded material, fig. 7.12. Due to the deformation which takes place in the material during twin formation the originally austenitic material can be subjected to a martensitic transformation while the twins are forming. If such a sample after multiple shots loading is etched, fig. 7.14, the surface regions between and in the vicinity of the twins are much stronger affected by the etching agent than in the surface outside the transition zone. This behaviour of the material could be caused by the martensitic inclusions in the loaded area.

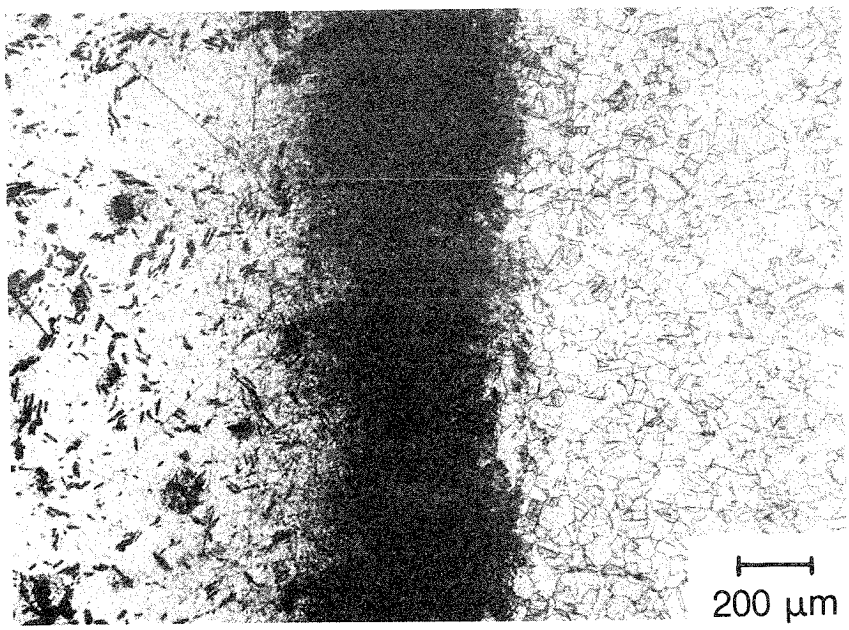

Fig. 7.14: Surface of an alloy 1.4311 sample after electron beam fatigue experiment (5 MW m^{-2}, pulse duration 1 s, interval time 9 s, 1000 pulses); the metallographically prepared sample is etched for the indication of martensitic transformation

After thermal fatigue, that means multiple shot experiments which raise the sample surface temperature above the melting point multilayer remelt zones are generated which are seperated from the unaffected material by recrystallized, coarse grained transition zones. Fig. 7.15 shows this generally known effect in a sample of the alloy 1.4311 which has been loaded with 100 electron beam pulses with a beam power density of 20 MW m^{-2} at a pulse length of 1 s and an interval time of 9 s.

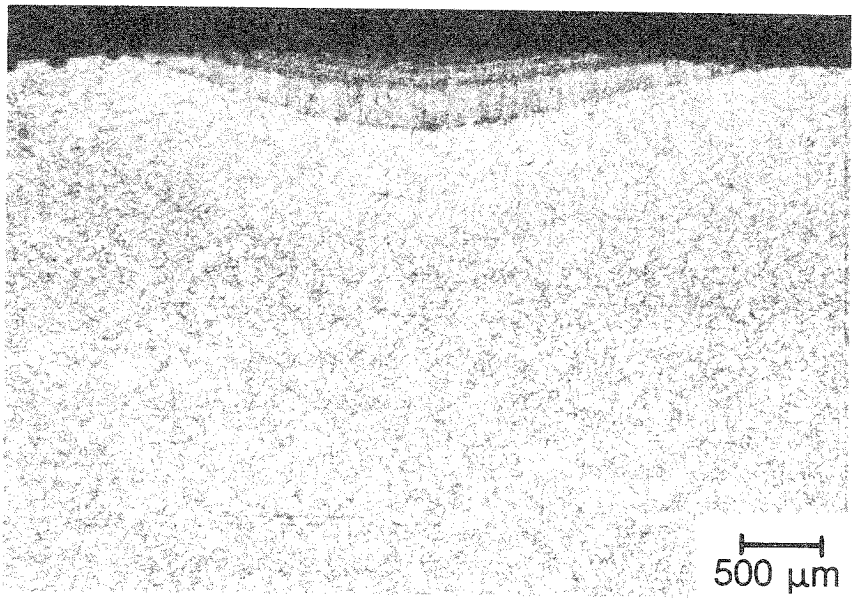

Fig. 7.15: Metallographic section through crater and multi-layer remelt zone in an alloy 1.4311 sample after an electron beam thermal fatigue experiment (20 MW m^{-2}, pulse duration 1s, interval time 9 s, 100 pulses)

Since a coarse grained, recrystallized structure has worse mechanical properties than a fine grained this structural aging as a consequence of the thermal fatigue may increase the probability for crack initiation and enhance crack propagation during subsequent thermal shock loadings. This possibility has to be examined in a forthcoming test series.

A very similar effect should be produced by the preferential evaporation (or erosion) of some alloying constituents during multiple melting in thermal fatigue experiments, fig. 7.16. Here, a line scan for the element Manganese (Mn) shows a distinct decrease of the concentration of this element in the melt crater area after 10 electron beam pulses with a beam power density of 30 MW m^{-2} and pulse lengths of 1 s with interval times of 9 s.

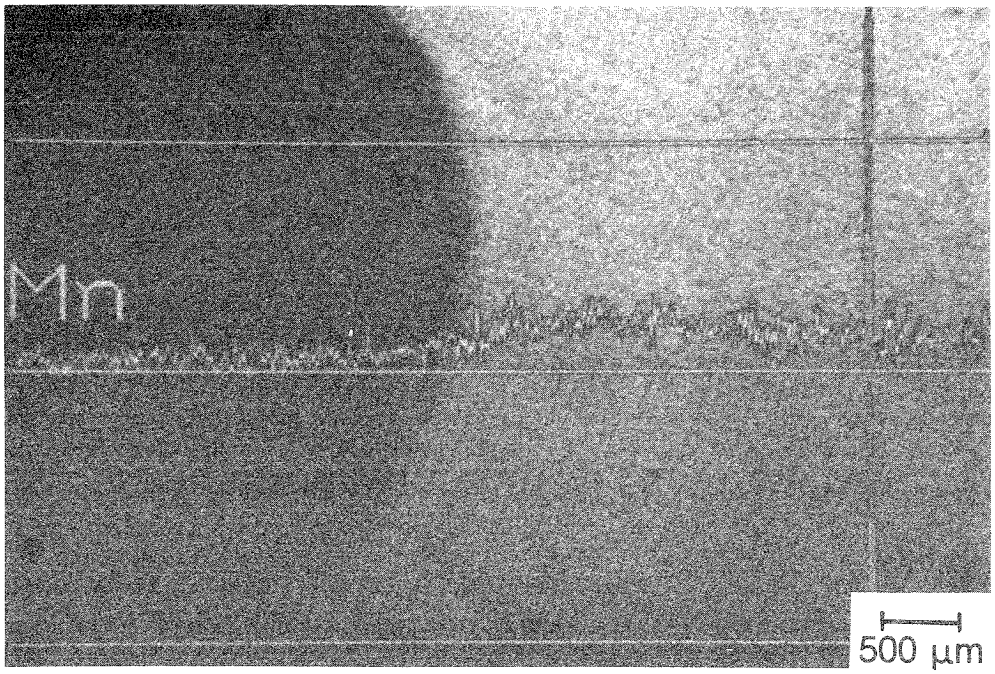

Fig. 7.16: Concentration decrease of the alloying constituent Mn in the alloy 1.4311 after an electron beam thermal fatigue test; SEM micrograph, EDX-analysis for Mn, line scan

Other experiments give rise to the assumption that perferential evaporation and/or erosion of alloying constituents occurs already below the melting point in thermal fatigue loading of first wall material. So, this effect may become an important process for the estimation of the lifetime of a first wall component and therefore should be investigated in further experiments.

7.5 Discussion

The alloys 1.4311 - CRONIFER 1810 - and 2.4816 - INCONEL 600 - as representatives for the high-alloyed Fe- and Ni-base alloys are at present often used as first wall materials for operating plasma machines. So in principle they have proved themselves acceptable for plasma facing structures in todays Tokamaks. To get a better understanding of plasma induced material damages and to examine their behaviour under the operating conditions of next-generation machines they have been tested for their thermal shock and thermal fatigue behaviour.

The following summarizing and evaluating conclusions shall be drawn from the presented results:

- During thermal shock and thermal fatigue loading no material cracking occurs except in the molten area, even at the highest beam power densities and largest pulse numbers.

- Cracks propagate, if at all, only few ten micrometer into the original material in the vicinity of the melt crater.

- The melted volume during thermal shock loading increases rapidly with increasing power density as soon as the threshold load for melting is exceeded but decreases to very short pulse lengths.

- The same result is found for the thermal shock - induced material loss, primarily by evaporation. Under the circumstances considered here a maximum material loss of about 6 mg per cm^2 was measured after one single beam pulse.

- Surface temperature of the materials can well exceed 2000°C already during the comparatively moderate loading of 30 MW m^{-2} for 1 s duration.

- As related to microhardness the molten, recrystallized material in the melt craters behaves as is expected from similar metallic structures: It shows a hardness reduced by roughly 20 % and, with respect to the crack behaviour, a reduced strength.

- Already below the threshold for surface melting thermally induced material damage occurs in the form of grain boundary step formation.

- Grain boundary step formation and, still earlier, twin formation occur markedly in thermal fatigue experiments, far below the threshold loading for surface melting, if only the pulse number is high enough. Both processes should reduce the mechanical strength of the material surface, grain boundary step formation additionally should increase the tendency for arcing and erosion considerably.

- In the area of twin formation the originally austenitic material can be subjected to martensitic transformation which again reduces the erosion resistivity and may reduce the mechanical strength in the material surface.

- During thermal fatigue loading a preferential evaporation of some alloying constituents occurs which may give rise to an unacceptable contamination of the plasma, an uncontrolled redeposition of these elements and, as a consequence of redeposition, an undesirable alloying of the first wall, and again a decrease of the original mechanical and chemical properties of the plasma facing surface of the materials.

- In multiple shot, thermal fatigue experiments in which the melting point of the resp. material is exceeded marked grain growth occurs in a transition zone surrounding the molten material. It can be assumed that the coarse grained material has a reduced resistance against crack initiation and crack propagation.

So the conclusion is obvious that thermal shock and thermal fatigue loading of first wall materials will have life-limiting consequences even under loading conditions which do no destroy a first wall component by one single plasma wall interaction event.

8. Summary and Objectives

The more "conventional" Fe- and Ni-base alloys 1.4311 and 2.4816 and the more uncommon - at least from the standpoint of present Tokamaks - refractory metals and their alloys have been investigated. The idea of this work was to quantify the material damages which are caused by high heat fluxes during - simulated - plasma wall interaction. The tool for this simulation was an electron beam welding machine, an experimental device which is at present often used for that purpose, independent of the respective instrumentation and experimental equipment.

The most important results of the test series can be drawn up in the following statements:

- The available electron beam facility is convenient for material tests of the thermal shock behaviour and of the thermal fatigue behaviour at least of the highly loaded first wall components.

- The characterization procedures available in the Institute for Reactor-materials make it possible to examine and quantify the induced structural changes and material damages very exactly.

- As compared with the effects of plasma wall interaction in real Tokamaks and the resulting variations in the plasma facing materials the results of the simulation tests allow a realistic, quantitative detection of acceptable material loadings and thus a first approach of lifetime prediction.

- Both classes of metals investigated here proved to be good for first wall application on the plasma facing side: for low and medium energetic plasma disruptions, i.e. for thermal shock loaded components, and for the highly loaded first wall components during normal plasma operation, i.e. for thermal fatigue loading. The thermal fatigue of the low-loaded, major part of the first wall should therefor have no life-limiting relevance.

- At low steady state, base temperatures the Fe- and Ni-base alloys show a better crack behaviour than the refractory alloys, at elevated temperatures the refractory alloys seem to be superior to the conventional metals.

- The weight loss, i.e. the material removel from the loaded samples above the melting point, is considerably higher for the refractory alloys than for the Fe- and Ni-base alloys, especially for short energy pulses with high power densities.

From the discussed results of the material tests and with consideration of the present specifications of the requirements for the plasma facing first wall materials in the next-generation Tokamaks some future material tests and experimental extensions should be carried out:

- The material tests should be extended to shorter load pulses with higher power densities - thermal shock - and longer pulses with lower power densities - thermal fatigue.

- Special emphasis should be laid on the tests of thick coatings and especially the bonding technique, e.g. brazing, of thick coatings to metallic substrates.

- The thermal shock behaviour of alloys has to be tested which have been pre-damaged by thermal fatigue, and vice versa.

- The material tests have to be repeated with an hydrogen/deuterium ion or atom beam instead of the electron beam.

Finally it has to be pointed out that the empirically determined effects of plasma wall interaction on and in the alloys neccessarily have to enter into theoretical-mathematical calculations for the lifetime of first wall components in future Tokamaks.

9. References

/1/ Pinkau, K., U. Schumacher: Physik in unserer Zeit, 13, 1982, 138

/2/ Fachausschuß Physik - Industrie - Energie der Österreichischen Physikalischen Gesellschaft (Herausgeber): Kernfusionsforschung, Technische Universität, Wien, 1980

/3/ Dietz, K.J., et al.: J. Nucl. Mat. 128 + 129, 1984, 10

/4/ JET Joint Undertaking, Annual Report 1985, EUR-10615-EN, 1986

/5/ Verhoeven, A.G.A.: 14th Symp. Fusion Techn., Abstracts, CI 01, Avignon, 1986

/6/ Feist, J.F.: 14th Symp. Fusion Techn., Abstracts, DI 01, Avignon, 1986

/7/ Marmy, P.; U. Stiefel: EIR-Bericht Nr. 515, Würenlingen, 1984

/8/ Dietz, K.J., K. Sonnenberg, E. Deksnis, R. Shaw: Conf. Tokamak Start-Up-Problems and Scenarios, Erice, Italy, Proceedings, 1985

/9/ Cecchi, J.L.: 9th Symp. Engineering Problems of Fusion Research, Chicago, Proceedings, Vol. II, 1981, 1378

/10/ Conn, R.W.: J. Nucl. Mat. 128 + 129, 1984, 407

/11/ Pontau, E.A., et al.: J. Nucl. Mat. 128 + 129, 1984, 434

/12/ Samm, U.: 11th Conf. Controlled Fusion and Plasma Physics, Aachen, Abstracts Part II, 413

/13/ Winkler, P., S. Fixler, W.V. Timlen: 9th Symp. Engineering Problems of Fusion Research, Chicago, Proceedings, Vol. II, 1387

/14/ Miyahara, A.: J. Nucl. Mat. 111 + 112, 1982, 461

/15/ Hoven, H., K. Koizlik, J. Linke, H. Nickel, E. Wallura: Berichte der Kernforschungsanlage Jülich, Jül-2002, Jülich, 1985

/16/ Roberto, J.B., R. Behrisch: J. Nucl. Mat. 128 + 129, 1984, 764

/17/ Philipps, V., K. Flaskamp, E. Vietzke: J. Nucl. Mat. 111 + 112, 1982, 781

/18/ Mc. Cracken, G.M., D.H.J. Goodall: Culham Laboratory Report CL M-P 509, 1977

/19/ Vernickel, H.: J. Nucl. Mat. 111 + 112, 1982, 531

/20/ Hassanein, A.M., G.L. Kulcinski, W.G. Wolfer: Nucl. Eng. Design/ Fusion, 1, 1984, 307

/21/ Hassanein, A.M., G.L. Kulcinski, W.G. Wolfer: J. Nucl. Mat. 111 + 112, 1982, 554

/22/ Bohdansky, J.: Physica Scripta, 23, 1981, 119

/23/ Ashby, C.I.H.: SNLA-Report SAND-83-0941 C, 1983

/24/ Cook, T.B., P.W. King, J.B. Roberto, K.A. Stewart, K.E. Yokoyama: J. Nucl. Mat. 128 + 129, 1984, 253

/25/ Gauster, W.B., J.A. Koski, R.D. Watson: 3rd Topical Conf. Fusion Reactor Mat., Albuquerque, 1983, Proceedings

/26/ Russ, J.C.: "Fundamentals of Energy Dispersive X-ray Analysis", Butterworth, London, 1984

/27/ Galambos, J., G. Miley: J. Nucl. Mat. 108 + 109, 1982, 385

/28/ Saidoh, M., R. Yamada, K. Nakamura: J. Nucl. Mat. 111 + 112, 1982, 848

/29/ Gotoh, Y., H. Hoven, K. Koizlik, J. Linke, E. Wallura, M. Ulrickson: 13th Symp. Fusion Technology, Varese, 1984, Proceedings, Vol. 2, 1247

/30/ Croessmann, C.D., G.L. Kulcinski: J. Nucl. Mat. 128 + 129, 1984, 816

/31/ Hassanein, A.M., G.L. Kulcinski, W.G. Wolfer: J. Nucl. Mat. 103 + 104, 1981, 321

/32/ Koizlik, K., H. Nickel: 11th Int. Plansee-Seminar, Reutte, 1985, Proceedings Vol. 2, 851

/33/ Miyake, M., S. Yamanaka, H. Nagae, P. Son, Y. Higashiguchi: J. Nucl. Mat. 122, 1984, 159

/34/ Mullendore, A.W., J.B. Whitley, D.M. Mattox: Thin Solid Films, 83, 1981, 79

/35/ Zito, R.R., W.S. Bickel, W.M. Bailey: Thin Solid Films, 114, 1984, 241

/36/ Guy, A.G.: "Metallkunde für Ingenieure", Akademische Verlagsgesellschaft, Wiesbaden, 1978

/37/ Rosenhain, W., D. Erven: J. Inst. Metals 8, 1912, 149

/38/ Chalmers, B., R. King, R. Shuttleworth: Proc. Roy. Soc. 193, 1948, 465

/39/ NEXT EUROPEAN TORUS: Status Report, Dec. 1985, EURATOM-Report EU-FU/XII-80/86/51, 1986

/40/ JOINT EUROPEAN TORUS: EURATOM-Report EUR-8306 EN, 1982

/41/ Clausing, R.E., L. Heatherly, L.C. Emerson, R.J. Colchin: J. Nucl. Mat. 111 + 112, 1982, 180

/42/ Doyle, B.L., W.R. Wampler, H.F. Dylla, D.K. Owens, M.L. Ulrickson: Sandia-Report SAND 83-2614, 1984

/43/ Bolt, H., H. Hoven, K. Koizlik, J. Linke, H. Nickel, E. Wallura: Berichte der Kernforschungsanlage Jülich, Jül-2024, 1985

/44/ Saidoh, M.: J. Nucl. Mat. 128 + 129, 1984, 540

/45/ Hofer, W.O.: 11. Koll. Metallkundliche Analyse, Wien, 1982, Proceedings,

/46/ Wolf, G.H.: J. Nucl. Mat. 122 + 123, 1984, 1124

/47/ Gotoh, Y., H. Hoven, K. Koizlik, J. Linke, U. Samm. B. Thiele, E. Wallura: J. Nucl. Mat. 133 + 134, 1985, 257

/48/ Shibui, M., et al.: 11th Symp. Fusion Engineering, Austin, 1985, Proceedings

/49/ Croessmann, C.D., G.L. Kulcinski, J.B. Whitley: Sandia-Report SAND 86-0764, 1986

/50/ Koizlik, K., H. Nickel: High Temperatures - High Pressures, 18, 1986, 127

/51/ Hassanein, A.M.: J. Nucl. Mat. 122 + 123, 1984, 1453

/52/ Fukutomi, M., M. Fujitsuka, M. Okada: J. Nucl. Mat., 128 + 129, 908

/53/ Mattox, D.M., A.W. Mullendore, J.B. Whitley, H.O. Pierson: Thin Solid Films, 73, 1980, 101

/54/ Brossa, F., E. Tranconi, P. Moretto, G. Rigon: 2nd Int. Conf. Fusion Reactor Mat., Chicago, 1986, Proceedings, 198

/55/ Stritzker, B.: "Dünne Schichten und Schichtsysteme", 17. IFF-Ferienkurs, KFA Jülich, 1986, 257

/56/ Quataert, D., F. Brossa, P. Moretto, G. Rigon: 13th Symp. Fusion Technology, Varese, 1984, Proceedings Vol. I, 401

/57/ Schiller, S., U. Heisig, S. Panzer: "Electron Beam Technology", J. Wiley - Interscience, Berlin, 1982

/58/ Reimer, L., G. Pfefferkorn: "Raster-Elektronenmikroskopie", Springer-Verlag, Heidelberg, 1973

/59/ Miyahara, A.: Workshop on Plasma-Wall Interaction Data Needs, Sandia National Laboratories, Livermore, 1985, Conference-Report No. 8506177 USDOE, Vol. 1, 269

/60/ Bückle, H.: "Hochschmelzende Metalle", 3. Plansee-Seminar, Reutte, 1958, Springer-Verlag, Wien, 1959, 151

/61/ Alani, R., H. Azodi, M. Naraghi, B. Safaii, A. Torabi-Fard: J. Nucl. Mat. 113, 1983, 25

/62/ Abdou, A.M., R.F. Mattas, D.L. Smith, G.L. Kulcinski: J. Nucl. Mat. 103 + 104, 1981, 41

/63/ Easoz, J.R., R. Bajaj: J. Vac. Sci. Techn. A 3 (3), 1985, 1119

/64/ Touloukian, Y.S., Editor: "Thermophysical Properties of High Temperature Solid Materials", Macmillan, New York, 1970

/65/ Behrisch, R.: Nucl. Fusion 12, 1972, 695

/66/ Behrisch, R.: J. Nucl. Mat. 93 + 94, 1980, 498

/67/ Neumann, G., G.M. Neumann: "Surface Self Diffusion of Metals", Diffusion Monograph Series No. 1, Ohio, 1972

/68/ Schumann, H.: "Metallographie", VEB Deutscher Verlag für Grundstoffindustrie, Leipzig, 1960